Contact of Orthotropic Laminates with a Rigid Spherical Indentor

by

Chun-Fu Chen

Dissertation submitted to the Faculty of the

Virginia Polytechnic Institute and State University

in partial fulfillment of the requirements for the degree of

Doctor of Philosophy

in

Engineering Mechanics

APPROVED:

Daniel Frederick, Chairman

Charles W. Smith

Michael W. Hyer

Liviu Librescu

Michael Renardy

April 29, 1991

Blacksburg, Virginia

Contact of Orthotropic Laminates with a Rigid Spherical Indentor

by

Chun-Fu Chen

Daniel Frederick, Chairman

Engineering Mechanics

(ABSTRACT)

Three dimensional contact problems of square orthotropic laminates indented by a rigid spherical indentor are solved. Simplified problems of indentations of beam and isotropic square plate are studied first to develop an efficient numerical technique and to gather the knowledge of the shape of the contact area in order to solve for the three dimensional orthotropic cases. The approach combines an exact solution method in conjunction with a simple discretization numerical scheme. Numerical sensitivity due to the ill-posed nature of the problem was experienced but was cured by enhancing the numerical approach with a least square spirit. Well agreement is obtained by comparing the results of these simplified studies with available published solutions. For isotropic plate, contact area is found to be either a circle or a hypotrocoid of four lobes featured with a shorter length of contact along the through-the-corner directions of the plate. Hertz's theory fails earlier than assuming the contact area to be a circle. In-plane dependence of the contact stress is presented to illustrate the difference of contact behavior between a square plate and a circular plate. Load-indentation relation reveals indenting a square plate is harder than indenting a circular plate of a diameter equal to the side length of the square plate.

Solutions of multi-layered orthotropic cases are achieved by employing a modified analytical approach with the same numerical method. Three different configurations of plate are implemented for the orthotropic case, namely, a single layered magnesium (Mg) plate, which is slightly orthotropic, and a single and double layered plates of graphite-epoxy (G-E), which are highly orthotropic. Results for the (Mg) plate agrees with the previous isotropic case. Concept of modifying the previous hypotrocoids is introduced to seek for the contact stresses for comparatively large indentation conditions. Single-layered (G-E) plate was implemented for small indentations. The result supports the validity of Hertz's theory for small indentation and shows a relatively longer contact length in the direction of less stiffness. Two layered (G-E) plate illustrates similar distributions for the contact stresses along both of the in-plane directions with a smaller range of validity of Hertzian type behavior than the previous cases. The boundary effect prevails at the initial stage of indentation but is overcome by the effect of material orthotrpy as the indentation proceeds. Thus, the contact area for small indentation appears to be the same kind of hypotrocoids as located in the isotropic case but changes to be the other type of hypotrocoids as the indentation advances.

Acknowledgements

I would like to thank my advisor, Dr. Daniel Frederick, for his guidance, supervision, and his encouragement during the years of my Ph. D. study.

I am also grateful to Dr. Charles W. Smith, Dr. Michael W. Hyer, Dr. Liviu Librescu, and Dr. Michael Renardy of the Mathematics Department for their kindly serving as members of my advisory committe. Especially, I would like to express my special appreciation to Dr. Smith for the many hours spent figuring and discussing the contact area and his inspiration of the hypotrocoidal curves. Dr. Renardy's conceptual help about the convergence problem also deserves my further gratitude.

Finally, I would like to thank my family, my mother, my brothers and sisters-in-law, for their continuous encouragement which makes the completion of this study possible.

TABLE OF CONTENTS

LIST OF TABLES

LIST OF FIGURES

Nomenclature

General Symbols used throughout this Dissertation

σ_{ij} $(i, j = 1,2,3)$	Stress Components
u_i $(i = 1,2,3)$	Displacement Compoments
U_i $(i = 1,2,3)$	Displacement Functions
L	Length of the Beam or the Plate
c	Semi-Contact Length
h	Thickness of the Beam or the Plate
R	Radius of the Indentor

Specific Notations used in the individual Chapters

In Chapter II

E	Young's Modulus
ν	Poisson's ratio
λ, μ	Lame' Constants
$\bar{\lambda}$	$\frac{5\lambda + 6\mu}{3\lambda + 2\mu}$
$f(x), f(x, y)$	Unknown Contact Stress
$q_i(x)$	Typical Subload on Beam
t_n	Fourier Coefficient
p	$\frac{n\pi}{L}$; (n = Any integer)
D	$\frac{d}{dz}$
K_j, ρ	Arbitrary Constants

a_i, b_i	Coefficients for U_j
$\bar{C}_{12}$	$\dfrac{2\lambda\mu}{\lambda+2\mu}$
$\bar{C}_{11}$	$2\mu+\bar{C}_{12}$
Γ, $\bar{K}_1$, $\bar{K}_2$	Defined in equation (13)
D_a, D_b	Defined in equation (17)
$u_{3,i}$	u_3 due to q_i
$(u_3)_0$	u_3 at the Loading Center
$(u_3)_j$	u_3 at x_j
$(u_3)_{0,i}$	$(u_3)_0$ due to q_i
$(u_3)_{j,i}$	$(u_3)_j$ due to q_i
$U_{3,i}$	U_3 due to q_i
K	Number of Divisions on c.
P_i	Magnitude of subload q_i
$\{P\}$	Matrix for P_i's
$[A]$	Coefficient Matrix for $\{P\}$
$\{\underset{\sim}{X}\}$	Matrix of $\underset{\sim}{X}_k=\dfrac{(x_k-L/2)^2}{2R}$
$[\bar{A}]$	$[A]^T[A]$

In Chapter III

C_a	$\lambda+2\mu$
C_b	$\lambda+\mu$
r_s, t	Hypotrocoidal Parameters
k_x	Intersection of hypotrocoid with coordinate axes

f_{kl}	Uniform Sub-load
T_{nm}'s	Fourier Coefficients for f_{kl}
p	$\frac{n\pi}{L}$
q	$\frac{m\pi}{L}$
r	$\sqrt{p^2+q^2}$
$a_{ij}(i,j=1,2,...6)$	Coefficients for U_j's
C_α	$\frac{\lambda+3\mu}{\lambda+\mu}$
$Z_i(i=1,2,...6)$	Defined in equations (45)
$B_\alpha(\alpha=a,b,...e)$	Defined in equations (45)
g_a, g_b	Defined in equations (45)
C_+	$\cosh(rh/2)$
S_+	$\sinh(rh/2)$
H_T	$\frac{S_+}{C_+}$
H_C	$\frac{C_+}{S_+}$
K_T, K_C, k_a, k_b	Defined in equations (48)
U_{3t}	U_3 on the top surface
k_c, k_d	Defined in equations (50)
$(u_3)_0$	u_3 at $(L/2, L/2)$
$(u_3)_{ij}$	u_3 at (x_i, y_j)
$(u_3)_{0,kl}$	$(u_3)_0$ due to f_{kl}
$(u_3)_{ij,kl}$	$(u_3)_{ij}$ due to f_{kl}
P_{kl}	Magnitude of f_{kl}
$[A']$	Coefficient Matrix for P_{kl}
$\{P'\}$	Matrix of P_{kl}'s
$\{\underline{X}\}$	Matrix of $\underline{X}_L = \frac{(x-L/2)^2+(y-L/2)^2}{2R}$
$[\bar{A}']$	$[A]^T[A]$

P	Total Contact Load
σ_{al}	Intimated Average Contact stress, $\frac{P}{c \times c}$
C_k	$\frac{t}{r_s}$
$\bar{x}$	$(x - L/2)/c$
$\bar{y}$	$(y - L/2)/c$
$\bar{r}$	$\sqrt{(\bar{x}^2 + \bar{y}^2)}$
Δ	Indentor Displacement
D	Bending Rigidity

In Chapter IV

C_i	$C_{i(i)}(i = 1,2,...6)$
C_7	$C_{12} + C_{66}$
C_8	$C_{13} + C_{55}$
C_9	$C_{23} + C_{44}$
n	Index for the n^{th} layer
N	Total Number of layers
z_1, z_b	z coordinate for top/bottom surface
z_{n+1}	z coordinate for n^{th} interface
a, b	Semi-Contact lengths along x, y directions respectively
$\lambda_m(m = 1, 2, 3)$	Roots of the characteristic equation (62)
C_{mz}	$\cosh(\lambda z)$
S_{mz}	$\sinh(\lambda z)$
a_i's , b_i's , d_i's	Coefficients for U_j's

F_{im} $(i = 1,2,3;\ m = 1,2,...6)$	Defined in equations (65)
$[K_A]$, $[K_B]$	Defined in equations (68), (69)
G_{ij} $(i = 1,2,3;\ j = 1,2,...6)$	Defined in equations (73)
V_{ij} $(i, j = 1,2,...6)$	Defined in equations (75)
H_{ij} $(i, j = 1,2,...6)$	Defined in equations (77)
$[M]$	Coefficient Matrix for U_j's, defined in equations (79)
σ_{ai}	$\frac{P}{a \times b}$
h_N	Layer Thickness
Y_c	A constant multiplier

CHAPTER I

INTRODUCTION

1.1 Physical Background

Composite material are widely used because of the benefit of high stiffness-to-weight ratio and superior corrosion resistance. For a laminated composite structure, however, a price is often paid due to the weakness in the direction transverse to the enhancement. The sensitivity of laminated composite structures to a lateral projectile has long been experienced and studied extensively in the aerospace industry. A very typical example is the impact damage induced by a foreign object. Such impacts may occur due to the dropping of a tool (Jones, et. al., 1988), or a bird hitting on the aircraft during landing, take-off, or low-altitude maneuvers (Brockman, 1988). The effect is highly localized and will cause fiber breakage and layer delamination or there may be damage of more complicated nature through the thickness of the composite which may be composed of various staking sequences and layer orientations. In general, the damage is induced underneath the impact site in the interior or on the back side of the structure and is usually undetectable by visual inspection. Although NDI (Non-Destructive Inspection) procedures may be used to detect this kind of damage, full-scale NDI is, however, very expensive and time-consuming (Jones, et. al., 1988). Therefore it is necessary to develop and rely on other techniques to access and cure this type of damage.

Theoretically, a typical bird-striking event, termed soft body impact, is believed to be a combination of nonlinear structural behavior, fluid-structure interaction, varying contact surfaces, and free surface flow phenomena (Brockman, 1988). In the case of stiff projectiles, the characterization may be even more complicated. For instance, in a high speed impact event, a stiff impactor may penetrate through the structure (Schonberg, et. al., 1987). In addition, the impact duration may be short enough to

induce a structural dynamics effect, namely the phenomenon of stress wave propagation. In reality, a full-scale solution for such a problem may require both static and dynamic consideration of linear and nonlinear elasticity, inelasticity, modal analysis, techniques of plasticity, fracture mechanics and perhaps knowledge of some other fields. In general, the number of involved fields is beyond what one can handle in practice. A major concern at present is the consideration of low speed impact in which the structural behavior remains in the elastic range and penetration and wave propagation are precluded (Schonberg, et. al., 1987; Sun and Sankar, 1985). In this case, the results of a quasi-static study can be of significant help in understanding the structural response in a typical impact condition (Sankar, 1987).

1.2 Present Study

The aim of this study is to investigate the local contact stress of orthotropic laminates indented by a rigid spherical indentor simulating the low speed impact condition. In the first chapter, a literature review on related studies is presented at the beginning. The motivation behind this study and the research objectives are also illustrated. The second chapter deals with a simplified problem of a single-layered isotropic beam indented by a cylindrical indentor in order to compare the results obtained by the methodolology used in this study with some published results. The approach incorporates Pagano's exact solution technique (1970) for a sandwich plate and a point matching method proposed by Sankar and Sun (1983). Sensitivity observed during the numerical implementation and the curing methods are illustrated. An investigation of the numerical convergence is made to conclude an efficient programming technique.

The solution methods developed in solving the beam problem are then employed and extended for studying three dimensional contact problems. First, since isotropy is a special case of orthotropy, the problem of an isotropic square plate indented by a rigid sphere is solved in chapter three. Because of the simplicity arising from the assumption of isotropy, the algebraic effort is significantly reduced, and the solution gives rise to an exact form for the expression of the displacement field which is much simpler than the approach presented by Pagano (1970). Conditions of both small and large contact areas are considered. While the contact area for the former case is found to preserve a circular shape, the Hertzian type distribution of contact stress shows only a limited range of application. For the case where the contact area is large enough to be affected by the boundary support conditions, the contact area is

sought by introducing the concept of an irregular contact boundary and is proven to be a hypotrocoid of four lobes. For large indentation, contact stress obtained for the present square plate are compared with a circular plate solution to illustrate the relative distinction.

The solution methods are further extended in chapter four to solve three dimensional contact problems of typically layered orthotropic square laminates indented by the same indentor. The approach superposes the previously developed methods for the isotropic beam and plate problems with Chen and Frederick's technique (1990) for solving the problems of multi-layered laminates. For the purpose of demonstration, the developed approach is implemented for both single-layered and multi-layered laminates. In investigating the single layer case, a nearly isotropic material is considered first in order to compare the results with those obtained in solving the previous isotropic plate problem. A highly orthotropic material such as high modulus graphite-epoxy used in typical laminated composites is then considered. Of this material, the single layer laminate is studied for small indentation conditions in which the contact area remains an elliptic shape. The major emphasis is the visualization of different rates of increasing the contact length along different in-plane directions as the indentation proceeds. Finally, a two layer laminate of the same material with a 0°/90° staking sequence is taken for implementation for various magnitudes of indentation. A strong intention is placed on investigating the variance of the correct contact area with the amount of indentation. The phenomenon that the contact area changes its shape from one family of hypotrocoids to the other as the indentation increases will be illustrated. Quantities of primary interest are the contact area and the associated contact stress distributions for various sizes of contact lengths along a prescribed direction. The load-indentation relations are also presented for both of the

three dimensional studies. Discussions of the numerical results will be addressed in each chapter in which comparison of the obtained solutions with the Hertzian type behavior will be made. Some concluding remarks are presented in chapter five to summarize this study.

1.3 Review of Previous Studies

A large number of related investigations involving both theoretical and experimental methods have been conducted over the past decades. The purpose of these studies was to make progress in providing a better simulation and understanding about the real problem. Due to the complexity of the real phenomenon, primarily experimental approaches were used to study this type of problem in the early years when composite materials were first introduced. The number of experimental investigations is still increasing at present. Some empirical equations have been developed for both the load-indentation relation and the expression of residual strength as a function of impact energy. For example, Yang and Sun (1982) presented a static indentation law to relate the magnitude of the applied load and the amount of indentation. It was applied to an impact analysis by Tan and Sun (1985). Due to the formidability in finding the contact forces analytically, they suggested that experimental measures be undertaken in studying an impact problem. A dynamic contact law relating force and strain for the transverse impact of beams was proposed by Doyle (1984). However, some difficulities in conducting a test were experienced (Yang and Sun, 1982; Sun, et. al., 1981). On the other hand, theoretical approaches seemed to be less productive. Nevertheless, theoretical methodology must be further developed not only for the purpose of interpreting and furnishing a better understanding of the experimental results but also for providing an accurate prediction of the structural response during the entire event of impact.

Of the analytical approaches, the earliest theory for the transverse indentation or punch type problem was the classical contact law established by Hertz (1881) over one hundred years ago. It was derived for the frictionless contact between an elastic

sphere and an elastic half space both of which were assumed to be isotropic and homogeneous. In many practical problems of the present time, the theory is still applicable in cases where the physical model of an isotropic half space can be employed. On the introduction of anisotropy, which is a typical property of composite materials, the earliest study was due to Willis (1966, 1967) who applied Hertz's contact law to an anisotropic semi-infinite body but presented some explicit formulas for the transversely isotropic case only. Several other analytical solutions for the contact or indentation problem of an isotropic body were published in 1960s, e. g., Popov (1961, 1962), Keer (1964), Meijers (1968) and Tsai (1969). A quasi-static impact on a multi-layered isotropic semi-infinite medium was studied later by Chen and Engel (1972). Several investigations in which the so-called transfer matrix approach was proposed to treat almost the same type of problem were made by Leon (1972, 1975). However, prior to the advent of sophisticated computational mechanics techniques, most of the analytical solutions were limited to very simplified cases. As the result of the development of modern high-speed computers, extensive numerical techniques have been developed to study the afore-mentioned problems. Most of studies which have been done on contact problems up to about 1980 may be found in the complete listing in Gladwell's book (Gladwell, 1980). However, they were mostly confined to plane problems or isotropic cases only.

In the mean time, another branch of contact mechanics dealing mainly with problems of wheel/rail contact was developed as well. By nature, most of these studies were to deal with rolling or sliding contacts which were usually non-Hertzian problems since consideration of the friction effect was required. Moreover, the local surfaces of the contacting bodies were quite often not quadratic although elementary studies of this type were usually to simulate a wheel/rail pair with two crossly contacted cyl-

inders. A review and survey of studies in this field was made by Kalker (1979, 1980). A detailed definition of a Hertzian contact problem was presented by Paul (1983), who also briefly classified contact problems in two categories according to the size of the contact length. When the contact length is small in comparison to the principal radii of the undeformed surfaces, the contact is classified as antiformal (or counterformal), when large it is conformal. One of the numerical solutions for the non-Hertzian type of contact problem was published by Singh and Paul (1974) by using a simple discretization method. The concept of the so-called interpenetration curves between contacting bodies was introduced. In particular, the numerical sensitivities of this type of problem were experienced and the required curing methods were presented. The problem was said to be inherently ill-posed. Significantly, this means that the boundary conditions of the problem, including the applied load and the corresponding area were not well defined. They are usually unknown as well and have to be considered in the solution procedure. Consequently, large differences in the results may be obtained upon slight changes in the manner of pursuing the approximate solution. The approach developed in this study was later modified by Paul and Hashemi (1978) who pointed out the cause of the previous numerical difficulities and presented an improved numerical method for solving this type of problem. In the improved method, a similar discretization technique was employed, however, the problem was posed in a different manner which was claimed to be able to avoid the aforementioned numerical sensitivity automatically. This improved method was further extended to solve a conformal contact problem (Paul and Hashemi, 1980) and problems of contact between wheels and rails of arbitrary profiles (Paul and Hashemi, 1980). A general numerical approach, termed the flexibility method, for elastic contact problems was presented by Hartnett (1980). Meanwhile, numerous studies were made to develop algorithms for the contact problems in this field (Kalker, 1980, 1981,

1983; Duffek, 1981, 1983). However, most of the analytical and numerical approaches of these studies were to deal with isotropic bodies which were assumed to be elastic half spaces with respect to the local contact regions. In this manner, a sophisticated contact problem could be reasonably solved by considering numerous simplified problems such as the Boussinesq problem in which the displacement field was easily obtained by the Boussinesq force-displacement relation (Timoshenko and Goodier, 1970).

In the structural mechanics field, although many of the structures may be built with a more regular geometry and shape than the wheel/rail system, technical difficulties may arise if different material properties exist, especially over the same in-plane surface or if the domain of the structure is finite and is poorly approximated by assuming it to be a semi-infinite medium. In both cases, the problem of obtaining the local response around the contact area is formidable. However, for the isotropic case, studies were initiated in the early 1980s to investigate the local contact behavior as well as the global bending action of a finite beam or plate structure. More studies were made for the beam problem than for the plate. For example, Keer and Miller (1983) superposed the solution based on an integral transform technique for an infinite layer with a pure bending beam theory to calculate the contact stresses and the overall beam compliance for a finite isotropic beam. Sankar and Sun (1983) solved the same problem by taking the contact force to be a sum of various uniform loads in a manner similar to a stepwise constant pressure method which was apparently first introduced by Conway, et. al. (1966). A subsequent extension to an orthotropic case including the effect of initial stress was made later by Keer and Ballarini (1983) and Sun and Sankar (1985). All of these studies indicated an agreement of the Hertzian type stress distribution for the small indentation condition, and

a deviation from the Hertzian behavior for the local contact stress in the case of a large contact area. In the meantime, the receding/advancing concept, namely decreasing/increasing the contact area or the so-called Dundurs problem for the case of a beam was studied by Pawlak et. al. (1985). Incorporating the dynamic effect, Keer and Miller's approach for the isotropic beam (Keer and Miller, 1983) was extended by Keer and Lee (1985) to treat a low speed impact problem of a beam with a large contact area.

Solutions for the three dimensional contact problem of a finite plate apparently were first obtained by Keer and Miller (1983), who extended their original approach for the beam to a circular plate by the method of Hankel transform. In a similar manner, the subsequently formulated impact problem was studied by Keer and Woo (1984). However, both studies were limited to the isotropic case. In the past few years, other approaches for solving the contact problem for a beam or a half space were proposed. For example, the Green function technique as presented by Sankar (1987), Miller (1986) and Koshnareva, et. al. (1987) were used. However, interest in the impact problem of a laminated plate increased. For example, Shivakumar, et. al. (1985) presented both energy-balance and spring-mass models to predict the impact force and duration in the low speed impact for a transversely isotropic laminate. Large deflections and transverse shear effects were both considered but the impact stress distribution was not described. Cairns and Lagace (1987) were able to solve the contact problem of a thick composite circular plate subjected to a lateral load. However, their solution was based on the consideration of cylindrical orthotropy without including the in-plane dependence of the response, which is one of the characteristics of the behavior of composite plates. Moreover, Hertz's law was assumed for the representation of the contact stress, which is true only for the case of a small in-

dentation as noted earlier. Sankar (1988) calculated the contact and interlaminar shear stresses of both single and multi-layered circular plates by using a finite difference approach. The influence of a soft layer on reducing the transverse shear stresses was investigated for the isotropic case only. Schonberg et. al. (1987) extended Keer and Woo's method (1984) to investigate the static and dynamic impact problem of transversely isotropic beams and plates. The in-plane dependence of the response was not considered; however, a thorough use of integral transforms in solving this type of problem was illustrated. For the elasto-static case of a transversely isotropic plate, another approach was formulated by Tsai (1986) without presenting the non-Hertzian type contact stress. A study of the effect of the transverse shear on an impact loaded plate was made by Mittal (1987), in which Hertz's contact law was also employed to calculate the impact force.

Recently, an experimental study was conducted by Poe (1988) to investigate the impact damage on the case of a solid rocket booster. It should be noted that the specimens were all taken from the full-scale structure to account for the exact curvature. The specimens contained off-axis layers but were considered as transversely isotropic bodies. Hertz's law was applied in representing the contact stresses for a correlation study with finite element solutions. Meanwhile, another impact problem of a rectangular laminated composite plate was solved by Aggour and Sun (1988). Results were obtained by using a two dimensional finite element method based on a laminated plate theory. The contact stress between the plate and the impactor was assumed to be uniformly distributed and was calculated for each time step during the entire duration of impact by using Hertz's contact law. A three dimensional finite element investigation on impact induced deformations as well as the locations and sizes of the resulting delamination in more general composite plates including off-

axis layers was studied by Wu and Springer (1988). Various boundary conditions were considered but the assumption of a point load for the contact force was introduced and was obtained from Hertz's contact law. Apparently, an analytical solution for this type of problem for the case of orthotropy or general anisotropy has not been published. Hertz's contact law, which in fact has been indicated by Tan and Sun (1985) to be invalid for a thin layered type structure such as a typical composite laminate has been employed by most researchers for treating a wide variety of plate problems. The effect of in-plane material orthotropy or general anisotorpy on the local contact behavior of the structure seems to have not been considered. In fact, it is anticipated that the task of finding the real contact profile when the in-plane material anisotropy exists, especially, for a thin and layered structure such as a fiber reinforced laminated composite will be very tedious.

Most recently, Chen and Gurdal (1990) investigated the effect of material orthotropy on the interlaminar normal stress for a laterally loaded orthotropic plate on an elastic foundation by using a double Fourier transform technique. The approach was modified and extended by Chen and Frederick (1990) to solve a multi-layered orthotropic case with an emphasis on the interlaminar normal as well as shear stresses at the layer interfaces through the thickness. Both of these two studies did not account for the real contact problem since the assumption of a uniform distribution of the applied load was introduced. However, the in-plane dependence of the responses, especially the interlaminar normal and shear stresses, due to the material orthotropy were well illustrated.

1.4 Motivation

Primarily, the motivation behind this study concerns the transverse impact of an aircraft structure by lateral projectiles. Due to the inherent invisibility of the impact damage, the residual strength of the structure after impact is extremely desirable since it completely determines the subsequent load carrying capability. On the other hand, knowledge of the damage initiation is equally important a priori information since the subsequent damage or failure mechanism will depend on it. Among the possible induced damages, two of the better known ones are fiber breakage and layer delamination (Brockman, 1988). Although an individual cause of damage may be due to transverse shear or interlaminar tensile normal stress, influences of both effects are likely to be mixed and depend on the relative stiffness, geometry, and hardness between the impactor and the structure. However, regardless of the possible configuration, an understanding of the real contact behavior between both bodies is required in order to predict the possible failure occurrences before any damage is produced. This requires the determination of the contact stress distribution over the contact area once the foreign object has come in contact with the structure. Following determination of the contact stress, information on the structural response, in particular, the layer-by-layer stress state in the vicinity of the contact area through the thickness can be obtained. Predictions of where the damage will be initiated and how it will be propagated is then possible.

The second motivation in conducting this study has to do with the need for a three dimensional analysis of an anisotropic contact problem since none of the existing publications in the literature have dealt with the three dimensional contact for a general anisotropic material. From the existing literature, two dimensional problems of

this type, namely a cylindrical indentation condition, seem to have been well studied and developed except for the case of contact for an off-axis layered beam. Although a two dimensional analysis may provide the technical foundation for a three dimensional study, the results may be of little value in predicting the actual behavior of the structure in practice since the real problem is always three dimensional. Unless the structure and the material properties are both axisymmetric, a three dimensional analysis is required in general. However, the three dimensional anisotropic case is very different from a two dimensional beam or a three dimensional axisymmetric problem. Physically, the difference is due to the possible inhomogeneity over the in-plane surface in the former case. Thus, for any magnitude of the applied load, although the contact length along any in-plane direction for the latter case is the same, it will be different for the general three dimensional anisotropic case. Therefore, one can always assume the contact length, for a beam or an axisymmetric problem to be known a priori from which the total applied load can be accordingly defined. For a three dimensional anisotropic case, however, only the contact length along one of the in-plane directions can be prescribed to correspond to a certain amount of the applied load. Knowing this contact length, the length of contact along any other direction will be a single-valued function subsequently. This function and thus the ratio between the contact lengths along different in-plane directions has to be found. Such a task, which amounts to finding the real contact area for a certain contact length along one of the in-plane directions, is believed to be the most difficult step in solving problems of this type.

In reviewing related publications, although some studies have been concerned with three dimensional investigations (Cairns and Lagace, 1987; Mittal, 1987; Wu and Springer, 1988), the importance of the local contact behavior seems to have been ig-

nored. As far as the local contact stress is concerned, for simplicity, it has been either assumed to be uniform or obtainable by Hertz's law for all types of indentation. To satisfy the static equilibrium condition, an accurate calculation of the contact stress should produce all compressive stresses and satisfy the free stress condition along the contact boundary as long as it is a smooth indentation, i. e. frictionless, and the indentor has no sharp edge. In accordance with the physical assumption of an isotropic homogeneous half space on which Hertz's law is based, the Hertzian type behavior can only be true for axisymmetric contact problems for small indentations (Schonberg, et. al., 1987). Although a circular plate may be of practical interest, the properties of general anisotropy or orthotropy are usually manufactured into rectangular plates. Obviously, a thin structure of a laminated composite violates the hypothesis of a half space. The material inhomogeneity and the asymmetric properties of a typical composite laminate also violate the conditions for Hertzian contact. The previously mentioned in-plane inhomogeneity of a typical laminated composite will result in different bending rigidities and thus different tendencies for wrapping around the curvature of a given indentor along different in-plane directions at any instant of an impact event. This condition may prevail in an asymmetric isotropic structure as well. Hence, calculation of the contact stresses in these cases requires a technique which is capable of taking into account the possibility of an irregular shape for the contact area, rather than arbitrarily applying Hertz's theory.

This study is also motivated by the need for quasi-static investigations of impact problems. Although the elasto-dynamic condition exists in reality, it can be reasonably assumed that the indentation occurs over a longer period of time in a low speed impact. The local deformations and stresses can therefore be approximated by an elasto-static solution. In fact, a static indentation study conducted by Sankar (1987)

has been shown to be able to provide useful information about failure mechanisms and failure loads for a low speed impact event. The present study is accordingly motivated.

1.5 Objectives

In this study, the main objective is to investigate the contact stress distribution for typical finite orthotropic laminated composite plates indented by a rigid spherical indentor. The low speed impact phenomenon of laminated composite structures induced by a foreign impactor will be simulated by using the quasi-static condition. Major emphasis will be placed on the investigation of the effect of the in-plane material orthotropy on the distribution of the contact stresses. In this regard, the contact stress distribution along different in-plane directions will be displayed for various sizes of the contact area. A strong intention is aimed at solving the correct contact area for a general three dimensional contact problem and investigating the effect of finite boundaries alone or the coupled effect of material orthotropy and finite boundary on the local contact behavior. Another intention is to test the validity of Hertz's contact law and accordingly to evaluate the limits of its application. A subsequent objective is to investigate and present the load-indentation as well as the load-contact size relations.

Theoretically, the purpose of this study is to demonstrate the use of elementary and tractable approaches, namely a series expansion technique in conjunction with a point matching method, in solving a sophisticated contact problem. In the computational/numerical phase, the major aim is to illustrate the cautions necessary to achieve a satisfactory convergence and accuracy of the results. Due to the necessity of considering a rectangular plate, numerical implementation which accounts for both in-plane directions is required and will be demonstrated. A subsidiary objective in conducting this study is to detect inherent numerical sensitivities similar to those experienced by Singh and Paul (1974). Appropriate techniques for an appro-

priate remedy will be demonstrated. For the purposes of comparing the results and attaining the guidances in treating the three dimensional orthotropic problems, some simplified cases such as the problems of an isotropic beam and an isotropic square plate will be studied. Another intention is to introduce the concept of irregular shape of the contact area in solving the three dimensional contact problems for the case of large contact area. In summary, this dissertation is to serve as a fundamental study for the three dimensional contact problems of laminated composites in the framework of the theory of elasticity.

CHAPTER II

AN ISOTROPIC BEAM PROBLEM

2.1 Introduction

In this chapter, a cylindrical indentation problem of a two dimensional isotropic beam, the same as the one presented by Keer and Miller (1983) and Sankar and Sun (1983), is solved. In addition to the aim of reproducing previously published results, one of the major objectives in studying the beam problem is to detect any possible numerical sensitivity and to demonstrate remedial approaches for dealing with it. The other reason for solving this simplified problem is to find an efficient technique for numerical convergence which will be useful in treating the three dimensional cases. Since, for the latter cases, it is known that implementation along both of the in-plane directions is required, a question of interest is whether the convergence behavior will be the same and whether can it be assured along both of the in-plane directions. For implementation, a technique to detect the convergence behavior along an individual direction is needed. A study of the two dimensional beam problems can therefore provide significant information for this purpose. To begin the study, a brief description of the beam problem will be given first. It will be followed by a detailed approach for solving this problem. The numerical technique will be used to obtain results for several examples. The convergence problems, numerical sensitivities, and the required suplemental methods are discussed also.

2.2 Description of the Problem

The two dimensional case of an isotropic beam, subjected to a cylindrical indentation is shown in Figure 2. The beam is taken to be homogeneous through the thickness and composed of a single layer. It is indented by a rigid cylinder at the center of its

length on the top surface and is simply supported at both ends. Friction between the cylindrical indentor and the beam is neglected. The governing field equations in this case are

$$(\bar{\lambda}+1)u_{1,11}+(\bar{\lambda}-1)u_{1,33}+2u_{3,13}=0 \tag{3.1}$$

$$(\bar{\lambda}-1)u_{3,11}+(\bar{\lambda}+1)u_{3,33}+2u_{1,13}=0 \tag{3.2}$$

where u_1 and u_3 represent displacements along the x and z directions respectively, and $u_{1,11}=\frac{\partial^2 u_1}{\partial x^2}$, ... etc. As for the plane stress condition considered by Keer and Miller (1983) and Sankar and Sun (1983), $\bar{\lambda}=\frac{5\lambda+6\mu}{3\lambda+2\mu}$. Here, λ and μ are the Lame constants expressible as $\mu=\frac{E}{2(1+\nu)}$, $\lambda=\frac{2\mu\nu}{1-2\nu}$, and E and ν are Young's modulus and Poisson's ratio, respectively. The boundary conditions for the beam in the through-the-thickness direction are

$$\sigma_{33}(x,\frac{h}{2})=\sigma_{31}(x,\frac{h}{2})=\sigma_{31}(x,-\frac{h}{2})=0 \tag{4.1}$$

$$\sigma_{33}(x,-\frac{h}{2})=-f(x), \quad |x-\frac{L}{2}|\leq c \tag{4.2}$$

$$\sigma_{33}(x,-\frac{h}{2})=0, \qquad |x-\frac{L}{2}|\geq c \tag{4.3}$$

where h is the thickness of the beam, $f(x)$ is the unknown contact stress beneath the cylindrical indentor. and L is the length of the beam. The contact length $2c$ is assumed to be a known value. Meanwhile, the transverse displacement, u_3, of the points in the contact region has to satisfy the contact relation due to the indentor, i. e.,

$$u_3(0, -\frac{h}{2}) - u_3(x, -\frac{h}{2}) = \frac{(x - \frac{h}{2})^2}{2R}, \quad |x - \frac{L}{2}| \leq c \tag{4.5}$$

where R is the radius of curvature of the indentor. Furthermore, the simply supported edge conditions require that

$$\sigma_{11}(0,\ z) = \sigma_{11}(L,\ z) = u_3(0,\ z) = u_3(L,\ z) = 0 \tag{4.6}$$

2.3 Formulation of the Solution

Basically, the approach used in obtaining the solution is along the lines proposed by Sankar and Sun (1983). At the very beginning, the unknown contact stress $f(x)$ for a prescribed contact length $2c$, is assumed to be a summation of various uniform sub-loads each over an individual interval inside the contact length as shown in Figure 3. To solve for the magnitudes of the sub-loads, the solution will be obtained in two steps. First, the transverse displacements u_3 at points along the length c due to all of the sub-loads of unit magnitude are to be solved. However, instead of superposing a bending theory for a beam and an elasticity approach as employed by Sankar and Sun (1983) at this stage, an exact solution following the method presented by Pagano (1970) will be found for the displacement field directly. The second step will be to establish algebraic simultaneous equations for the magnitudes of various sub-loads based on the contact relation given in equation (4.5). Finally, the magnitudes of all of the sub-loads will be found by solving these equations to obtain an approximate solution for the unknown contact stress $f(x)$.

2.3.1 Displacements due to a typical sub-load

Following Pagano's method (1970), in satisfying the boundary conditions, a typical sub-load $q_i(x)$ will be expressed in terms of a Fourier series as follows

$$q_i(x) = \sum_{n=1}^{\infty} t_n \sin(px) \tag{5}$$

where $p = \frac{n\pi}{L}$ and t_n is the Fourier coefficient. Accordingly, the displacements due to q_i will be a superposition of those induced by each term in the series. Hence, it is necessary to find the displacements due to a typical term in equation (5).

2.3.1.1 Expressions for the Displacements and Stresses

To solve for the responses of the beam for the prescribed edge support conditions, a form similar to that of equation (5) for a sub-load will be used for the displacement components. Thus,

$$u_1(x, z) = U_1(z)\cos(px)\,, \quad u_3(x, z) = U_3(z)\sin(px) \tag{6}$$

where U_1, U_3 are unknown displacement functions which must be determined. To accomplish this, expressions (6) are substituted into the governing equations (3). These give rise to the equations

$$[(\bar{\lambda} - 1)D^2 - (\bar{\lambda} + 1)p^2]U_1 + 2pDU_3 = 0 \tag{7.1}$$

$$-2pDU_1 + [(\bar{\lambda} + 1)D^2 - (\bar{\lambda} - 1)p^2]U_3 = 0 \tag{7.2}$$

where $D = \frac{d}{dz}$. The fundamental solution for the U_j's is $K_j e^{\rho z}$ $(j = 1, 3)$, where the K_j's and ρ are constants. To obtain non-trivial solutions for the U_j's, the characteristic equation derived from equations (7) has to be satisfied, which is,

$$\begin{vmatrix} (\bar{\lambda} - 1)\rho^2 - (\bar{\lambda} + 1)p^2 & 2p\rho \\ -2p\rho & (\bar{\lambda} + 1)\rho^2 - (\bar{\lambda} - 1)p^2 \end{vmatrix} = 0 \tag{8}$$

The roots of this characteristic equation are $\rho = p, p, -p, -p$. Therefore, with two repeated roots, the solutions for U_1, U_3 can be written as,

$$U_1 = (a_1 + a_3 z)C_z + (a_2 + a_4 z)S_z\,, \quad U_3 = (b_1 + b_3 z)C_z + (b_2 + b_4 z)S_z \tag{9}$$

where $C_z = \cosh(pz)$, $S_z = \sinh(pz)$, and the a_k's, b_k's $(k = 1, 2, 3, 4)$ are constants. However, a_k's and b_k's are related by equations (7). Upon substituting expressions (9) into equation (7.1), performing some rearranging, and recognizing that C_z, S_z, zC_z, zS_z are independent functions, it is possible to express the b_k's in terms of a_k's as,

$$b_1 = a_2 - \frac{\bar{\lambda}}{p} a_3\,, \quad b_3 = a_4 \tag{10.1}$$

$$b_2 = a_1 - \frac{\bar{\lambda}}{p} a_4\,, \quad b_4 = a_3 \tag{10.2}$$

Therefore, the transverse displacement function $U_3(z)$ can be further written as

$$U_3 = a_1 S_z + a_2 C_z + a_3\left(zS_z - \frac{\bar{\lambda}}{p} C_z\right) + a_4\left(zC_z - \frac{\bar{\lambda}}{p} S_z\right) \tag{11}$$

From the expressions for the displacement components, the stress components, in the case of plane stress, can be readily derived. In terms of the displacements, these are (Sokolnikoff, 1956),

$$\sigma_{11} = \bar{C}_{11} u_{1,1} + \bar{C}_{12} u_{3,3}\,, \quad \sigma_{33} = \bar{C}_{12} u_{1,1} + \bar{C}_{11} u_{3,3}\,, \quad \sigma_{13} = \mu(u_{1,3} + u_{3,1}) \tag{12}$$

In equation (12), $\bar{C}_{11} = 2\mu + \bar{C}_{12}$, and $\bar{C}_{12} = \dfrac{2\lambda\mu}{\lambda + 2\mu}$.

Upon substituting the displacements of equations (6), into equations (12), and employing equations (9) and (11), the expressions for the stress compoments may be written as

$$\sigma_{11} = \{\Gamma(a_1 C_z + a_2 S_z) + a_3[\bar{K}_2 S_z + \Gamma z C_z] + a_4[\bar{K}_2 C_z + \Gamma z S_z]\} \sin(px) \tag{13.1}$$

$$\sigma_{33} = \{a_3[\bar{K}_1 S_z - \Gamma z C_z] - \Gamma(a_1 C_z + a_2 S_z) + a_4[\bar{K}_1 C_z - \Gamma z S_z]\} \sin(px) \tag{13.2}$$

$$\sigma_{13} = \mu\{2p(a_1 S_z + a_2 C_z) + a_3[(1-\bar{\lambda})C_z + 2pz S_z] + a_4[(1-\bar{\lambda})S_z + 2pz C_z]\} \cos(px) \tag{13.3}$$

where $\Gamma = -2\mu p$, and $\bar{K}_1 = (1-\bar{\lambda})\bar{C}_{11}$, $\bar{K}_2 = (1-\bar{\lambda})\bar{C}_{12}$.

2.3.1.2 Solutions for the Unknown Coefficients

In the previous equations (13), the unknown coefficients a_k's are to be found by applying the boundary conditions through the thickness of the beam. Thus,

$$\sigma_{33}(x, \frac{h}{2}) = 0 \rightarrow$$

$$2\mu p(C_+ a_1 + S_+ a_2) + [\bar{C}_{11}(1-\bar{\lambda})S_+ + \mu p h C_+]a_3 + [\bar{C}_{11}(1-\bar{\lambda})C_+ + \mu p h S_+]a_4 = 0 \tag{14.1}$$

$$\sigma_{13}(x, \frac{h}{2}) = 0 \rightarrow$$

$$2p(S_+ a_1 + C_+ a_2) + [(1-\bar{\lambda})C_+ + p h S_+]a_3 + [(1-\bar{\lambda})S_+ + p h C_+]a_4 = 0 \tag{14.2}$$

$$\sigma_{33}(x, -\frac{h}{2}) = -t_n \sin(px) \rightarrow$$

$$2\mu p(C_+ a_1 - S_+ a_2) - [\mu p h C_+ + \bar{C}_{11}(1-\bar{\lambda})S_+]a_3 + [\bar{C}_{11}(1-\bar{\lambda})C_+ + \mu p h S_+]a_4 = -t_n \tag{14.3}$$

$\sigma_{13}(x, -\frac{h}{2}) = 0 \rightarrow$

$$2p(-S_+a_1 + C_+a_2) + [(1-\bar{\lambda})C_+ + phS_+]a_3 - [(1-\bar{\lambda})S_+ + phC_+]a_4 = 0 \tag{14.4}$$

where $C_+ = \cosh(ph/2)$ and $S_+ = \sinh(ph/2)$. Rearranging equations (14) gives

(14.1) + (14.3)→

$$-4\mu pC_+a_1 + 2[\bar{C}_{11}(1-\bar{\lambda})C_+ - \mu phS_+]a_4 = -t_n \tag{15.1}$$

(14.1) − (14.3)→

$$-4\mu pS_+a_2 + 2[\bar{C}_{11}(1-\bar{\lambda})S_+ - \mu phC_+]a_3 = t_n \tag{15.2}$$

(14.2) + (14.4)→

$$2pC_+a_2 + [(1-\bar{\lambda})C_+ + phS_+]a_3 = 0 \tag{15.3}$$

(14.2) − (14.4)→

$$2pS_+a_1 + [(1-\bar{\lambda})S_+ + phC_+]a_4 = 0 \tag{15.4}$$

Solving the above equations (15) for the a_k's, it follows from (15.1) and (15.4) that,

$$a_1 = \frac{-t_n}{D_a}[(1-\bar{\lambda})S_+ + phC_+], \quad a_4 = \frac{2pS_+t_n}{D_a} \tag{16.1}$$

Similarly, equations (15.2) and (15.3) give,

$$a_2 = \frac{t_n}{D_b}[(1-\bar{\lambda})C_+ + phS_+], \quad a_3 = \frac{-2pC_+t_n}{D_b} \tag{16.2}$$

where,

$$D_a = 4\mu p[2C_+S_+ + ph], \quad D_b = 4\mu p[2C_+S_+ - ph] \tag{17}$$

Basically, the quantity of the primary interest is the transverse displacement u_3 on the top surface where the indentation occurs. This is,

$$u_{3,i}(x, -\frac{h}{2}) = \sum_{n=1}^{\infty} U_{3,i}(-\frac{h}{2}) \sin(px) \tag{18}$$

where, as can be seen from equation (11),

$$U_{3,i}(-\frac{h}{2}) = -S_+a_1 + C_+a_2 + (\frac{h}{2}S_+ - \frac{\bar{\lambda}}{p}C_+)a_3 + (\frac{\bar{\lambda}}{p}S_+ - \frac{h}{2}C_+)a_4 \tag{19}$$

The a_k's were previously found in equations (16) and expressed in terms of t_n.

2.3.2 The Indentation Problem

Having solved for the transverse displacement u_3 for any x location on the top surface of the beam due to any sub-load $q_i(x)$ with unit magnitude, the next step is to solve for the magnitude of each sub-load. Employing the point matching method as presented by Sankar and Sun (1983), the indentation problem requires the development of as many equations, similar to equation (4.5), as the number of sub-load, due to the same number of distinct points over the length, c, i. e.,

$$(u_3)_0 - (u_3)_j = \frac{(x_j - L/2)^2}{2R} \tag{20}$$

provided the contact length, $2c$, is small in comparison with R. In equation (20), $j = 1, 2, ..., K$, for the case of K reference points x_j's selected along the length, c. Next, the following definitions are introduced,

$(u_3)_0$ = displacement u_3 at the center on the top surface

$(u_3)_j$ = displacement u_3 at x_j on the top surface

However, upon considering the contribution due to all of the sub-loads q_i's, it is obvious that

$$(u_3)_0 \simeq \sum_{i=1}^{K} (u_3)_{0,i} P_i \ , \quad (u_3)_j \simeq \sum_{i=1}^{K} (u_3)_{j,i} P_i \tag{21}$$

where $(u_3)_{0,i}$, and $(u_3)_{j,i}$ are $(u_3)_0$, and $(u_3)_j$ due to the sub-load $q_i(x)$, respectively. P_i is the magnitude of $q_i(x)$. Therefore,

$$\sum_{i=1}^{K} [(u_3)_{0,i} - (u_3)_{j,i}] P_i \simeq \frac{(x_j - L/2)^2}{2R} \ , \ j = 1, 2, ..., K. \tag{22}$$

Equations (22) define a set of K simultaneous equations for the K unknown magnitudes P_i's for all of the sub-load q_i's, ($i = 1, 2, ..., K$). Solving these equations for the P_i's, an approximate representation for the unknown contact stress can be constructed.

2.4 Numerical Implementation

2.4.1 Summary of the Numerical Procedures

The numerical procedure for solving the beam problem starts with the discretization of the presumed semi-contact length c into K segments, where K is a prescribed finite number. It should be noted here that since the indentor is smooth with no sharp edges, a prescribed contact length, $2c$, automatically implies a zero contact stress right at the contact boundary, $x = \frac{L}{2} + c$, which is known a priori without any calculation. Along the length c, a set of K points with the coordinates x_{j+1}'s ($j = 1, 2, ..., K$) can be identified upon which various uniform sub-loads are to be constructed. Typically, a uniform sub-load $q_i(x)$ of unit magnitude can be defined in a manner such that,

$$q_i(x) = -1, \quad L - x_{i+1} \leq x \leq x_{i+1}$$

$$= 0, \quad \textit{elsewhere} \tag{23}$$

One way of discretizing the length c, for example, is to take a uniform division with $x_{j+1} = \frac{L}{2} + \frac{j}{K} \times c$ such that the K points x_{j+1}'s are equally spaced. Due to this set of sub-loads, the displacements at any location inside the contact length can be calculated by the forthgoing solution procedures to obtain the coefficients $(u_3)_{0,i} - (u_3)_{j,i}$ of equations (22). Based on the solutions for the P_i's in equations (22), an approximate contact stress distribution along c is available. By the nature of approximation, the solutions for the P_i's give the contact stress at a location x, where $x_j < x < x_{j+1}$ with magnitude

$$\sigma_{33}(x, -\frac{h}{2}) = \sum_{k=j}^{K} P_j \tag{24}$$

In an average sense, the afore-mentioned location x can be reasonably taken to be $x = \frac{1}{2}(x_j + x_{j+1})$, i. e., the mid-point between the boundaries of the adjacient sub-loads. In performing the calculation of $(u_3)_{0,i} - (u_3)_{j,i}$, however, concerns about numerical convergence arise in this step and thus consume most of the numerical effort. Before obtaining any numerical results, further investigation into this step of implementation may be required.

2.4.2 Convergence Problems

Lack of convergence may arise from two sources, the first arises from the approximation of the total contact stress by the constructed sub-loads, and the other from the summation of the series expansion in calculating the displacements. The first source has been discussed by Sankar and Sun (1983) which relates to the required number of subdivisions, i. e., the number of sub-loads used in representing the unknown contact stress. Although 10 to 40 uniform divisions were made by these authors it was stated that the required number depends upon the relative size of the contact length with respect to the thickness of the beam. A higher number of divisions will be required if a relatively large contact length is considered because of the greater likelihood that the contact stress will deviate from the Hertzian type distribution. Due to the intention that the approach developed for the present beam problem will be extended to the solution of three dimensional contact problems, a more efficient technique to accelerate the convergence must be found. In this regard, it is reasoned

that the distribution of contact stress in the central region of the contact area will be more uniform than the distribution in the vicinity of the contact boundary, in particular, in the case of a large contact area. A non-uniform discretization on the contact length which gives a finer cut around the contact boundary is feasibly more accurate than the uniform discretization scheme. Therefore, this concept will be employed in this study. Accordingly, the points in the semi-contact length c on which various sub-loads will be constructed are defined by,

$$x_{j+1} = \frac{L}{2} + c \times \sin\left(\frac{j}{2K}\pi\right), \quad j = 1, 2, \ldots, K. \tag{25}$$

As will be shown later, such a non-uniform discretization method provides the numerical results with the same accuracy, but with a fewer number of sub-loads in comparison to the uniform discretization scheme employed by Sankar and Sun (1983).

The second source of lack of convergence is due to the need to take a finite number of Fourier terms in the calculation of the coefficients $(u_3)_{0,l}$ and $(u_3)_{j,i}$. In concept, one can visualize that, due to the nature of the discontinuity at the ends of any sub-load, many more terms will be required to give accurate calculations for the displacements for locations close to the loading boundary to overcome the well known Gibb's phenomenon (Arfkan, 1973). On the other hand, a narrow sub-load may require more terms as well in the calculation for the displacement as mentioned by Sankar and Sun (1983) because the load tends to behave as a delta function. However, if the point of interest is relatively far from the loading ends, fewer terms will be required in accurately calculating the displacement. Thus, questions arise as to the fewer number of terms required in this case and the manner in which convergence can be guaran-

teed. In fact, the potential answers to these questions are imbedded in the expressions for the displacements themselves. First, for a typical sub-load $q_i(x)$ of unit magnitude defined in equation (23), the Fourier coefficient t_n in equation (5) can be easily derived to be $t_n = \frac{4\cos(px_{i+1})}{pL}$. In performing such a derivation, it is observed that the even-numbered terms give no contribution and thus only odd numbers for n need to be considered in the definition of p in equation (5). Next, in view of the expressions (18), (19), and (16), equation (18) may be rewritten as

$$u_3(x, \frac{-h}{2}) = \sum_{n=1}^{\infty} \bar{U}_{3,i} \cos(px_{i+1}) \sin(px) \tag{26}$$

where $\bar{U}_{3,i}$ is an expression similar to that given in equation (19) with the term $\cos(px_{i+1})$ factored out of the definition of t_n, i. e., similar to the expression for the a_i's in equations (16). Hence, alternatively, equation (26) becomes

$$u_{3,i}(x, \frac{-h}{2}) = \sum_{n=1}^{\infty} \frac{\bar{U}_{3,i}}{2} \{ \sin[\frac{p}{2}(x + x_{i+1})] - \sin[\frac{p}{2}(x - x_{i+1})]\} \tag{27}$$

where $\bar{U}_{3,i}$ are terms free of any trigonometric functions and are of asymptotically decaying nature similar to the transformed responses mentioned by Chen and Gurdal (1990). Therefore, from equation (27), it is possible to determine the term at which the individual summations should be truncated to produce a local maximum or minimum value. Meanwhile, since x and x_{i+1} both have non-negative values, in general, the first summation gives the dominant term which has a higher magnitude and higher frequency of oscillation whereas the second summation gives a relatively lower magnitude and lower oscillating frequency, i. e., it will converge slower than the first summation. The relative magnitudes of the individual summations can be calculated and compared by including all terms up to the critical terms where their local extrema

occur. In this way, it is possible to determine the number of terms which will be needed for the displacement calculation at any location due to the sub-load q_i, for any specified accuracy of convergence. Although Sankar and Sun (1983) mentioned that at least 1000 terms should be taken into account, a precise answer depends on the relative position between the point of interest and the loading ends as previously mentioned. In fact, it was found that more than 2000 terms may be required for locations close to the boundary of a sub-load. However, for a typical sub-load, fewer than 200 terms may be required for most of the remaining points.

Based on the previous effective technique, it is observed that up to 80 % of the required CPU time can be saved although the calculation without this consideration generally takes less than one minute. However, as will be discussed later, by extending the current idea of detecting terms to a three dimensional problem, it is possible to obtain a more significant saving of effort of numerical calculation.

2.4.3 Examples and Results

The intention here is to test the current simplified approach against published results. Thus, the numerical examples presented by Keer and Miller (1983) and Sankar and Sun (1983) are adopted. Consistent with these publications, the same material properties and geometry are considered, i. e.,

Length of the Beam (L) :	2.0 in.
Thickness of the Beam (h) :	0.1 in.
Lame' Constants (λ, μ) :	Both $1.0 * 10^6$ (Psi)
Radius of the Spherical Indentor (R) :	1 in.

For the purpose of comparison, results are presented for two cases, a small indentation condition with $c = 0.5h$ and a large indentation with $c = 4.0h$. In the first example, the small indentation case is considered. In order to verify the previous argument of taking the magnitudes of various sub-loads to calculate the contact stress at an average location, both the uniform and non-uniform discretization schemes are implemented. For the uniform discretization scheme, the sub-loads were constructed on the points $x_{j+1} = \frac{L}{2} + \frac{j}{K} \times c$, which were also the points chosen in calculating the displacements $(u_3)_{j,l}$ in equations (22) in order to solve for the unknown magnitude P_i's. The contact stress distribution in this case was found to be convergent by taking $K \geq 10$ and after taking 1500 terms in calculating the series expansion (18). For $K = 10$, the magnitudes of the various sub-loads, the normalized magnitudes of sub-loads with respect to two times of the average applied stress, and the amount of the total contact force are listed in Table 1. It should be noted that the magnitude of the outermost sub-load is not zero. For the second implementation, the non-uniform division method as shown in equation (25) is employed in order to achieve a finer cut close to the contact boundary. Using the same number for K and taking up to 4000 terms in the series expansion (18), results for the same quantities are shown in Table 2. In this case, it was found that although the magnitude of the outermost sub-load was reduced substantially, it still had not become exactly zero. However, the total contact force calculated by both methods of discretization were found to be different in less than 1 %. In addition, it is observed that by following the averaging methods proposed in equation (24), the contact stress distributions obtained by both techniques were found to be indistinguishable and are both in full agreement with the results of Keer and Miller (1983) and Sankar and Sun (1983). The results are shown in Figure 3, where the contact stress was normalized with respect to the average applied stress multiplied by two and was plotted against the normal-

ized coordinate along the semi-contact length c, i. e., $\bar{x} = (x - L/2)/c$. As expected, the stress profile in this case preserved the Hertzian type behavior. Therefore, It can be stated conclusively that, the previously mentioned technique of averaging is required when seeking an approximate solution for the problems of this type. Furthermore, the previously mentioned free stress condition along the contact boundary may serve as a guideline as well in treating three dimensional problems.

Next, the case of large indentation with $c = 4.0h$ is considered. Employing the same type of non-uniform discretization and normalization schemes, an agreement with Sankar and Sun's (1983) result is also obtained as shown in Figure 4. In this case, a larger number of divisions on the contact length and terms in the Fourier series are taken to increase the likelihood of convergence. A very severe deviation from the Hertzian type distribution for the contact stress is obtained. Peaking occurs close to the contact boundary and the contact stress in the central portion is zero which, as has been mentioned by Sankar and Sun (1983), indicates a wrapping phenomenon of the beam along the curvature of the cylinder.

2.4.4 Numerical Sensitivities

It should be noted here that the contact stress presented so far are all obtained by calculating the displacements at the same points which define all of the sub-loads in order to enter into the second step of the indentation problem. In fact, for a set of sub-loads, i. e., an approximate solution for the contact stress, the selection of the points at which the displacements will be calculated in the application of equation (22) is supposed to be arbitrary. Several trials were thus made in solving for the contact

stresses by finding the displacements at the points of coordinates $x = \frac{1}{2}(x_i + x_{i+1})$ where x_{i+1}'s are the points defining the sub-loads q_i's ($i = 1, 2, ..., K$) and $x_1 = \frac{L}{2}$. In the case where $c = 0.5h$, for example, the problem was solved by taking the same number for K, i. e., $K = 10$, and the same number of terms in the Fourier series (18). However, the result for the contact stresses in this case was found to be entirely different from the solution presented by Sankar and Sun (1983). In order to attempt an improvement, the number of terms used in the series for calculating the displacement was increased; however, the result was not improved. Both the stress distribution and the magnitude of the total contact force were found to disagree with Sankar and Sun's (1983) solution more strikingly by such an attempt. By taking up to 10000 terms, which is in fact much more than required according to the previously mentioned technique of detecting terms, the distribution of the contact stress as shown in Figure 5 arises. A very steep peak value close to the contact boundary arises while the magnitude of the contact stress in the central portion is significantly reduced in comparison to Sankar and Sun's (1983) result. In view of these differences, it is obvious that the same kind of numerical sensitivities as experienced by Singh and Paul (1974) exist in the present problem.

A very detailed explanation of this sensitive behavior was given by Singh and Paul (1974) who indicated that the ill-posed nature of the problem itself caused these kinds of numerical difficulities. Mathematically, this means that the boundary conditions, in particular, the applied load in the current beam case were not well defined. Thus, in solving such a problem with an approximate method, accordingly, some errors will be introduced in the solution steps. In the present solution technique for the beam problem, correspondingly, significant errors were imbedded in equations (22) which interpret the contact relations (20) in an approximate sense. Although the right hand

side of equation (22) is exact, unfortunately, the coefficients on the left hand side are inexact. Singh and Paul (1974) mentioned that in solving such a set of K simultaneous equations, the solution which arises will be for a problem other than the one desired. They reasoned that the inexactness which occurs in the coefficients of such approximate equations is perhaps random in nature. Consequently, instead of a formulation using just the same number of equations as the number of unknown sub-loads, a possibility of reducing the random errors may exist by a formulation employing more than the regularly required number of equations thereby averaging off the inexact coefficients. Following this idea, Singh and Paul (1974) presented the Redundant Field Point method (RFP) which is essentially based on the spirit of the well-known least square technique which is used regularly for curve fitting. This approach will be employed in the present study. Thus, M additional points were chosen in the calculation of the displacements and equations (22) were modified to take the following form

$$[A]\{P\} = \{\underset{\sim}{X}\} \tag{28}$$

where $[A]$ is a $(K+M)\times K$ coefficient matrix with the elements A_{ki}'s defined by $A_{ki} = (u_3)_{0,i} - (u_3)_{k,i}$, and $(u_3)_{k,i}$ is the displacement u_3 at x_k due to q_i. $\{P\}$ is an $K \times 1$ column matrix composed of the magnitudes of the sub-loads P_i and $\{\underset{\sim}{X}\}$ is a $(K+M)\times 1$ right hand side vector with components $\underset{\sim}{X}_k = \dfrac{(x_k - L/2)^2}{2R.}$ $(k = 1, 2, ..., K)$. From equation (28), it is obvious that the definition of mean-square error, ε^2, will be given by

$$(K+M)\times \varepsilon^2 = (A_{ki}P_i - \underset{\sim}{X}_i)(A_{kj}P_j - \underset{\sim}{X}_j) \tag{29}$$

To minimize ε^2, it is necessary that $\frac{\partial \varepsilon^2}{\partial P_i} = 0$ $(i = 1, 2, ..., K)$. A set of K simultaneous equations similar to equations (22) will be obtained which can be cast in the matrix form

$$[\bar{A}]\{P\} = [A]^T[A]\{P\} = [A]^T\{\underset{\sim}{X}\} \tag{30}$$

where $[\bar{A}]$ is a $K \times K$ matrix defined by $\bar{A}_{ij} = A_{ki}^T A_{kj} = A_{ki}A_{kj}$ $(i, j = 1, 2, ..., K)$. Thus, instead of solving equations (22), the problem is to solve equations (30) for the unknown magnitude P_i's of the sub-loads q_i's.

To demonstrate the power of the RFP method, the previous condition of numerical sensitivity was reconsidered. M was taken to be equal to K and u_3 was calculated at coordinates $\underset{\sim}{x}_j (j = 1,2,...2k)$ where $\underset{\sim}{x}_i = \frac{1}{2}(x_i + x_{i+1})$, $\underset{\sim}{x}_{(2i)} = x_{i+1}$ and the x_{i+1}'s are the coordinates which define the domains of the various sub-loads q_i's $(i = 1, 2,...., K)$. The contact stresses given by employing the above method is identical to those shown in Figure 5, thus indicating that the problem associated with numerical sensitivity has been cured. Feasibly, the RFP method should prove useful in solving three dimensional problems as will be discussed later.

CHAPTER III

INDENTATION OF AN ISOTROPIC SQUARE PLATE

3.1 Introduction

In this chapter, contact problem of an isotropic square plate indented by a rigid spherical indentor is solved. There are several reasons to conduct this investigation. First, although the main objective of this dissertation is to solve a three dimensional contact problem for an orthotropic laminate, isotropy is a special case of orthotropy. Thus, solving the isotropic problem can provide knowledge of both theoretical and numerical concerns. Theoretically, a three dimensional contact problem must deal with a surface for the contact area, rather than a length as has been treated in a two dimensional beam problem. Feasibly, the characteristics of the contact surface may be gleaned from the isotropic case. Furthermore, since the problems considered in this dissertation involve a finite boundary, knowledge of the effect of the boundary support conditions upon both the contact surface and the structural behavior is extremely desirable before introducing any material anisotropy. Moreover, such knowledge may also be of importance for an experimental study. For example, during an indentation test of composites, the specimen is usually supported by some type of mechanical fixtures. Therefore, information is often needed about the circumstances under which the experimental results will not be affected by the specific support conditions. Numerically, a three dimensional problem usually requires implementations along both of the in-plane directions. To develop step-by-step numerical implementation procedures, especially the procedures which are able to assure numerical convergence for an anisotropic case, it is necessary to have a thorough understanding of the approach when the material anisotropy vanishes.

The present study will begin with a description of the physical problem. The main emphasis will be placed on developing an approach to achieve a solution. Basically,

the approach follows the method used for the previous beam problem. In other words, the displacement field in a prescribed contact area will be determined first to establish the contact relations, in order to obtain an approximate solution for the contact stresses. However, presentation of the detailed approach will be preceded by a discussion concerning the distinction between a three dimensional problem and the two dimensional case and the required caution in extending a two dimensional approach to solve the present problem. In solving for the displacement field, the simplicity due to material isotropy is illustrated and used to obtain an expression for the transverse displacement which is much simpler than the approach presented by Pagano (1970). Numerical results are presented for cases ranging from a small indentation to a large contact area. For the latter cases, the so-called hypotrocoidal shape for the contact area is introduced. The limits of validity of both the circular contact area and the Hertzian type distribution for the contact stresses are investigated.

3.2 Statement of the Problem

A single-layered isotropic square plate is considered, as shown in Figure 6. It is simply supported on all edges so that only normal displacement but no tangential displacement is allowed along each edge. The plate is indented by a rigid sphere at the center of the top surface. Friction between the plate and the indentor is neglected. Both the domain of the contact region, $Q(x, y)$, and the contact stresses, $f(x, y)$, under the indentor are to be determined. The expressions for the stress components in this case are (Love, 1954),

$$\begin{bmatrix} \sigma_{11} \\ \sigma_{22} \\ \sigma_{33} \end{bmatrix} = \begin{bmatrix} \lambda + 2\mu & \lambda & \lambda \\ \lambda & \lambda + 2\mu & \lambda \\ \lambda & \lambda & \lambda + 2\mu \end{bmatrix} \begin{bmatrix} u_{1,1} \\ u_{2,2} \\ u_{3,3} \end{bmatrix} \tag{31.1}$$

$$\begin{bmatrix} \sigma_{23} \\ \sigma_{31} \\ \sigma_{12} \end{bmatrix} = \mu \begin{bmatrix} u_{3,2} + u_{2,3} \\ u_{3,1} + u_{1,3} \\ u_{2,1} + u_{1,2} \end{bmatrix} \tag{31.2}$$

where $u_j\,(j = 1, 2, 3)$ are the displacement components along the three coordinate axes and $u_{1,1} = \dfrac{\partial u_1}{\partial x}$,.....etc. Also, λ and μ are the same Lame constants as those used in the previous beam problem. Therefore, the governing field equations in terms of the displacement components are

$$C_a u_{1,11} + \mu u_{1,22} + \mu u_{1,33} + C_b u_{2,12} + C_b u_{3,13} = 0 \tag{32.1}$$

$$C_b u_{1,12} + \mu u_{2,11} + C_a u_{2,22} + \mu u_{2,33} + C_b u_{3,23} = 0 \tag{32.2}$$

$$C_b u_{1,13} + C_b u_{2,23} + \mu u_{3,11} + \mu u_{3,22} + C_a u_{3,33} = 0 \tag{32.3}$$

where $u_{1,11} = \frac{\partial^2}{\partial x^2} u_1(x,\ y,\ z)$, $u_{2,22} = \frac{\partial^2}{\partial y^2} u_2(x,\ y,\ z)$...etc. In addition, $C_a = \lambda + 2\mu$ and $C_b = \lambda + \mu$. The origin of the z coordinate is at the mid-plane of the plate. Therefore, the boundary conditions along the through-the-thickness direction are,

$$\sigma_{33}(x, y, -\frac{h}{2}) = -f(x,\ y), \quad \textit{for } (x,\ y) \textit{ in } Q(x,\ y) \tag{33.1}$$

$$\sigma_{33}(x, y, -\frac{h}{2}) = 0, \qquad \textit{elsewhere} \tag{33.2}$$

$$\sigma_{31}(x, y, -\frac{h}{2}) = \sigma_{32}(x, y, -\frac{h}{2}) = 0 \tag{33.3}$$

$$\sigma_{33}(x, y, \frac{h}{2}) = \sigma_{32}(x, y, \frac{h}{2}) = \sigma_{31}(x, y, \frac{h}{2}) = 0 \tag{33.4}$$

where $\sigma_{ij}\ (i,\ j = 1, 2, 3)$ are the stress components and h is the thickness of the plate. Next, in correspondence to equation (4.5), a certain contact relation must be satisfied by the points in contact between the plate and the indentor, i. e.,

$$u_3(L/2, L/2, -h/2) - u_3(x, y, -h/2) = \frac{(x - L/2)^2 + (y - L/2)^2}{2R}, \quad (x, y) \textit{ in } Q(x, y) \tag{33.5}$$

where L is the edge length of the square plate. Meanwhile, the simply supported edge conditions require

$$\sigma_{11} = u_2 = u_3 = 0, \quad \textit{for } x = 0,\ L \tag{33.6}$$

$$\sigma_{22} = u_1 = u_3 = 0, \quad \textit{for } y = 0,\ L \tag{33.7}$$

3.3 Overview of a Three Dimensional Contact Problem

In this dissertation, an attempt is made to solve the three dimensional contact problem by applying and extending the previous approach for the beam problem. Attention has to be paid to the distinction between a three dimensional problem and a two dimensional study in order to understand the additional considerations required in making the extension. The major consideration basically concerns the fulfillment of a correct contact area. Prior to the presentation of the solution method for the present isotropic case, the possible shape of the contact area will be discussed to introduce the hypotrocoidal shape of contact area.

3.3.1 Criterion for a Correct Contact Area

In solving an impact problem, one of the major concerns is the history of the varying contact surface. Correspondingly, for a three dimensional indentation problem, the main issue is the domain of the contact area for any magnitude of indentation. Excluding any material anisotropy, knowledge of the effects of the edge support conditions upon the shape of the contact area may still be formidable. At the initial stage of indentation, the contact area may be small enough so that the effect of the boundary conditions is negligible. In such a case, the contact area is feasibly a circle and the distribution of the contact stresses is likely to follow Hertz's law. However, three questions may be posed for such a solution. The first two are associated with the validity of Hertz's law and the circular shape of contact area. The third one has to do with the shape of the contact area and the contact stress profile when the effects

of boundary conditions prevail. An additional question may be raised as to whether the validity of Hertz's law or the circular contact shape will break down first.

Answers to the afore-mentioned questions will provide clues for the solution of the orthotropic contact problem. In comparison to the present problem, the previous beam problem with cylindrical indentation is much easier since the contact area is simply a length. Thus, the significant difference between these two problems is obvious. For the previous cylindrical indentation problem, the contact length is always a permissible one regardless of the magnitude of the length. Alternatively, this means any length of contact is practically possible from which the total indentation load may be determined. In contrast, for a general three dimensional problem, the ratio between the contact lengths along different in-plane directions is fixed for a certain length along an in-plane direction as has been mentioned in the first chapter. Therefore, an arbitrarily prescribed contact area may not be physically possible, especially when the effects of the finite boundary conditions are significant. For an arbitrary contact area, the contact length in one direction may be either longer or shorter than the correct one with respect to the contact length in another direction. Subsequently, the following implications will be demonstrated, which is in the spirit of the approaches for the studies made by Singh and Paul (1974) and Paul and Hashemi (1978, 1980). For a length which is longer than the correct one, a tendency of separation between the indentor and the plate may exist along that direction. Thus the contact stress near the contact boundary is likely to be tensile. On the other hand, if the prescribed contact length is shorter than the exact one, the contact stress in the neighborhood of the contact boundary may exhibit a higher compressive value than the correct magnitude. Thus, the length of contact along that direction has to be increased to redistribute the undue high parts of the contact stress profile. In

summary, the contact stress around the contact boundary along some of the in-plane directions may be tensile if the contact area is imposed arbitrarily in solving the problem. Alternatively, a correct contact area is one which is subjected only to all compressive contact tractions in the vicinity of the contact boundary, as will be illustrated later in this chapter.

3.3.2 Hypotrocoids of Four Lobes

Following the afore-mentioned arguments, a question still exists as to the shape of the contact area when the effects of the boundary conditions influence the local contact behavior. For the present isotropic case with symmetric loading and boundary conditions, there is no distinction between the x and the y axes. Therefore, the contact lengths in the x and the y directions will be the same regardless of the magnitude of the contact length and the amount of indentation. However, the behavior along a 45° direction which passes through the corners of the plate will be different. The length along this direction is greater than those along the coordinate axes and thus it is comparatively easier to bend and induce a transverse deflection along the diagonals of the plate. However, the relative fraction of the total load carried along different directions is unknown. Therefore, without any further investigation, it is not possible to predict whether the contact length along the 45° direction will be longer or shorter than that along the x or the y axis. In any case, a curve which evenly intersects the x and the y axes and gives either a greater or a shorter length along the 45° direction is appropriate for representing the contact boundary. Geometrically, a curve possessing such properties is a hypotrocoid, which is often used in designing gears and rotors for a transmission system. Specifically, the desired curve is a

hypotrocoid of four lobes which satisfies the symmetry pattern for an isotropic square plate. Referring to Holmes (1978), a typical hypotrocoid of four lobes is shown in Figure 7. It can be defined by the following coordinates, termed the freedom equations,

$$x = 3r_S \sin(\theta) - t \sin(3\theta) \ , \quad y = 3r_S \cos(\theta) + t \cos(3\theta) \tag{34}$$

where r_s and t are the parameters which control the appearance of the hypotrocoidal curves. Both r_s and t are positive with $0 < t \leq r_s$, and θ is the angle measured clockwise from the positive y direction. The intersection of this curve with the coordinate axes occurs at a distance $k_x = 3r_s + t$, away from the origin. Therefore, to generate a set of such curves with a fixed intersection on the coordinate axes, it is only necessary to impose different values for t and take $r_s = (k_x - t)/3$. For the purpose of demonstration, such a set of constant-intersection hypotrocoids which give shorter lengths along the 45° direction than the distance from the intersection with a coordinate axis to the origin is displayed in Figure 8, and is referred as group A. The parameter t is taken to range from 0.02 to 0.12 and the coordinate of the intersection along the coordinate axes k_x is taken to be 1.0. To produce a set of similar curves which give longer lengths along the 45° direction, referred as group B, a coordinate transformation is made in equations (34). The freedom equations in this case can be shown to be

$$x = 3r_S \sin(\theta) + t \sin(3\theta) \ , \quad y = 3r_S \cos(\theta) - t \cos(3\theta) \tag{35}$$

A set of curves of group B with the same parameters r_s, t, and intersection k_x, is illustrated in Figure 9. However, as will be verified later, only the curves of group A are useful in pursuing the correct contact area for the relative large indentation condition in which the effect of boundary conditions are important.

3.4 Analytical Procedures

To develop the method for solving the present problem, the same precedures as used in the previous approach for the beam problem are followed. Since, in concept, both the contact area $Q(x, y)$ and the distribution of contact stresses $f(x, y)$ are unknown, the problem is more ill-posed than the previous beam problem. The only known information is that the contact area will be deformed so that its transverse displacements u_3 remain in contact with the surface of the indentor thus giving rise to identical curvatures. In consideration of these factors, the problem will be solved in several steps. First of all, a candidate contact area will be proposed. Although the contact area for the present problem is possibly either a circle or a hypotrocoid as mentioned earlier, it should be noted that any proposed contact area is subject to numerical verification. A discretization over the contact area will be made in order to define various uniform sub-loads over each sub-area in the contact region in order to construct an approximate representation of the unknown contact stresses. Next, similar to the approach used in treating the previous beam problem, the magnitudes of the sub-loads will be solved in two steps. In the first step, the transverse displacement at the each point in the contact area due to each sub-load of unit magnitude is found. In this step, however, instead of superposing a bending theory and an elasticity solution as was used in the approach by Sankar and Sun (1983), a closed form solution for the transverse displacements is obtained based on the exact solution method developed by Pagano (1970). However, although Pagano's approach can be immediately applied, the formulation employing exponential functions as used by Pagano (1970) requires dealing with large numbers for the coefficients in the final algebraic equations. His procedures is inefficient and inconvenient for numerical implementation, especially if a multi-layed plate is considered. Therefore, in solving

for the displacement field in the present problem, Pagano's approach (1970) will be modified by using hyperbolic functions. Furthermore, because of the necessity of considering a polygonal region to approximate the proposed contact area, an extensive effort will be undertaken in deriving the expressions for the Fourier coefficients for the series expansion of a typical sub-load. A complete algebraic formulation is then conducted which will result in closed form expressions for the transverse displacement field and the other field quantities.

Although the current study of the isotropic problem deals with only a single layer, it is expected that the approach developed here will prove to be very useful in the study of multi-layered isotropic plates. Based on the transverse displacements obtained for the points in the proposed contact area, a set of simultaneous contact relations are established in a three dimensional manner by following the same procedures for indentation as used in solving the beam problem. A candidate approximate solution for the unknown contact stresses can be obtained by solving the formulated simultaneous equations for the magnitudes of various sub-loads. The candidate solution is then checked to see if compressive stresses are obtained at all points inside and around the contact boundary. In case of any violation of the afore-mentioned criterion of contact, the solution procedures are repeated by proposing a modified candidate for the contact area based on the previous one. This procedure is performed until the contact criterion is satisfied everywhere.

3.4.1 Composition / Discretization of Candidate Contact Area

In extending Sankar and Sun's method (1983) for a beam, to the problem of a plate, It is noted that differences arise in the representations of the contact area and contact stress profile. For a beam, the contact area, i. e., the contact length, is always the exact one regardless of the manner of discretizing the contact area to establish the sub-loads and to obtain the real contact stress distribution. For a plate however, a typical proposed contact area, whether it is circular or non-circular, can only be approximated by a polygonal region composed of various sub-areas as shown in Figure 10. Each sub-area is subjected to an individual uniform sub-load. The exact prescribed contact area is thus approached asymptotically when the divisions are made increasingly small along both of the in-plane directions in the contact area. Furthermore, because of logical reasoning that the contact stress distribution will be more uniform in the central portion than around the boundary of the contact area, the non-uniform discretization scheme used in solving the beam problem will be employed along both of the in-plane directions for the present problem. Thus, taking into account the symmetry of the problem, only one quarter area of the contact region will be considered and a loading factor of 4 will be used for each sub-loading area.

Following the above arguments, it is possible to label all the sub-loads as well as the sub-areas as follows. For example, for a typical sub-load f_{kl}, where $k = 1, 2,..., K$; $l = 1, 2,....,, K - k + 1$ for the case of K divisions on each of the semi-contact lengths a and b along x and y axes respectively, the corresponding sub-area will be

$$A_{k\,l} = 4(x_{k+1} - x_1)(y_{l+1} - y_1), \quad k + l \neq K + 1 \tag{36.1}$$

$$A_{1\,K} = A_{1(K-1)} + 2(x_2 - x_1)(y_{K+1} - y_K), \quad A_{K\,1} = A_{(K-1)1} + 2(y_2 - y_1)(x_{K+1} - x_K) \tag{36.2}$$

$$A_{k(K+1-k)} = A_{k(K-k)} + 2(x_k + x_{k+1} - 2x_1)(y_{K+2-k} - y_{K+1-k}), \quad k = 2, 3, ..., K - 1. \tag{36.3}$$

Apparently, the sub-area is a rectangle if $k + l \neq K + 1$. If $k + l = K + 1$, the sub-area is the summation of a rectangle and a small triangle or a tapered area. The total number of sub-loads (or sub-areas) is $K \times (K + 1)/2$ and the approximated polygonal region will underestimate the exact candidate contact area. However, by allowing the number of divisions to increase, which implies involving more points in obtaining the approximate contact stresses, the approximated area will approach the exact one.

3.4.2 Response due to a Typical Sub-load

Consider a typical sub-load f_{kl}, which is symmetric with respect to the center of the plate over the corresponding sub-area A_{kl}. For this sub-load, the governing equations are the field equations (32) and the boundary conditions (33). Employing Pagano's approach (1970), the load f_{kl} will be expanded in a double Fourier series, i. e.,

$$f_{kl} = \sum_{n=1}^{\infty} \sum_{m=1}^{\infty} T_{nm} \sin(p\,x) \sin(q\,y) \tag{37}$$

where the T_{nm}'s are the Fourier coefficients and $p = \frac{n\pi}{L}$, $q = \frac{m\pi}{L}$. The expressions for the T_{nm}'s for the various sub-loads are derived and listed in Appendix-A. Obviously, the response due to f_{kl} is the sum of all the contributions given by all of the T_{nm}'s. Therefore, it is necessary to formulate the method to be used in solving for the response due to each T_{nm}.

3.4.2.1 Expressions for the Displacement Functions

At the outset, the expressions for the displacement components are assumed to be in the following form in order to satisfy the boundary support conditions posted in equations (33.6) and (33.7), i. e.,

$$u_1 = U_1(z)\cos(p\,x)\sin(q\,y) \tag{38.1}$$

$$u_2 = U_2(z)\sin(p\,x)\cos(q\,y) \tag{38.2}$$

$$u_3 = U_3(z)\sin(p\,x)\sin(q\,y) \tag{38.3}$$

where the functions U_j ($j = 1, 2, 3$) are functions of z only. Substituting equations (38) into equations (32), this give rise to the equations for the U_j's. ($j = 1, 2, 3$)

$$[\mu D^2 - (C_a p^2 + \mu q^2)]U_1 - C_b pqU_2 + C_b pDU_3 = 0 \tag{39.1}$$

$$-C_b pqU_1 + [\mu D^2 - (\mu p^2 + C_a q^2)]U_2 + C_b qDU_3 = 0 \tag{39.2}$$

$$-C_b pDU_1 - C_b qDU_2 + [C_a D^2 - \mu(p^2 + q^2)]U_3 = 0 \tag{39.3}$$

where $D = \dfrac{d}{dz}$. Following the previous approach used for the beam problem, the U_j are expressed as $K_j e^{\rho z}$ where the K_j's ($j = 1, 2, 3$) are constants. The characteristic equation derived from equations (39) is

$$\begin{vmatrix} \mu\rho^2 - C_a p^2 - \mu q^2 & -C_b pq & C_b p\rho \\ -C_b pq & \mu\rho^2 - \mu p^2 - C_a q^2 & C_b q\rho \\ -C_b p\rho & -C_b p\rho & C_a\rho^2 - \mu(p^2 + q^2) \end{vmatrix} = 0 \tag{40}$$

Solutions for the characteristic equation (40) are in the form of triply repeated pairs of roots $\rho = \pm r$, where $r = \sqrt{p^2 + q^2}$. The displacement functions can therefore be expressed in terms of the exponential functions as presented by Pagano (1970).

However, instead of using the exponential functions, the hyperbolic functions are employed here for convenience. Thus, the displacement functions may be expressed as

$$U_i = (a_{1i} + a_{3i}z + a_{5i}z^2)C_h + (a_{2i} + a_{4i}z + a_{6i}z^2)S_h \tag{41}$$

where $i = 1, 2, 3$, and a_{ji} ($j = 1, 2, ..., 6$) are unknown constants to be determined. In addition, $C_h = \cosh(rz)$, and $S_h = \sinh(rz)$. In equation (41), there are 18 constants of which only 6 are independent. To deduce the various relations between the unknown constants, equations (41) are substituted into equations (39). This results in 18 equations for the a_{ji}'s. Solving these equations, the following relations are obtained.

$$a_{5j} = a_{6j} = 0 \quad (j = 1, 2, 3) \tag{42.1}$$

$$a_{(2+i)2} = \frac{q}{p} a_{(2+i)1} \quad (i = 1, 2); \qquad \begin{bmatrix} a_{43} \\ a_{33} \end{bmatrix} = \frac{r}{p} \begin{bmatrix} a_{31} \\ a_{41} \end{bmatrix} \tag{42.2}$$

$$\begin{bmatrix} a_{13} \\ a_{23} \end{bmatrix} = \frac{1}{r} \left[p \begin{bmatrix} a_{21} \\ a_{11} \end{bmatrix} + q \begin{bmatrix} a_{22} \\ a_{12} \end{bmatrix} \right] - \frac{C_\alpha}{p} \begin{bmatrix} a_{31} \\ a_{41} \end{bmatrix} \tag{42.3}$$

where $C_\alpha = \dfrac{\lambda + 3\mu}{\lambda + \mu}$. Thus, the independent constants are taken to be a_{11}, a_{21}, a_{12}, a_{22}, a_{31}, a_{41}. In this way, the expressions for the U_i's can be rewritten as

$$U_1 = (a_{11} + za_{31})C_h + (a_{21} + za_{41})S_h \tag{43.1}$$

$$U_2 = (a_{12} + z\frac{q}{p} a_{31})C_h + (a_{22} + z\frac{q}{p} a_{41})S_h \tag{43.2}$$

$$U_3 = \left[\frac{pa_{21} + qa_{22}}{r} - \frac{C_\alpha a_{31} - zra_{41}}{p} \right] C_h + \left[\frac{pa_{11} + qa_{12}}{r} - \frac{C_\alpha a_{41} - zra_{31}}{p} \right] S_h \tag{43.3}$$

It should be noted that, similar to equations (42), the relationships between the unknown constants have been proposed by Pagano (1970) with the use of exponential functions. In particular, equations (42.1) are found to be identically obtained. However, the remaining relations are different from the results derived by Pagano (1970).

3.4.2.2 Expressions for the Out-of-Plane Stress Components

To solve for the unknown constants appearing in equations (43), it is necessary to derive the expressions for the stress components and then apply the boundary conditions (33). Of primary interest are the out-of-plane stress components σ_{3j} ($j = 1, 2, 3$) since the boundary conditions are in terms of out-of-plane stresses only. Taking the appropriate derivatives of the displacement functions (43), and recalling the stress-displacement relations (31), the out-of-plane stresses can be deduced to take the form

$$\sigma_{33} = \{2\mu[p(a_{11}C_h + a_{21}S_h) + q(a_{12}C_h + a_{22}S_h)] + Z_1 a_{31} + Z_2 a_{41}\} \sin(px) \sin(qy) \quad (44.1)$$

$$\sigma_{32} = \mu\{\frac{pq}{r}(a_{11}S_h + a_{21}C_h) + B_b(a_{12}S_h + a_{22}C_h) + Z_3 a_{31} + Z_4 a_{41}\} \sin(px) \cos(qy) \quad (44.2)$$

$$\sigma_{31} = \mu\{\frac{pq}{r}(a_{12}S_h + a_{22}C_h) + B_d(a_{11}S_h + a_{21}C_h) + Z_5 a_{31} + Z_6 a_{41}\} \cos(px) \cos(qy) \quad (44.3)$$

where,

$$Z_1 = g_a z C_h + B_a S_h, \quad Z_2 = g_a z S_h + B_a C_h, \quad Z_3 = g_b z S_h + B_c C_h \quad (45.1)$$

$$Z_4 = g_b z C_h + B_c S_h, \quad Z_5 = 2rz S_h + B_e C_h, \quad Z_6 = 2rz C_h + B_e S_h \quad (45.2)$$

$$g_a = \frac{2\mu r^2}{p}\ ,\quad g_b = \frac{2rq}{p}\ ,\quad B_a = (\lambda + 2\mu)\frac{r}{p}B_e\ ,\quad B_b = \frac{q^2}{r} + r \tag{45.3}$$

$$B_c = \frac{q}{p}B_e\ ,\quad B_d = \frac{p^2}{r} + r\ ,\quad B_e = 1 - C_\alpha \tag{45.4}$$

3.4.2.3 Imposing the Boundary Conditions

The boundary conditions in the through-the-thickness direction, i. e., equations (33.1) to (33.4) will be satisfied next. For a typical term T_{nm} in equation (37), the following equations can be deduced.

$\sigma_{33}(x, y, \frac{h}{2}) = 0 \quad \rightarrow$

$$2\mu[p(a_{11}C_+ + a_{21}S_+) + q(a_{12}C_+ + a_{22}S_+)] + Z_{1\,+}a_{31} + Z_{2\,+}a_{41} = 0 \tag{46.1}$$

$\sigma_{33}(x, y, -\frac{h}{2}) = -T_{nm}\ \sin(px)\sin(qy) \quad \rightarrow$

$$2\mu[p(a_{11}C_+ - a_{21}S_+) + q(a_{12}C_+ - a_{22}S_+)] + Z_{1\,-}a_{31} + Z_{2\,-}a_{41} = -T_{nm} \tag{46.2}$$

$\sigma_{32}(x, y, \frac{h}{2}) = 0 \quad \rightarrow$

$$\frac{pq}{r}(a_{11}S_+ + a_{21}C_+) + B_b(a_{12}S_+ + a_{22}C_+) + Z_{3\,+}a_{31} + Z_{4\,+}a_{41} = 0 \tag{46.3}$$

$\sigma_{32}(x, y, -\frac{h}{2}) = 0 \quad \rightarrow$

$$\frac{pq}{r}(-a_{11}S_+ + a_{21}C_+) + B_b(-a_{12}S_+ + a_{22}C_+) + Z_{3\,-}a_{31} + Z_{4\,-}a_{41} = 0 \tag{46.4}$$

$\sigma_{31}(x, y, \frac{h}{2}) = 0 \quad \rightarrow$

$$B_d(a_{11}S_+ + a_{21}C_+) + \frac{pq}{r}(a_{12}S_+ + a_{22}C_+) + Z_{5\,+}a_{31} + Z_{6\,+}a_{41} = 0 \tag{46.5}$$

$\sigma_{31}(x, y, -\frac{h}{2}) = 0 \quad \rightarrow$

$$B_d(-a_{11}S_+ + a_{21}C_+) + \frac{pq}{r}(-a_{12}S_+ + a_{22}C_+) + Z_{5\_}a_{31} + Z_{6\_}a_{41} = 0 \tag{46.6}$$

where the Z_{j+}'s and the Z_{j-}'s ($j = 1, 2, ..., 6$) are the values for the functions Z_j's evaluated at $z = \frac{h}{2}$ and $z = -\frac{h}{2}$ respectively. It can be shown that $Z_{j-} = -Z_{j+}$ if $j = 1, 4, 6$, and $Z_{j-} = Z_{j+}$ if $j = 2, 3, 5$. In addition, $C_+ = \cosh(rh/2)$ and $S_+ = \sinh(rh/2)$. Rearranging equations (46) gives

(46.1) + (46.2)→

$$2\mu(pa_{11} + qa_{12}) + (\frac{g_a}{2}hH_T + B_a)a_{41} = \frac{-T_{nm}}{2C_+} \tag{47.1}$$

(46.1) − (46.2)→

$$2\mu(pa_{21} + qa_{22}) + (\frac{g_a}{2}hH_C + B_a)a_{41} = \frac{T_{nm}}{2S_+} \tag{47.2}$$

(46.3) + (46.4)→

$$\frac{pq}{r}a_{21} + B_b a_{22} + (B_c + \frac{rq}{p}hH_T)a_{31} = 0 \tag{47.3}$$

(46.3) − (46.4)→

$$\frac{pq}{r}a_{11} + B_b a_{12} + (B_c + \frac{rq}{p}hH_C)a_{41} = 0 \tag{47.4}$$

(46.5) + (46.6)→

$$B_d a_{21} + \frac{pq}{r}a_{22} + (B_e + rhH_T)a_{31} = 0 \tag{47.5}$$

(46.5) − (46.6)→

$$B_d a_{11} + \frac{pq}{r}a_{12} + (B_e + rhH_C)a_{41} = 0 \tag{47.6}$$

where $H_T = \frac{S_+}{C_+}$, $H_C = \frac{C_+}{S_+}$. The above equations can be readily solved for the unknown constants appearing in them. These solutions are

$$a_{12} = \frac{q}{p}a_{11}, \quad a_{41} = \frac{-2r}{K_C}a_{11}, \quad a_{22} = \frac{q}{p}a_{21}, \quad a_{31} = \frac{-2r}{K_T}a_{21} \tag{48.1}$$

and,

$$a_{11} = \frac{-T_{nm}}{4k_a C_+}, \quad a_{21} = \frac{T_{nm}}{4k_b S_+} \tag{48.2}$$

where,

$$K_T = B_e + rhH_T, \quad K_C = B_e rhH_C \tag{48.3}$$

$$k_a = \frac{r^2}{p}\{\mu - \frac{1}{K_C}[\mu rhH_T + C_a B_e]\}, \quad k_b = \frac{r^2}{p}\{\mu + \frac{1}{K_T}[\mu rhH_C + C_a B_e]\} \tag{48.4}$$

3.4.2.4 Transverse Displacement on the Top Surface

Substituting $z = -\frac{h}{2}$ into equation (43.3), the displacement function U_3 on the top surface, referred as U_{3t}, will be

$$U_{3t} = \frac{1}{r}[p(a_{21}C_+ - a_{11}S_+) + q(a_{22}C_+ - a_{12}S_+)] + \frac{1}{p}[(\frac{rhS_+}{2} - C_\alpha C_+)a_{31} + (C_\alpha S_+ - \frac{rhC_+}{2})a_{41}]$$

Via equations (48), the above expression may be written as

$$U_{3t} = \frac{T_{nm}}{4}(1 + C_\alpha)(\frac{H_T}{k_c K_C} + \frac{H_C}{k_d K_T}) \tag{49}$$

where,

$$k_c = \frac{p}{r}k_a = r[\mu - \frac{1}{K_C}(\mu rhH_T + C_a B_e)] \tag{50.1}$$

$$k_d = \frac{p}{r}k_b = r[\mu - \frac{1}{K_T}(\mu rhH_C + C_a B_e)] \tag{50.2}$$

Thus, from equation (38.3), the transverse displacement at any point $P(x, y)$ on the top surface, due to a typical term T_{nm} in equation (37), is $U_{3t}\sin(p\,x)\ \sin(q\,y)$. By summing

up the contributions due to all of the T_{nm}'s, the transverse displacement u_3 at $P(x, y)$, due to a typical sub-load f_{kl}, will be

$$(u_3)_{,kl} = \sum_{n=1}^{\infty}\sum_{m=1}^{\infty} U_{3t}(n, m)\sin(p\,x)\sin(q\,y) \tag{51}$$

3.4.3 The Indentation Problem

Having solved for the transverse displacement for any point of interest $P(x, y)$ on the top surface of the plate due to a typical sub-load f_{kl}, the procedures of the Point Matching Method employed in treating the beam problem can be easily employed in a three dimensional manner to solve for the magnitude of various sub-loads P_{kl}. First, in view of equations (20), the simultaneous equations based on the contact relations on the top surface of the plate for the present case will be

$$(u_3)_0 - (u_3)_{ij} = \frac{(x_i - \frac{L}{2})^2 + (y_j - \frac{L}{2})^2}{2R}\ ;\quad i, j = 1, 2, \ldots, K. \tag{52}$$

where $(u_3)_0 = u_3$ at $x = y = \frac{L}{2}$, and $(u_3)_{ij} = u_3$ at (x_i, y_j). Meanwhile, upon considering the contributions due to all of the sub-loads f_{kl}'s, equation (21) can readily be modified to take the form

$$(u_3)_0 \simeq \sum_{k=1}^{K}\sum_{l=1}^{K-k+1} (u_3)_{0,\,kl}P_{kl}\,,\quad (u_3)_{ij} \simeq \sum_{k=1}^{K}\sum_{l=1}^{K-k+1} (u_3)_{ij,\,kl}P_{kl} \tag{53}$$

for the case of K divisions made on both of the semi-contact lengths a and b. In equation (53), $(u_3)_{0,kl}$ is the displacement $(u_3)_0$ due to sub-load f_{kl}, and P_{kl} is the magnitude of f_{kl}. Consequently,

$$\sum_{k=1}^{K}\sum_{l=1}^{K-k+1}[(u_3)_{0,kl}-(u_3)_{ij,kl}]P_{kl} \simeq \frac{(x_i-\frac{L}{2})^2+(y_j-\frac{L}{2})^2}{2R}, \quad i,j=1,2,....,K. \tag{54}$$

3.5 Numerical Implementation

3.5.1 Technical Remarks

The numerical procedures employed for the present isotropic plate problem are the same, in spirit, as those used for the previous beam problem. However, due to the inherent difference between a three dimensional problem and a two dimensional one, the present problem requires a more extensive caution in the numerical implementation. First of all, for a certain contact length along one of the in-plane directions (taken to be the x axis, for example), the problem is to find the correct associated contact area. For this, it may be necessary to propose several trials for the contact area to implement the development of the method of solution. As can be seen from the derivation of the solution procedures, each trail requires double summations in finding the displacement field. Therefore, the CPU cost is expected to be much higher than in the previous beam case. Technically, The non-uniform discretization scheme proposed in equation (25) will be used along both of the in-plane directions to discretize the present contact region. The method of detecting terms developed in solving the beam problem will be similarly applied here along both the x and the y directions. Meanwhile, the Redundant Field Points Method (Singh and Paul, 1974) will be employed as well to preclude the extreme numerical sensitivity which has been experienced previously. In this regard, M more points are chosen along both the x and the y directions to calculate the displacements. Due to the involvement of double summation, equation (54) is now modified to read

$$[A']\{P'\} = \{\underset{\sim}{X}'\} \tag{55}$$

where $[A']$ is a $M_K \times K_T$ coefficient matrix with $M_K = (K+M) \times (K+M+1)/2$, $K_T = K(K+1)/2$, and the elements A'_{IJ}'s are defined by $A'_{IJ} = (u_3)_{0,J} - (u_3)_{I,J}$ where $I = K + (K-1) + \ldots + (K-i+1) + j$, and $J = K + (K-1) + \ldots + (K-k+1) + l$. $\{P'\}$ is a $K_T \times 1$ column matrix containing the magnitudes of the sub-loads P'_J's, and $\{\underset{\sim}{X'}\}$ is a $M_K \times 1$ right hand side vector with components $\underset{\sim}{X'}_I = [(x_i - \frac{L}{2})^2 + (y_j - \frac{L}{2})^2]/(2R)$. As a counterpart of equation (29), the definition of the mean-square error ε^2 in the current case will be given by

$$M_K \times \varepsilon^2 = (A'_{IJ}P'_J - \underset{\sim}{X'}_J)(A'_{I\bar{J}}P'_{\bar{J}} - \underset{\sim}{X'}_{\bar{J}}) \tag{56}$$

Minimizing ε^2 requires $\frac{\partial \varepsilon^2}{\partial P'_J} = 0$ $(J = 1, 2, \ldots, K_T)$. A set of K_T simultaneous equations equivalent to equations (29) can be obtained in the following form

$$[\bar{A}']\{P'\} = [A']^T[A']\{P'\} = [A']^T\{\underset{\sim}{X'}\} \tag{57}$$

where $[\bar{A}']$ is an $K_T \times K_T$ matrix defined by $\bar{A}'_{ij} = A'_{\bar{I}k}A'_{kj} = A'_{ki}A'_{kj}$ $(i, j = 1, 2, \ldots, K_T)$. Equations (57) are to be solved to conclude the numerical procedures in finding an approximate solution for the unknown contact stress.

As to the problem of numerical convergence, it is clear that the rates of convergence along both of the in-plane directions should be the same. Because of isotropy, this implies that the number of terms required to calculate $(u_3)_{ij,kl}$ and $(u_3)_{ji,lk}$ are the same. Thus, $(u_3)_{ij}$ should be calculated in the same way as $(u_3)_{ji}$, and eventually $P_{kl} = P_{lk}$, to be consistent with physical reality. The afore-mentioned argument can serve as an additional check against the results obtained for the contact stress distribution.

3.5.2 Numerical Results and Discussion

For the purpose of demonstration and with an intention of maintaining consistency with previous study of the beam problem, the same material properties will be used for the isotropic plate and its edge will have a length equal to the length of the previous beam. The thickness of the previous beam will be adopted here as well. In the numerical examples, various lengths of contact along the coordinate axes are considered ranging from a small indentation with semi-contact length $a = c = 0.5h$ to a large contact area in which $a = c = 4.0h$.

First, the case of $c = 0.5h$ is implemented. The contact area is taken to be a circle with various numbers of divisions on the length c. The contact stress are found to be all compressive over the contact area and thus the proposed circular shape for the contact area is correct for such a small indentation condition. The convergence of the total contact force with respect to the number of divisions, K, on c is investigated at the beginning and is shown in Figure 11. It is obvious that the total contact load converges very quickly even with a small number of K which may be less than 10. For $K = 8, 9, 10$, for example, the total contact force is essentially constant. For $K = 10$, the distribution of contact stresses along the y direction for various x locations is shown in Figure 12. The contact stress was normalized with respect to an intimated average contact stress, $\sigma_{AI} = \frac{P}{c \times c}$, where P is the total contact load and the y coordinate was normalized with respect to the semi-contact length c, i. e., $\bar{y} = (y - L/2)/c$. As can be reasonably expected, the distribution in this case retains the Hertzian type behavior and is close to an ellipsoid in shape. In particular, it should be noted that the curve of contact stress along $\bar{x} = 0.0 (\bar{x} = (x - L/2)/c)$ in Figure 12, i. e., the radial direction, is the same as the result presented by Keer and Miller (1983) for a contact problem of a circular plate with the same contact length. Apparently, this indicates that the size of the contact region in this case is sufficiently small

so that the local contact behavior is not affected by the finite boundary of the plate, regardless of its shape.

For the case of $c = 1.0h$, the contact area is also taken to be a circle for the first attempt and is proven to be correct as well since the contact stresses over the circular area are found to be all compressive. With the same scheme, the normalized contact stress for $c = 1.0h$ is plotted in Figure 13 versus the normalized y coordinate along the length c. It is clear that the distribution in this case can not be represented by the Hertzian type solution. However, although the deviation of the contact stress from Hertz's law is visible, it is still not very appreciable.

The next example to be considered is the case of $c = 2.0h$. For the first attempt, the circle is still proposed to be the candidate contact area. A three dimensional surface plot is displayed in Figure 14 using the same normalization scheme to illustrate the contact stress distribution over a quarter region of the proposed circular contact area. There is a abrupt ascending, i. e., a steep jump of compressive contact stress near the end of the contact lengths along both of the x and the y directions. Whereas, numerically, it is observed that contact stresses in the neighborhood of the contact boundary around the 45° direction exhibit a small tension. Thus, the proposed circular contact area fails to represent the true contact region. Due to the presence of a slight tension along the the 45° direction and a steep compression along 0° and 90° directions, an implication can be drawn that the contact length along the 45° direction should be reduced from the original length or, alternatively, the contact lengths along the x and the y directions should be increased comparatively. This suggests the consideration of a hypotrocoidal shape of group A as shown in Figure 8 as a candidate to represent the contact area. For the second attempt, a hypotrocoidal curve

with a small parameter $C_k = \frac{t}{r_s} = 0.01$ is taken to implement the solution approach. Even such a small parameter C_k is found to produce all compressive stresses over the contact area as shown in Figure 15 in a three dimensional manner for the normalized contact stress. The distribution is further demonstrated in Figure 16 in a two dimensional fashion by plotting the similarly normalized contact stress along various radial directions with respect to the x axis versus a normalized radius, $\bar{r} = \sqrt{\bar{x}^2 + \bar{y}^2}$, where $\bar{x} = (x - L/2)/c$, $\bar{y} = (y - L/2)/c$. Due to isotropy and the symmetry of the plate, only the directions ranging from 0° to 45° passing through the corners of the plate are included. It is obvious that the contact stress distribution in this case deviates significantly from the Hertzian type solution. Peaking occurs near the boundary of the contact region. Similar to the phenomenon detected by Keer and Miller (1983), a slight wrapping of the plate around the spherical indentor prevails in the central portion of the plate where the magnitude of the contact stress is reduced considerably. As can be seen from Figure 16, the maximum value of the contact stress is located at approximately $\bar{r} = 0.8$ in this case and can be as high as 45 % of σ_{Al}. While, the minumum contact stress which occurs at the center of the contact region is just about 13 %. Thus, although the correct contact area deviates only slightly from a circle, the distribution of contact stresses is far from the Hertzian type result. The aforementioned wrapping also diminishes the directional dependence of the contact stress over the corresponding region. As can be seen for $\bar{r} \leq 0.7$, for example, the contact stresses are distributed equally along all of the in-plane directions. In the outer region of the contact area, the orientational dependence of the contact stress distribution is visible. The 0° direction passing through the mid-span of the plate contains the maximum profile of the stress. The magnitude is reduced gradually when one goes from the 0° direction to the 45° direction where the contact stress profile reaches

its minimum. However, it is evident that the distinction between the contact stresses along different in-plane directions in this case is nearly negligible.

The last example to be considered is the case of a comparatively large indentation with $c = 4.0h$. In order to obtain a thorough understanding of how the solution for this case is achieved, the first choice for the contact area is taken to be a circle. Results for the corresponding candidate solution for the contact stress is presented in Figure 17. Severe tensile stresses are observed in the vicinity of the contact boundary in a direction of oriented approximately 45° with respect to axes x and y. Along the directions of the x and the y axes, on the other hand, sharp peaks of compressive contact stress appear near the contact boundary. Because the proposed circular area fails to represente the correct contact region, the use of a hypotrocoidal curve with $C_k = 0.02$ is motivated in the second attempt at proposing the shape of contact area. The corresponding solution for the contact stress distribution is shown in Figure 18. As can be seen, a serious reduction in the amount of tension obtained by previously proposing a circle for the contact area is not visible in the current attempt. In the next trial, the previous C_k is doubled, i. e., C_k is taken to be 0.04. The contact stress distribution for this attempt is displayed in Figure 19. It is obvious that the reduction of the severe tension is still marginal. For the next attempt, the magnitude of C_k is taken to be 0.06. As shown in Figure 20, apparently, the abrupt tension still exists in this case although it is decreased in magnitude by a considerable amount. Finally, by taking $C_k = 0.075$, the tension is eliminated. Normalizing by the same scheme as used in the previous case, the contact stress versus radial distance relation for this case is presented in Figure 21. For comparison and for the purpose of revealing the influence of the boundary effects arising from different geometries of the plate, Keer and Miller's solution (1983) for the same amount of indentation is

displayed. It is obvious that the contact stress in this case is extremely non-Hertzian. Near the central region of contact where $r/c \leq 0.25$ approximately, the contact stress is essentially zero for all the directions. While close to the contact boundary along any direction, a steep peaking of the stress is observed. As mentioned by Keer and Miller (1983), this indicates full wrapping of the plate over the indentor is developed in this case which results in zero shear stresses on the plate over this region. As to the directional dependence of the contact stress, apparently, the contact stress is distributed identically along any in-plane direction for a circular isotropic plate. The result for the present case is quite different from Keer and Miller's solution (1983). The first distinction which is to be noted from Figure 21 is the size of the region of zero contact stress. For the square plate, it is evident that, from the central region to the border of the contact area, the contact stress along any direction gains in magnitude earlier than for the circular plate. This implies that, near the center of the contact area, the domain of the region free of contact stress in the square plate will be smaller than in the circular plate for the same magnitude of indentation. In addition, from center to the boundary of the contact area, the contact stress distributions along different directions reach their peak values at different locations and have different magnitudes which are all different from the result for the circular plate. For $\theta = 0^{\circ}$, for example, the peak value of the contact stress can be higher by 25 % than the circular plate result, although their locations are nearly the same. Thus, the contact stress along the directions of coordinate axes, i. e., passing through the mid-span the square plate, is distributed over a wider region than in the circular plate. Due to a shorter length of contact, the contact stress along the 15° direction is distributed over a narrower range than along the 0° direction. However, in comparison with the case of a circular plate, the peak value of the contact stress along this direction is higher by about 15 % and the corresponding location is closer to the

center of indentation. From the 15°- to the 30°-direction, both the maximum contact stress and the contact length are reduced by about the same amounts as those from the 0°- to the 15°-direction. Along both the 30°- and the 45°-directions, the contact stresses are distributed over a similarly narrower width and their peak values are found to be smaller than in the circular plate.

Finally, the relation between the total contact load and the displacement of the indentor is established and shown in Figure 22 for various magnitudes of indentation. Keer and Miller's solution (1983) is also included for the purpose of comparison and their normalization scheme is employed. Clearly, a difference between the two solutions is visible for most of the magnitudes of indentation although for relatively small indentation condition, the difference is apparently negligible. First, the load-displacement relation for the present square plate is found to be located above the curve for the circular plate. In other words, in order to have the same amount of indentation, the required load for a square plate has to be higher than that required to indent the circular plate. Accordingly, although the square plate has a larger domain since its edge length is equal to the diameter of the circular plate, and because of the geometry and the boundary support conditions, the circular plate is still easier to indent comparatively. Meanwhile, as similarly obtained for the circular plate, the relation is almost linear for $\frac{\Delta R}{(h \times h)} \leq 15$ which corresponds to $\Delta = 0.15$ inch and $RP/D = 2.47$ or a total load $P = 522.75\,(lb.)$. Beyond these values, relation increases its slope gradually and most likely the nonlinear behavior is initiated. This is in effect compatible with the results obtained by the previous investigation for the contact stress where the circular contact area becomes invalid and it is necessary to introduce a hypotrocoidal contact area.

CHAPTER IV

INDENTATION OF ORTHOTROPIC LAMINATES

4.1 Introduction

Following the foregoing studies of the cylindrical indentation of a beam and the indentation of an isotropic plate, the main focus of this dissertation, i. e., a three dimensional contact problem of orthotropic laminates, will be studied in this chapter. Guided by the techniques developed and the experiences gained from studying the isotropic beam and plate problems, the current problem is to investigate the local contact behavior in the indentation site due to the influence of the in-plane dependence due to material orthotropy, the finite boundary effect, and the multi-layer configuration. Feasibly, the major concern is to seek the correct contact area over which the unknown contact load is applied for any extent of indentation. A successful siting of the contact area will lead to a correct contact stress distribution as a consequence. To initiate the study, a description of the problem will be given first with the consideration of material orthotropy and a multi-layer structure. A brief discussion will then be presented concerning the possible shape of contact area for the current problem. Next, the analytical solution method will be developed along with a description of the numerical implementation procedures. Several examples are implemented to demonstrate the results for various sizes of indentation for both single and multi-layered laminates. The examples will be based on two different materials and two different geometries. An extensive investigation will be made of the effect of material orthotropy on the shape of contact area and the distribution of the contact stress. Different contact stress distributions along different in-plane directions will be illustrated. The distinction of the results for the present problem from the previous isotropic problems will be visualized.

4.2 Description of the Problem

Indented by the same spherical indentor that was employed in the isotropic plate problem, an N —layered specially orthotropic laminate is considered. The plate geometry and coordinate system used for the previous isotropic square plate as shown in Figure 6 will be adopted here. The same type of simple supports will be employed along the boundaries of the laminate, i. e., only normal but no transverse displacement components is allowed along each edges. The out-of-plane coordinate, z, is further illustrated in Fig. 23 to show the through-the-thickness configuration. The axes of symmetry in each layer are along either the x or y global coordinate axes. Friction between the laminated plate and the indentor is also neglected. The objective is to find the correct contact area, $Q(x, y)$, and the unknown contact stress distribution, $f(x, y)$, under the indentor. The governing field equations for any layer in terms of the displacement components $u_j(x, y, z); j = 1, 2, 3$ along the three coordinate axes (Pagano, 1970) are,

$$(C_1 u_{1,11} + C_6 u_{1,22} + C_5 u_{1,33}) + C_7 u_{2,12} + C_8 u_{3,13} = 0 \tag{58.1}$$

$$C_7 u_{1,12} + (C_6 u_{2,11} + C_2 u_{2,22} + C_4 u_{2,33}) + C_9 u_{3,23} = 0 \tag{58.2}$$

$$C_8 u_{1,13} + C_9 u_{2,23} + (C_5 u_{3,11} + C_4 u_{3,22} + C_3 u_{3,33}) = 0 \tag{58.3}$$

where $u_{1,11} = \frac{\partial^2}{\partial x^2} u_1(x, y, z)$, $u_{2,22} = \frac{\partial^2}{\partial y^2} u_2(x, y, z)$...etc, and C_k; $k = 1,2,...9$, are defined in terms of the elements of the constitutive matrix C_{ij} $(i, j = 1,2,...6)$ to be $C_i = C_{i(i)}$ $(i = 1, 2, ...6)$, and $C_7 = C_{12} + C_{66}$, $C_8 = C_{13} + C_{55}$, $C_9 = C_{23} + C_{44}$.

The boundary conditions in the through-the-thickness direction includes those on the top and the bottom surfaces as well as the continuity conditions on the stress and displacement components at the interfaces of the layers, i. e.,

$$\sigma_{33}^{1}(x, y, z_1) = -f(x, y), \quad for(x, y) \ in \ Q(x, y), \tag{59.1}$$

$$\sigma_{33}^{1}(x, y, z_1) = 0, \quad elsewhere \tag{59.2}$$

$$\sigma_{31}^{1}(x, y, z_1) = \sigma_{32}^{1}(x, y, z_1) = 0 \tag{59.3}$$

$$\sigma_{3j}^{n}(x, y, z_{n+1}) = \sigma_{3j}^{n+1}(x, y, z_{n+1}) \tag{59.4}$$

$$u_j^{n}(x, y, z_{n+1}) = u_j^{n+1}(x, y, z_{n+1}) \tag{59.5}$$

$$\sigma_{3j}^{N}(x, y, z_{N+1}) = 0 \tag{59.6}$$

where $z_1 = 0$ and $z_{N+1} = z_b$ are the z coordinates for the top and the bottom surfaces of the N —layered lamina respectively, and z_{n+1} is the z coordinate for the n^{th} interface between the n^{th} and the $(n+1)^{th}$ layers with $n = 1, 2, ..., N-1$. σ_{ij}^{n} $(i, j = 1, 2, 3)$ are the stress components and the superscripts represent the indices for the layers. In addition to the above boundary conditions, the same type contact relation as proposed in equation (32.5) are valid over a similarly defined contact area and will be employed here. Furthermore, the simply-supported edge conditions as described in equations (32.6) and (32.7) will be employed.

4.3 Prospective Shape of the Contact Area

It has to be re-emphasized that finding the correct contact area is the most important issue in solving contact problems of the type considered here. Following the determination of the shape of the contact area, the remaining task in achieving a solution will be simply a matter of applying techniques of numerical approximation. However, the previously mentioned criterion for a correct contact area is valid for any three dimensional contact problem. Therefore, the primary interest is in finding the shape of the contact area for the current problem which includes the effects of material orthotropy, finite boundary conditions and the multi-layer configuration. Since the present problem deals with specially orthotropic laminates, the laminates may have either a balanced or an unbalanced layup. For a balanced layered laminate, first of all, it is reasonable that the bending rigidities along both the x and the y directions be approximately the same. Therefore, the contact area may resemble that for the isotropic plate problem. However, it is definitely of interest to study the differences in the results between these two cases. In Particular, the limit of application of the circular contact area may be different. Furthermore, if the contact area is indeed a hypotrocoid, the hypotrocoidal parameters for the present problem may be different from those used for the previous isotropic problem for a certain contact length along an in-plane direction. Especially, the structural behavior along the 45° direction which passes through the corners of the plate and possesses lower stiffness may be more sensitive to the local indentation than the other direction comparatively. For an unbalanced layered laminate, on the other hand, the boundary effect is likely to be weak in the local contact region at the early stage of indentation. On the other hand, the effect of material orthotropy may be strong regardless of the magnitude of indentation. Hence, an ellipse seems to be a reasonable representation for the contact area

for small indentations. However, for a certain contact length on the major or minor semi-axis, i. e., *a* or *b* respectively, the length of contact along the other semi-axis is likely to be a fixed value for a correct contact area. Within the range where ellipses are applicable, the ratio between *a* and *b* has to be investigated since the ratio between them may not be a constant as *a* or *b* varies. As indentation proceeds, the influence of material orthotropy is likely to be coupled with the finite boundary effect. Recalling in the previous isotropic problem, a circle for a small indentation becomes a hypotrocoid for the case of a relatively large contact area. Therefore, an ellipse may change to become a distorted hypotrocoid in representing the contact area for large indentation conditions by multiplying the original hypotrocoid with a constant along one of the in-plane directions. However, the range of validity of the modified hypotrocoid has to be investigated as well.

4.4 Formulation of the Analytical Approach

Primarily, the approach to be used is based on the same technique used in solving the isotropic plate problem. Specifically, the previous discretization scheme will be employed over a proposed candidate contact area. Over the proposed area, various subareas will be identified as in the previous manner shown in Figure 10 to construct various uniform subloads in order to compose of an approximate representation for the unknown contact load, $f(x, y)$. Th method to be used in solving for the magnitudes of various subloads will be mostly the same as the previous approach. Thus, the displacement field over the proposed contact area due to various subloads of unit magnitude will be found first. In this step, however, Pagano's method for exact solution (1970) will not be solely employed. Instead, it will be incoorperated with Chen and Frederick's approach (1990) for treating a transverse loading problem for a multi-layer orthotropic laminate. Next, both the point matching Method (Sankar and Sun, 1983) and the Redundant Field Point Method (Singh and Paul, 1974) used in solving the previous problems will be similarly applied to solve for the magnitudes of various subloads. The candidate approximate solution for the unknown contact stress thus obtained will then be checked against the previously illustrated criteria for a correct contact area. A similar iterative execution for the solution procedure will be conducted as well until a satisfaction of the previous criteria are achieved.

4.4.1 Expressions for the Displacement Functions

Initially, Pagano's approach (1970) will be employed. The expressions for the displacement components proposed in equations (38) will be utilized for a typical n^{th}

layer in the laminate. To solve these expressions for the displacement functions, U_j's, equations (38) are substituted into the governing field equations (58). In equivalence to equations (39), this gives

$$C_5U_{1,33} - (C_1p^2 + C_6q^2)U_1 - C_7pqU_2 + C_8pU_{3,3} = 0 \tag{60.1}$$

$$-C_7pqU_1 - (C_6p^2 + C_2q^2)U_2 + C_4U_{2,33} + C_9qU_{3,3} = 0 \tag{60.2}$$

$$-C_8pU_{1,3} - C_9qU_{2,3} - (C_5p^2 + C_4q^2)U_3 + C_3U_{3,33} = 0 \tag{60.3}$$

Solutions for the U_j's are given by $U_j = K_je^{\lambda z}$ $(j = 1, 2, 3)$, where the K_j's are constants. The non-trivial solutions for U_1, U_2, U_3 will exist only when the determinant of the coefficients of the above equations vanishes, i. e.,

$$\begin{vmatrix} C_5D^2 - C_1p^2 - C_6q^2 & -C_7pq & C_8pD \\ -C_7pq & C_4D^2 - C_6p^2 - C_2q^2 & C_9qD \\ -C_8pD & -C_9qD & C_3D^2 - C_5D^2 - C_4q^2 \end{vmatrix} = 0 \tag{61}$$

where $D = \dfrac{\partial}{\partial z}$. After some rearranging, the characteristic equation for the unknown exponent λ can be written in the following form

$$\lambda^6 + e_1\lambda^4 + e_2\lambda^2 + e_3 = 0 \tag{62}$$

where e_j $(j = 1, 2, 3)$ are functions of p, q, and C_l $(l = 1, 2, ..., 9)$. By referring to Pagano (1970), the six roots, λ's, in equation (62) can be shown to be all distinct and real and will exist in three positive and negative pairs. Therefore, the expressions for the U_j's $(j = 1, 2, 3)$ can be written as

$$U_1 = a_{(2m-1)}C_{mz} + a_{(2m)}S_{mz} \tag{63.1}$$

$$U_2 = b_{(2m-1)}C_{mz} + b_{(2m)}S_{mz} \tag{63.2}$$

$$U_3 = d_{(2m-1)}C_{mz} + d_{(2m)}S_{mz} \tag{63.3}$$

where $C_{mz} = \cosh(\lambda_m z)$, $S_{mz} = \sinh(\lambda_m z)$ and λ_m ($m = 1, 2, 3$) are the positive roots of the characteristic equation (62) for any n^{th} layer in which $z_n \leq z \leq z_{n+1}$. The implication of the summation on m is also intended as well. The a's, b's, and d's are the unknown coefficients to be solved for the n^{th} layer. Although there are a total of 18 unknowns for a single layer, the unknown constants a's, b's, and d's are related one another through equations (60). By substituting the expressions (63) into equations (60), the various relations among the unknown constants can be derived. In summary, these relations are (Chen and Frederick, 1990),

$$b_{(2m-1)} = \frac{F_{3m}}{F_{4m}} a_{(2m-1)}, \quad b_{(2m)} = \frac{F_{3m}}{F_{4m}} a_{(2m)}, \tag{64.1}$$

$$d_{(2m-1)} = \frac{F_{5m}}{\lambda_m F_{6m}} a_{(2m)}, \quad d_{(2m)} = \frac{F_{5m}}{\lambda_m F_{6m}} a_{(2m-1)}, \quad m = 1,\ 2,\ 3. \tag{64.2}$$

where,

$$F_{3m} = F_{3m}(p, q) = qF_{1m} + q\frac{C_8}{C_9}p^2, \quad F_{4m} = F_{4m}(p, q) = pq^2 + p\frac{C_8}{C_9}F_{2m} \tag{65.1}$$

$$F_{5m} = F_{5m}(p, q) = F_{1m}F_{2m} - p^2q^2, \quad F_{6m} = F_{6m}(p, q) = \frac{C_9}{C_7}F_{4m} \tag{65.2}$$

$$F_{1m} = F_{1m}(p, q) = (C_5\lambda_m^2 - C_1p^2 - C_6q^2)/C_7 \tag{65.3}$$

$$F_{2m} = F_{2m}(p, q) = (C_4\lambda_m^2 - C_6p^2 - C_2q^2)/C_7 \tag{65.4}$$

Therefore, by replacing the b's and d's in terms of the a's, equations (63) can be re-written as

$$U_1 = \sum_{m=1}^{3} \{a_{(2m-1)} C_{mz} + a_{(2m)} S_{mz}\} \tag{66.1}$$

$$U_2 = \sum_{m=1}^{3} \frac{F_{3m}}{F_{4m}} \{a_{(2m-1)} C_{mz} + a_{(2m)} S_{mz}\} \tag{66.2}$$

$$U_3 = \sum_{m=1}^{3} \frac{F_{5m}}{\lambda_m F_{6m}} \{a_{(2m)} C_{mz} + a_{(2m-1)} S_{mz}\} \tag{66.3}$$

4.4.2 Local Stiffness Matrix Formulation

One may proceed to obtain a solution based on the expressions (66) for the U_j's, i. e., to derive the expressions for the stress components and then to apply the boundary conditions. In this manner, the total number of the unknown coefficients to be solved will be $6 \times N$ for an N –layer laminate. However, by using the approach presented by Chen and Frederick (1990) one is able to reduce the total number of unknowns considerably, for a multi-layer structure. This method is therefore employed for the present study. In this regard, a local z coordinate, $z^{(n)}$, originated at the mid-surface of any n^{th} layer as shown in Figure 23 is introduced. Next, by considering the displacement continuity at all of the interfaces of the laminate, the unknown coefficients can be shifted from the a's to the U_j's ($j = 1, 2, 3$) at the upper and the lower surfaces of any layer. To this end, equations (66) for any n^{th} layer are rearranged such that,

$$U_{1+} = \sum_{m=1}^{3} \{a_{(2m-1)} C_m^+ + a_{(2m)} S_m^+\} \tag{67.1}$$

$$U_{2+} = \sum_{m=1}^{3} \frac{F_{3m}}{F_{4m}} \{a_{(2m-1)} C_m^+ + a_{(2m)} S_m^+\} \tag{67.2}$$

$$U_{3+} = \sum_{m=1}^{3} \frac{F_{5m}}{\lambda_m F_{6m}} \{a_{(2m)} C_m^+ + a_{(2m-1)} S_m^+\} \tag{67.3}$$

$$U_{1-} = \sum_{m=1}^{3} \{a_{(2m-1)} C_m^- + a_{(2m)} S_m^-\} \tag{67.4}$$

$$U_{2-} = \sum_{m=1}^{3} \frac{F_{3m}}{F_{4m}} \{a_{(2m-1)} C_m^- + a_{(2m)} S_m^-\} \tag{67.5}$$

$$U_{3-} = \sum_{m=1}^{3} \frac{F_{5m}}{\lambda_m F_{6m}} \{a_{(2m)} C_m^- + a_{(2m-1)} S_m^-\} \tag{67.6}$$

where $U_{j+} = U_j[\frac{h_n}{2}]$, $U_{j-} = U_j[\frac{-h_n}{2}]$, $C_m^+ = \cosh\ [\lambda_m \frac{h_n}{2}]$, $C_m^- = \cosh\ [\lambda_m \frac{-h_n}{2}]$, $S_m^+ = \sinh[\lambda_m \frac{h_n}{2}]$, $S_m^- = \sinh[\lambda_m \frac{-h_n}{2}]$, and h_n is the thickness of the n^{th} layer. Since $C_m^+ = C_m^-$, $S_m^- = -S_m^+$, two sets of equations can be obtained from equations (67) for the unknown coefficients a_k's ($k = 1, 2,...,6$), in terms of U_{j+}'s and U_{j-}'s ($j = 1, 2, 3$), i. e.,

$$[K_A]\{a_A\} = \{U_A\}, \quad [K_B]\{a_B\} = \{U_B\} \tag{68}$$

where $[K_A]$ and $[K_B]$ are 3×3 matricies with the following expressions for their elements

$$K_{A1m} = C_m^+, \quad K_{A2m} = \frac{F_{3m}}{F_{4m}} C_m^+, \quad K_{A3m} = \frac{F_{5m}}{F_{6m}\lambda_m} S_m^+ \tag{69.1}$$

$$K_{B1m} = S_m^+, \quad K_{B2m} = \frac{F_{3m}}{F_{4m}} S_m^+, \quad K_{B3m} = \frac{F_{5m}}{F_{6m}\lambda_m} C_m^+; \quad (m = 1, 2, 3), \tag{69.2}$$

$\{a_A\}$ and $\{a_B\}$ are 3×1 column matricies defined by,

$$\{a_A\} = \frac{1}{2}\begin{bmatrix} a_1 \\ a_3 \\ a_5 \end{bmatrix}, \quad \{a_B\} = \frac{1}{2}\begin{bmatrix} a_2 \\ a_4 \\ a_6 \end{bmatrix}, \tag{70}$$

and $\{U_A\}$, $\{U_B\}$ are 3×1 column vectors composed of the U_{j+}'s and U_{j-}'s ($j = 1, 2, 3$), and take the form

$$\{U_A\} = \frac{1}{2}\begin{bmatrix} U_{1+} + U_{1-} \\ U_{2+} + U_{2-} \\ U_{3+} - U_{3-} \end{bmatrix}, \quad \{U_B\} = \frac{1}{2}\begin{bmatrix} U_{1+} - U_{1-} \\ U_{2+} - U_{2-} \\ U_{3+} + U_{3-} \end{bmatrix} \tag{71}$$

Therefore,

$$a_{(2m-1)} = \sum_{j=1}^{3} G_{mj}\{U_{j+} + (-1)^J U_{j-}\}, \quad a_{(2m)} = \sum_{j=1}^{3} G_{(m+3)j}\{U_{j+} - (-1)^J U_{j-}\} \tag{72}$$

where,

$$G_{mj} = \frac{1}{2}[K_A]^{-1}_{mj}, \quad G_{(m+3)j} = \frac{1}{2}[K_B]^{-1}_{mj}, \tag{73}$$

and $m, j = 1, 2, 3$, and $J = 0$ if $j = 1, 2$; $J = 1$ if $j = 3$. The expressions (66) now read,

$$U_1 = \sum_{j=1}^{3}\{V_{1j}U_{j+} + V_{2j}U_{j-}\} \tag{74.1}$$

$$U_2 = \sum_{j=1}^{3}\{V_{3j}U_{j+} + V_{4j}U_{j-}\} \tag{74.2}$$

$$U_3 = \sum_{j=1}^{3} \{V_{5j} U_{j+} + V_{6j} U_{j-}\} \tag{74.3}$$

where,

$$V_{1j} = \sum_{m=1}^{3} \{G_{mj} C_{mz} + G_{(m+3)j} S_{mz}\} \tag{75.1}$$

$$V_{2j} = \sum_{m=1}^{3} (-1)^j \{G_{mj} C_{mz} - G_{(m+3)j} S_{mz}\} \tag{75.2}$$

$$V_{3j} = \sum_{m=1}^{3} \frac{F_{3m}}{F_{4m}} \{G_{mj} C_{mz} + G_{(m+3)j} S_{mz}\} \tag{75.3}$$

$$V_{4j} = \sum_{m=1}^{3} (-1)^j \frac{F_{3m}}{F_{4m}} \{G_{mj} C_{mz} - G_{(m+3)j} S_{mz}\} \tag{75.4}$$

$$V_{5j} = \sum_{m=1}^{3} \frac{F_{5m}}{\lambda_m F_{6m}} \{G_{mj} C_{mz} + G_{(m+3)j} S_{mz}\} \tag{75.5}$$

$$V_{6j} = \sum_{m=1}^{3} (-1)^j \frac{F_{5m}}{\lambda_m F_{6m}} \{G_{mj} C_{mz} - G_{(m+3)j} S_{mz}\} \tag{75.6}$$

By the foregoing manipulations and the fact that $U_{j-}^{(n)} = U_{j+}^{(n-1)}$ ($j = 1, 2, 3$; $n = 2, 3,...,N$), the total number of unknowns is now reduced from $6 \times N$ to $3 \times N + 3$ for the $N-$ layer case. Following equations (74), the expressions for the stress components at any z location in the n^{th} layer can be expressed in terms of U_{j+}, U_{j-}; j = 1, 2, 3, as

$$\sigma_i = \sigma_{i(l)} = \sum_{j=1}^{3} \{H_{ij} U_{j+} + H_{i(j+3)} U_{j-}\} \sin(p\,x) \sin(q\,y); \quad i = 1, 2, 3. \tag{76.1}$$

$$\tau_{23} = \sum_{j=1}^{3} \{H_{4j} U_{j+} + H_{4(j+3)} U_{j-}\} \sin(p\,x) \cos(q\,y) \tag{76.2}$$

$$\tau_{31} = \sum_{j=1}^{3} \{H_{5j} U_{j+} + H_{5(j+3)} U_{j-}\} \cos(p\,x) \sin(q\,y) \tag{76.3}$$

$$\tau_{12} = \sum_{j=1}^{3} \{H_{6j} U_{j+} + H_{6(j+3)} U_{j-}\} \sin(p\,x) \sin(q\,y) \tag{76.4}$$

where the H_{kl} $(k, l = 1, 2, ..., 6)$ are defined as functions of C_{kl}, p, q, V_{kl}'s and z as given by

$$H_{ij} = -C_{i1} p \dot{V}_{1j} - C_{i2} q \dot{V}_{3j} + C_{i3} \dot{V}_{5j} \tag{77.1}$$

$$H_{i(j+3)} = -C_{i1} p \dot{V}_{2j} - C_{i2} q \dot{V}_{4j} + C_{i3} \dot{V}_{6j} \tag{77.2}$$

$$H_{4j} = C_{44}(\dot{V}_{3j} + q V_{5j}), \quad H_{4(j+3)} = C_{44}(\dot{V}_{4j} + q V_{6j}) \tag{77.3}$$

$$H_{5j} = C_{55}(\dot{V}_{1j} + q V_{5j}), \quad H_{5(j+3)} = C_{55}(\dot{V}_{2j} + q V_{6j}) \tag{77.4}$$

$$H_{6j} = -C_{66}(p V_{1j} + q V_{3j}), \quad H_{6(j+3)} = -C_{66}(p V_{2j} + q V_{4j}) \tag{77.5}$$

where $\dot{V}_{kl} = \dfrac{\partial V_{kl}}{\partial z}$. By imposing the reduced boundary conditions in which the displacement continuity condition at all of the interfaces have been absorbed, a set of $3 \times N + 3$ simultaneous equations can be established for the N –layer laminate for the unknown coefficients $U_{j+}^{(n)}$'s, $U_{j-}^{(n)}$'s with n being the index for the n^{th} layer, where $n = 1, 2, ..., N$, and $j = 1, 2, 3$. In a matrix form, these equations are

$$[M]\{\underset{\sim}{U}\} = \{\underline{R}\} \tag{78}$$

where $[M]$ is a $(3 \times N + 3) \times (3 \times N + 3)$ coefficient matrix with the following definitions for its elements,

$$M_{ij} = H^{(1)+}_{(i+2)j}, \quad M_i(j+3) = H^{(1)+}_{(i+2)(j+3)}, \tag{79.1}$$

$$M_{(3l+i)(3l-3+j)} = H^{(l)-}_{(i+2)j}, \quad M_{(3l+i)(3l+j)} = H^{(l)-}_{(i+2)(j+3)} - H^{(l+1)+}_{(i+2)j}, \tag{79.2}$$

$$M_{(3l+i)(3l+j)} = -H^{(l+1)+}_{(i+2)(j+3)}; \quad l = 1, 2, ..., N-1 \tag{79.3}$$

$$M_{(3N+i)(3N-3+j)} = H^{(N)-}_{(2+i)j}, \quad M_{(3N+i)(3N+j)} = H^{(N)-}_{(2+i)(j+3)} \tag{79.4}$$

with the remaining elements being zero. In the above, i, $j = 1, 2, 3$, and the superscript (k) $(k = 1, 2, ..., N)$ is the index for the k^{th} layer. Another superscript '-' or '+' indicates that the quantity will be calculated at the local z coordinate $z^{(n)} = z_n$ or $z^{(n)} = z_{n+1}$ respectively. In addition, $\{\underset{\sim}{U}\}$ is a $(3N+3) \times 1$ column matrix composed of the unknown coefficients, i. e., $\underset{\sim}{U}_j = U_j^{(1)}$, $\underset{\sim}{U}_{(3l+j)} = U_j^{(n)}$; $j = 1, 2, 3$; $l = 1, 2, ..., N$, and $\{\underline{R}\}$ is a $(3N+3) \times 1$ column vector filled with zeros except for the first term which is $\underline{R}_1 = T_{mn}$. Solving equations (78) simultaneously for the unknown coefficients $\{\underset{\sim}{U}\}$, the displacements and stresses at any z location in any layer can then be obtained via equations (74) and (76) respectively.

The remaining procedures for the solution will be the same as those used in solving the previous isotropic plate problem. Thus, the transverse displacement u_3 on the top surface of the laminate at any location (x, y), due to any typical subload f_{kl} has to be found in order to solve the indentation problem, as demonstrated in Section 3.4.3, to construct the contact relations and to solve for the magnitudes of the subloads.

4.5 Numerical Implementation

4.5.1 Comments on the Numerical Experience

It should be noted that in order to solve the present orthotropic contact problem, a fully different solution method has been developed. As can be seen from the formulation of the analytical approach, it is practically impossible to obtain a closed form solution for the present problem since the methodology involves extremely sophisticated algebraic procedures. Unlike the isotropic problem in which the expressions for the displacement functions can be obtained in a fairly straight forward manner, a difficulty in dealing with a three dimensional problem of orthotropy because of the impossibility of solving the characteristic equation given in (62) in a closed form. Therefore, the subsequent formulation of the approach and the final stage in the solution of the contact relation equations may require a great deal of numerical effort. Thus, more effective numerical procedures must be developed in order to obtain an approximate solution. However, in comparison with the previous isotropic plate problem, the present approach differs only in the manner of finding the displacement field on the top surface of the layered plate. As far as the local contact event is concerned, the way of locating the contact area, i. e., the scheme of determining whether a point lies inside the contact area or not is still the same regardless of the material properties. Therefore, it is not necessary to generate a new numerical technique other than what has been developed previously. Following the same numerical procedures as used in treating the foregoing isotropic problem; however, the numerical experience is entirely different. The major concern is the problem of numerical convergence. It is observed that orthotropy can cause considerably different rates of

convergence. Along the minor material direction, the convergence is betterr than along the major material direction. The greater the stiffness in the major direction, the slower the convergence. Furthermore, for a multi-layered case, the higher the number of the layers, the slower the convergence as well. Thus, in comparison with the previous isotropic problem, the calculation time for the present case is much greater. The present study was implemented on IBM 3090 machine with the use of vectorization. Employing the previously developed technique of detecting terms, all of the computer jobs based arising from the examples to be studied here are easily handled within the capability of the computer.

4.5.2 Results and Discussions

In order to demonstrate the present approach and to provide a further check on the results obtained by the current approach, several examples are implemented. Two different materials are employed, i. e., magnesium (Mg) and graphite-epoxy (G-E). Magnesium has been considered by Schonberg, et. al. (1987) for studying impact problems of transversely isotropic beams and plates. The material properties for magnesium used in their study will be used here. The corresponding magnitudes for the elements of the constitutive matrixes for both (Mg) and (G-E) are listed in Table 3. Although properties listed for magnesium represent only transversely isotropy, the intention in solving the (Mg) plate is to simulate an orthotropy by using a transversely isotropic material by taking C_{11} to be along the x direction and letting $C_{22} = C_{33}$. In this manner, a slight in-plane orthotropy can still be achieved so that the results obtained can be compared with those found for the previous isotropic plate. However, the question of whether this strategy can render valid three dimensional material prop-

erties must be answered by using a mathematical examination developed by Pagano (1970). It is stated that, in reality, for most of the composite materials, the roots of the characteristic equation (62), λ's, are all real. In effect, without performing the testing, the solution procedure can never be proceeded since the expression of the displacement functions U_j ($j = 1, 2, 3$) given in equation (63) will be no longer valid. The properties of magnesium and graphite-epoxy listed in Table 3 have been checked against the afore-mentioned criterion. The requirement is satisfied. Three different configurations of the plate will be considered. The first example to be considered is a single layered (Mg) plate with the same geometry as used in the previous isotropic plate, i. e., the edge length $L = 2.0$ inch and the thickness $h = 0.1$ inch. The second example is taken to be a single layered plate of (G-E) again with the same geometry. The last example to be considered is a two-layered G-E laminate with a 0°/90° stacking sequence where the edge length, L, is taken to be 1.0 inch. Both layers are assumed to have the same thickness of $h_N = 0.05$ inches so that the total thickness of the laminate is $h = 0.1$ inches.

For the (Mg) plate, the material property along the y direction is stronger than that along the x direction. The contact stress is investigated for various lengths of contact along the x direction with magnitudes of $a = 1.0h$, $2.0h$, and $3.0h$, respectively. For the semi-contact length $c = a = h$, for example, the contact area is taken to be an ellipse and the contact stress is sought by implementing several sizes for b. A completely compressive contact stress is obtained by taking $b = 0.96a$. The results are displayed in Figure 24 where the corresponding elliptical contact area is presented in the top figure. The contact stress is normalized again by a similar intimate average contact stress $\sigma_{ai} = \dfrac{P}{a \times b}$ and is plotted versus the normalized coordinates $\bar{x}$, and $\bar{y}$ along c for various locations of $\bar{y}$ and $\bar{x}$ respectively. Locations of the curves of contact stress

are further illustrated on the contact area shown. Due to the slight material orthotropy, it is obvious that the stress contours along both the x and the y directions in this case are nearly indistinguishable. Comparing the curves of $\bar{x} = 0.0$ and $\bar{y} = 0.0$ in Figure 24 with the corresponding curves in Figure 13, which is for an isotropic plate, the results are identical. Thus, a full agreement is obtained by the present approach.

For $c = a = 2.0h$, several attempts are tried by first taking the contact area to be an ellipse. However, no successful results are obtained. In the previous study of isotropic plate, a hypotrocoidal contact area has come into the picture for such an indentation magnitude. Therefore, further attempts are conducted by multiplying the original regular hypotrocoidal curves of Group A with a constant, Y_c, along the y direction to fulfill the slightly orthotropic condition needed to represent such contact areas. The correct contact area is found by employing a hypotrocoid parameter $C_k = 0.04$, and $Y_c = 0.975$. The normalized contact stress for this case is shown in Figure 25. Apparently, the difference between the contact stresses along the x and the y directions is negligible. Curves for $\bar{x} = 0.0$ and $\bar{y} = 0.0$ are found to be nearly equal to the results illustrated in Figure 16 for the isotropic plate for the same magnitude of c. However, it should be noted that the hypotrocoid parameter employed here is greater than that which used for the isotropic case. Thus, from $c = 1.0h$ to $c = 2.0h$, the contact length along approximately the 45° direction is reduced by a greater amount than that which occurs in the isotropic plate. The same scheme is employed in solving for the contact area and the contact stress for the case of $c = 3.0h$. The factor used to modify the hypotrocoids is taken to be the same, i. e., $Y_c = 0.975$. However, fully compressive contact stress is found by taking a slightly greater hypotrocoid parameter, $C_k = 0.05$. As shown in Figure 26, the result does not

suggest a significant distinction for the contact stresses along the two coordinate directions.

Next, the single-layered G-E plate is considered. Since C_{11} is much higher than C_{22}, the main purpose of this example is to reveal the rates at which the contact lengths increase along different in-plane directions as the indentation advances under the circumstances of severe orthotropy and small indentations. The contact stress is investigated with respect to the semi-contact length along the y direction, b. Two magnitudes for b are considered, i. e., $b = 0.5h$ and $b = 1.0$. For $b = 0.5h$, the contact area is assumed to retain an elliptic shape and is proven to be correct by taking $a = 0.4h$. Thus, the contact length along the major material direction is less than the length of contact along the minor material direction and the ratio is 80 %. Distribution of the contact stresses along the semi-axis, b, is presented in Figure 27 in which the previous schemes of normalization for both the ordinate and the abassica are employed. The contact stress along the other semi-axis, a, is found to be the same by using the same normalization scheme and thus it is not displayed. As expected, in a three dimensional sense, the contact stress preserves an ellipsoidal shape in this case, i. e., it is a Hertzian type distribution. In addition, the normalized magnitude of the contact stress is found to be very close to the result for the previous isotropic plate with the same magnitude for c. Thus, for small indentations, Hertz's theory is clearly applicable regardless of the properties of the material.

For $b = 1.0h$, the shape of the contact area is also assumed to be elliptic. The contact stresses are found to be all compressive by introducing $a = 0.64h$. This indicates that, as the indentation proceeds, the rate of increase of the contact length along a stiffer material direction will be less than that along a weaker material direction. The

corresponding contact stress is displayed in Figure 28. Clearly, the profile of the contact stress is still close to an ellipsoid in shape but the peak value of the contact stress which located at the center of the elliptic contact area has decreased by about 10 % of σ_{ai}, in comparison with the case for $b = 0.5h$.

Finally, the two layered G-E plate is considered. This example is of more practical value due to the existence of symmetric and balanced configuration. Feasibly, the material properties along the 45° direction passing through the corners of the laminate is different from those along the x and the y directions. Therefore, it is of interest to seek the contact stress under the joint effect of in-plane dependence of material properties and the finite boundary. However, based on the experience gained by studying the previous isotropic plate problem in which the material orthotropy did not exist, a reasonable prediction of the shape of the contact area for the present case can be made. Since the bending rigidities along both of the in-plane directions for the present case are likely to be the same regardless of the existence of different stiffness along the 45° direction, the contact lengths along both the x and the y directions should be very close although the length of contact along the 45° direction has to be investigated. Anyhow, the previously employed hypotrocoids are supposed to be well suited in representing the contact areas for the present case. Accordingly, the contact stresses will be sought based on certain lengths of contact, $c = a = b$, along the coordinate axes directions. However, the previous results for a single layered (G-E) plate illustrate a slower rate of increase for the contact length along a stiffer material direction. Therefore, an investigation based on gradual increases of the contact length is needed. In this regard, for demonstration, four magnitudes for the semi-contact lengths, c, will be considered, i. e., $c = 0.75h$, $1.0h$, $1.5h$, and $1.6h$.

For $c = 0.75h$, several trials were attempted by proposing the contact area to be a hypotrocoid of group A by introducing various values for the parameter C_k including the special case of $C_k = 0.0$, i. e., a circle. The contact stresses are All compressive only when $C_k = 0.03$. Using the previous normalization, the shape of the contact area and the corresponding stress distributions are presented in Figure 29. It is clear that the contact stress in this case has significantly deviated from a Hertzian type profile even under the condition of small indentation. However, along both directions, the contact stresses are distributed almost identically. For the curves of both $\bar{x} = 0.0$ and $\bar{y} = 0.0$, the maximum contact stress is located off the center of the contact area. The present plate is comparatively thicker than the foregoing studied configurations since the aspect ratio has been reduced by half. Recalling Keer and Miller's study (1983) for a beam, it should be noted that different aspect ratios do not produce different behaviors for the contact stresses for the same magnitude of indentation. Thus for the current magnitude of indentation, it may be expected that the contact stress should lie within the limit of Hertzian behavior or otherwise the deviation should be very small. However, the present spherical indentation of a layered plate reveals entirely different results, although it is possible to visualize that along the 45° direction, the contact stress deviates less from the Hertzian type distribution with a shorter length of contact.

For $c = 1.0h$, a similar hypotrocoid with $C_k = 0.05$ successfully represents the contact area. The corresponding contact stress is shown in Figure 30. Symmetry of the contact stress along both of the in-plane directions is observed. Meanwhile, it is clear that wrapping of the plate over the indentor has significantly developed since a considerable amount of peaking of the contact stress has occured close to the boundary of contact area as can be seen from the curves for $\bar{x} = 0.0$ and $\bar{y} = 0.0$. The

difference between the peak contact stress and the stress at the center of loading is found to be as much as 45 % of σ_{ai}. This is even greater than the corresponding difference shown in Figure 16 for an isotropic plate with $c = 2.0h$ by considering the current contact length c to be two times of the layer thickness for comparison. As to the contact length along different in-plane directions, it is obvious that from $c = 0.75h$ to $c = 1.0h$, the contact length along the 45° direction increases by a smaller amount than those along the coordinate axes directions. Thus, as for a similar phenomenon observed in the isotropic plate, the present geometry and boundary of the plate which contains a shorter dimension along the coordinate axis direction, have induced a shorter contact length in the 45° direction within the limit of present magnitude of indentation, although the structure is stiffer in the 0° and 90° directions than in the 45° direction. Alternatively, the boundary effect prevails up to this stage of indentation.

For $c = 1.5h$, the correct contact area is found by imposing $C_k = 0.02$. Illustrated in Figure 31, the contact stresses along both in-plane directions do not reveal any significant difference. The extent of the wrapping behavior is found to be slightly increased in comparison with the previous case of $c = 1.0h$. However, it should be noted that the employed hypotrocoid parameter is appreciably smaller than the previous cases. Thus, along the weaker material direction, the contact length begins to increase since, as far as wrapping is concerned, it is comparatively easier to deform along this direction than along the others. Thus, the effect of material orthotropy begins to be dominant at this instant of indentation.

Since the hypotrocoidal parameter is increased at the beginning but is then decreased up to this stage of indentation, a gradual look at the variance of the contact

behavior seems to be in order now. Therefore, the next case considers a slightly increased contact length with $c = 1.6h$. The contact area is found to be a member of the other kind of hypotrocoid, i. e., group B, with a parameter $C_k = 0.02$. The contact stress for this case is displayed in Figure 32 in which peaking of the contact stress is seen to be more severe than in the previous cases but no serious distinction are found for the distributions of the contact stresses along both of the in-plane directions. Apparently, the contact length along the 45° direction is greater than those along the directions of fibers in this case. Thus, the material effect has completely overcome the boundary effect for this case and the behavior of local contact which occured in the previous single layer case is recovered, i. e., the contact length along a material weaker direction is longer than the length along a stiffer direction.

CHAPTER V

CONCLUSIONS

Three dimensional contact problems of orthotropic layered square plates indented by a rigid spherical indentor are solved by combining an analytical elasticity approach with numerical procedures. The proposed problems involve both finite boundary and orthotropy, i. e., in-plane asymmetries due to both structural geometry and material properties. The approaches are based on the exact solution formulation developed by Pagano (1970) in conjunction with numerically the Point Matching (PM) method of Sun and Sankar (1983) and enhanced by the Redundant Field Point (RFP) method presented by Singh and Paul (1974) to overcome the inherent numerical sensitivity due to the ill-posed nature of the problems. Simplified problems obtained by degrading the problem to a two dimensional case and excluding the material orthotropy are studied thoroughly in order to develop the required techniques and approaches prior to solving the afore-mentioned three dimensional case.

For the two dimensional problem of cylindrical indentation of a beam, the results obtained are in good agreement with those obtained by Keer and Miller (1983) and Sankar and Sun (1983). An efficient numerical programming technique is developed via this study which is readily applicable in dealing with three dimensional contact problems.

For the three dimensional problem of contact between an isotropic square plate and a rigid spherical indentor, a nearly closed form expression for the displacement field due to any arbitrarily defined sub-load is obtained. Solutions for the contact stresses are achieved by extending the previous PM method and employing the RFP method. For the small indentation condition, the results retain Hertzian type behavior and are identical to the circular plate solutions obtained by Keer and Miller (1983). However, a comparatively limited range of applicability of Hertzian type solutions is revealed

with respect to the limit of the validity of a circular contact area. For comparatively large indentations, the contact area is located by introducing the concept of an irregular shape of contact based on the consideration of the geometry of the structure and is found to be a hypotrocoid of four lobes. In summary, the proposed boundary geometry causes a reduction of the contact length along the through-the-corner direction as the indentation proceeds. The load versus indentor displacement relation indicates a square plate is stiffer in indentation than a circular plate with a diameter which is equal to the edge length of the square plate.

Three dimensional contact problems of orthotropic laminates are solved by superposing the readily developed approach with Chen and Frederick's method (1990). A slightly orthotropic material, magnesium, is implemented first for a single layer case and the induced results are in a full agreement with those obtained for the purely isotropic case. A single-layered highly orthotropic plate of graphite-epoxy is studied and the result shows an appreciably greater rate of increasing contact length along the less stiffer material direction. A Hertzian type distribution for the contact stress is retained for small indentation conditions regardless of the existence of material orthotropy. A two layered plate of the same material with a 0°/90° staking sequence is investigated and demonstrates nearly the same patterns of contact stresses along both of the in-plane directions. In comparison with the previous isotropic case, the contact area departs from a circular shape much earlier and is associated with an appreciable amount of wrapping, i. e., an early deviation from the Hertzian type solution for the contact stresses. The boundary effect prevails initially in the early stage of indentation in which the contact area is proven to be a hypotrocoid of the same type which existed for the large indentation condition in the isotropic plate. As the indentation advances, however, the material effect participates in controlling the

contact shape and becomes dominant. Finally, the material effect overcomes the boundary effect and the contact area changes to the other type of hypotrocoid featured with a longer length of contact along the through-the-corner directions.

Overall, although a two dimensional study may not be able to precisely simulate the physical problem in reality, the approach developed for the two dimensional problem is extremely valuable and applicable for studying a three dimensional problem. Moreover, in solving a three dimensional contact problem, the most important issue is the knowledge of the shape of the contact area. Feasibly, a three dimensional contact problem involving general anisotropy could possibly feature a contact area which is far from physical imagination. Consequently, studies of this type still need to be further developed in order to truly understand the local indentation behavior for the event of a general three dimensional anisotropic structure subjected to impact due to a foreign projectile.

Bibliography

Jones, R., Paul, J., Tay, T. E., and Williams, J. F., 1988, "Assessment of the Effect of Impact Damage in Composites : Some Problems and Answers", Composite Structures , Vol. 10, No. 1, pp. 51-73.

Brockman, R. A., 1988, "Computational Methods for Soft-Body Impact Problems", Proceeding of the Second International Conference on Computational Engineering Science , pp. 6.vi.1-6.vi.4.

Yang, S. H., and Sun, C. T., 1982, "Indentation Law for Composite Laminates", Composite Materials : Testing and Design, ASTM STP 787, American Society for Testing and Materials, pp. 425-449.

Tan, T. M., and Sun, C. T., 1985, "Use of Static Indentation laws in the Impact Analysis of Laminated Composite Plates", ASME Journal of Applied Mechanics , Vol. 52, No. 1, pp. 6-12.

Doyle, J. F., 1984, "An Experimental Method for Determining the Dynamic Contact Law", Experimental Mechanics , Vol. 24, No. 1, pp. 10-16.

Doyle, J. F., 1984, "Further Developments in Determining the Dynamic Contact Law", Experimental Mechanics , Vol. 24, No. 4, pp. 265-270.

Sun, C. T., Sankar, B. V., Tan, T. M., 1981, "Dynamic Response of SMC to Impact of a Steel Ball", Advances in Aerospace Structures and Materials, The Winter Annual Meeting of the American Society of Mechanical Engineers, Washington, D. C., pp. 99-107.

Hertz, H., 1881, "Uber die Beruhrung fester Elastischer Korper", Journal Reine Angle Math. , Crelle, Vol. 92, pp. 155.

Willis, J. R., 1966, "Hertzian Contact of Anisotropic Bodies", Journal of the Mechanics of Physics and Solids , Vol. 14, No. 3, pp. 163-176.

Willis, J. R., 1967, "Boussinesq Problems for an Anisotropic Halfspace", Journal of the Mechanics of Physics and Solids , Vol. 15, No. 5, pp. 331-339.

Popov, G. I., 1961, "On an Approximate Method of Solution of Certain Plane Contact Problems of the Theory of Elasticity", Trans. Armen. Acad. Sci., SSR, Vol. 14.

Popov, G. I., 1962, "The Contact Problem of the Theory of Elasticity for the Case of A Circular Area of Contact", PMM (English Translation : Journal of Applied Mathematics and Mechanics) , Vol. 26, No. 1, pp. 207-225.

Keer, L. M., 1964, "The Contact Stress Problem for an Elastic Sphere Indenting an Elastic Layer", ASME Journal of Applied Mechanics , Vol. 31, No. 1, pp. 143-145.

Meijers, P., 1968, "The Contact Problem of a Rigid Cylinder on an Elastic Layer", Journal of Applied Scientific Research , Vol. 18, No. 5, pp. 353-383.

Tsai, Y. M., 1969, "Stress Distributions in Elastic and Viscoelastic Plates Subjected to Symmetrical rigid Indentation", Quarterly Journal of Applied Mathematics , Vol. 27, No. 3, pp. 371-380.

Chen, W. T., and Engel, P. A., 1972, "Impact and Contact Stress Analysis in Multi-layer Media", International Journal of Solids and Structures , Vol. 8, No. 11, pp. 1257-1281.

Leon, Y. B., 1972, "Transfer Matrix Approach to Layered Systems", Journal of the Engineering Mechanics Division, Proceeding of the American Society of Civil Engineers , Vol. 98, No. EM5, pp. 1159-1172.

Leon, Y. B., 1975, "Transfer Matrix Approach to Elastodynamics of Layered Media", Journal of the Acoustical Society of America , Vol. 57, No. 3, pp. 606-609.

Gladwell, G. M. L., 1980, "Contact Problems in the Classical Theory of Elasticity", Sijthoff and Noordhoff International Publishers B. V., Alphen aan den Rijn, The Netherlands.

Kalker, J. J., 1979, "Survey of Wheel-Rail Rolling Contact Theory", Vehicle System Dynamics , Vol. 8, No. 4, pp. 317-350.

Kalker, J. J., 1980, "Review of Wheel-Rail Contact Theories", Proc. of Syposium on the General Problem of Rolling Contact , AMD-Vol. 40, ASME, N. Y., pp. 66-92.

Paul, B., 1983, "Surface and Subsurface Stresses Associated with Non-Hertzian Wheel-Rail Contact", in **Contact Mechanics and Wear of Rail/Wheel Systems,** Edited by Kalousek, J., Dukkipati, R. V., and Gladwell, G. M. L., University of Waterloo Press, Waterloo, Canada, pp. 197-207.

Singh, K. P., and Paul, B., 1974, "Numerical Solution of Non-Hertzian Elastic Contact Problems", ASME Journal of Applied Mechanics , Vol. 41, No. 2, pp. 484-490.

Paul, B. and Hashemi, J., 1978, "An Improved Numerical Method and Computer Program for Counterformal Contact Stress Problems", in **Computational techniques for Interface Problems** , AMD-Vol. 30, Ed. by Park, K. C. and Gartlung, D. K., ASME, N. Y., pp. 165-180.

Paul, B. and Hashemi, J., 1980, "Contact Pressures on Closely Conforming Elastic Bodies", Proc. of Symposium on Solid Contact and Lubrication , AMD-Vol. 39, ASME, N. Y., pp. 67-78.

Paul, B. and Hashemi, J., 1980, "Contact Geometry Associated with Arbitrary Rail and Wheel Profiles", Proc. of Syposium on the General Problem of Rolling Contact , AMD-Vol. 40, ASME, N. Y., pp. 93-105.

Hartnett, M. J., 1980, "A General Numerical Solution for Elastic Body Contact Problems", Proc. of Symposium on Solid Contact and Lubrication , AMD-Vol. 39, ASME, N. Y., pp. 51-66.

Kalker, J. J., 1980, "Numerical Contact Elastostatics", in **Variational Methods in the Mechanics of Solids,** S. Nemat-Nasser, Editior, Pergamon.

Kalker, J. J., 1981, "The Numerical Calculation of the Contact Problem in the Theory of Elasticity", in **Non-linear Finite Element Analysis in Structural Mechanics,** Wunderlich, Stern and Bathe, Editors, Springer.

Kalker, J. J., 1983, "Two Algorithms for the Contact Problem in Elastostatics", in **Contact Mechanics and Wear of Rail/Wheel Systems,** Edited by Kalousek, J., Dukkipati, R. V., and Gladwell, G. M. L., University of Waterloo Press, Waterloo, Canada, pp. 103-120.

Duffek, W., and Jaschinski, A., 1981, "Efficient Implementation of Wheel-Rail Contact Mechanics in Dynamic Curving", Proceeding of the 7th IAVSD Symposium on the Dynamics of Vehicles on Roads and Tracks , Cambridge, United Kingdom.

Duffek, W., 1983, "Contact Geometry in Wheel Rail Vihicles", in **Contact Mechanics and Wear of Rail/Wheel Systems,** Edited by Kalousek, J., Dukkipati, R. V., and Gladwell, G. M. L., University of Waterloo Press, Waterloo, Canada, pp. 161-181.

Timoshenko, S. P., and Goodier, J. N., 1970, "Theory of Elasticity", Third Edition, Mcgraw-Hill, New York.

Keer, L. M., and Miller, G. R., 1983, "Smooth Indentation of Finite Layer", Journal of Engineering Mechanics , Vol. 109, No. 3, pp. 706-717.

Sankar, B. V., and Sun, C. T., 1983, "Indentation of a Beam by a Rigid Cylinder", International Journal of Solids and Structures , Vol. 19, No. 4, pp. 293-303.

Conway, H. D., Vogel, S. M., Farnham, K. A., and So, S., 1966, "Normal and Shearing Contact Stresses in indented Strips and Slabs", International Journal of Engineering Science , Vol. 4, pp. 343-359.

Keer, L. M., and Ballarini, 1983, "Smooth Contact Between a Rigid Indenter and an Initially Stressed Orthotropic Beam", AIAA Journal , Vol. 21, No. 7, pp. 1035-1042.

Sun, C. T., and Sankar, B. V., 1985, "Smooth Indentation of an Initially Stressed Orthotropic Beam", International Journal of Solids and Structures , Vol. 21, No. 2, pp. 161-176.

Pawlak, T. P., Salamon, N. J., and Mahmoud, F. F., 1985, "Beams in Receding / Advancing Contact : Dundurs Problems", ASME Journal of Applied Mechanics , Vol. 52, No. 4, pp. 933-936.

Keer, L. M., and Lee, J. C., 1985, "Dynamic Impact of An Elastically Supported Beam - Large Area Contact", International Journal of Engineering Science , Vol. 23, No. 10, pp. 987-997.

Keer, L. M., and Miller, G. R., 1983, "Contact Between an Elastically Supported Circular Plate and a Rigid Indenter", International Journal of Engineering Science , Vol. 21, No. 6, pp. 681-690.

Keer, L. M., and Woo, T. K., 1984, "Low Speed Impact on a Circular Plate", Advances in Aerospace Sciences and Engineering, ASME Winter Annual Meeting , pp. 1-8.

Sankar, B. V., 1987, "An Approximate Green's Function for Beams and Application to Contact Problems", ASME Journal of Applied Mechanics , Vol. 54, No. 3, pp. 736-737.

Miller, G. R., 1986, "A Green's Function Solution for Plane Anisotropic Contact Problems", ASME Journal of Applied Mechanics , Vol. 53, No. 2, pp. 386-389.

Koshnareva, V. A., Mel'nikov, Y. A., and Preobrazhenskii, I. N., 1987, "Solution of Plane Contact Problems of Elasticity By the Method of Green's Functions", Journal of Mechanics and Solids , Vol. 22, No. 4, pp. 148-155.

Shivakumar, K. N., Elber, W., and Illg, W., 1985, "Prediction of Impact Force and Duration Due to Low-Velocity Impact on Circular Composite Laminates", ASME Journal of Applied Mechanics , Vol. 52, No. 3, pp. 674-680.

Cairns, D. S., and Lagace, P. A., 1987, "Thick Composite Plates Subjected to Lateral Loading", ASME Journal of Applied Mechanics , Vol. 54, No. 3, pp. 611-616.

Sankar, B. V., 1988, "Axis-symmetric Contact Between a Rigid Sphere and a Layered Plate", Proceeding of the 2nd International Conference on Computational Engineering Science , pp.6.vii1-6.vii4.

Schonberg, W. P., Keer, L. M., and Woo, T. K., 1987, "Low Velocity Impact of Transversely Isotropic Beams and Plates", International Journal of Solids and Structures , Vol. 23, No. 7, pp. 871-896.

Tsai, Y. M., 1986, "Symmetrical Contact Problem of a Thick Transversely Isotropic Plate", Journal of Elasticity , Vol. 16, No. 2, pp. 179-188.

Mittal, R. K., 1987, "A Simplified Analysis of the Effect of Transverse Shear on the Response of Elastic Plates to Impact Loading", International Journal of Solids and Structures , Vol. 23, No. 8, pp. 1191-1203.

Aggour, H., and Sun, C. T., 1988, "Finite Element Analysis of A Laminated Composite Plate Subjected to Circularly Distributed Central Impact Loading", Computers and Structures , Vol. 28, No. 6, pp. 729-736.

Wu, H. T., and Springer, G. S., 1988, "Impacted Induced Stresses, Strains, and Delaminations in Composite Plates", Journal of Composite Materials , Vol. 22, No. 6, pp. 533-560.

Poe, C. C., 1988, "Simulated Impact Damage in a Thick Graphite / Epoxy Laminate Using Spherical Indenter", NASA Technical Memorandum 100539, National Aeronautics and Space Administration, Langley Research Center, Hampton, Virginia

Chen, C. F., and Gurdal, Z., 1990, "Stress Analysis of an Orthotropic Plate on an Elastic Foundation with a Transverse Point Load", ASCE Journal of Aerospace Engineering , Vol. 3, No. 1, pp. 64-77.

Chen, C. F., and Frederick, D., 1990, "Orthotropic Laminates on an Elastic Foundation Under Transverse Force", ASCE Journal of Engineering Mechanics , Vol. 116, No. 11, pp. 2434-2448.

Sankar, B. V., 1987, "Low-Velocity Impact Response of Graphite-Epoxy Laminates", Final Report, Dept. of Engineering Science, University of Florida, WPAFB Contract F33615-84-C-5070.

Pagano, N. J., 1970, "Exact Solutions for Rectangular Bidirectional Composites and Sandwich Plates", Journal of Composite Materials , Vol. 4, No. 1, pp. 20-34.

Arfkan, 1973, "Mathematical Methods for Physicists", Second Edition, Academic Press, Inc., New York.

Sokolnikoff, I. S., 1956, "Mathematical Theory of Elasticity", Second Edition, McGraw-Hill Book Company, New York.

Love, A. H. E., 1944, "Elasticity", Fourth Edition, Dover Publications, New York.

Holmes, W. T., 1978, "Plane Geometry of Rotors in Pumps and Gears", The Scientific Publishing Company, Manchester, Great Britain.

Appendix - A Expressions for the T_{nm}s in equation (36)

For $k + l \neq K + 1$,

$$T_{nm} = \frac{16}{\pi^2 pqL^2} \cos(px_{k+1}) \cos(qy_{l+1}) \qquad (A-1)$$

For $k = 1, l = K$,

$$T_{nm} = \frac{J_{nm}}{q} \left[\frac{1}{p} \sin(px'_2) \sin(qy'_K) + \frac{t_2}{p^2 - t_2^2} [\cos(t_1) - \cos(px'_2)] \right] \qquad (A-2)$$

where,

$$t_1 = qm_1 x'_2, \quad t_2 = qm_1, \quad m_1 = \frac{y_{K+1} - y_K}{x'_2}$$

For $k = K, l = 1$,

$$T_{nm} = \frac{J_{nm}}{p} \left[\frac{1}{q} \sin(px'_K) \sin(qy'_2) + \frac{t_2}{q^2 - t_2^2} [\cos(t_1) - \cos(qy'_2)] \right] \qquad (A-3)$$

where,

$$t_1 = pm_1 y'_2, \quad t_2 = pm_1, \quad m_1 = \frac{x_{K+1} - x_K}{y'_2}$$

For $k + l = K + 1$; $k = 2, 3, \ldots, K - 1$;

$$T_{nm} = J_{nm} \left[\frac{1}{pq} f_{s(k, K+2-k)} + \frac{\frac{p}{q} F_{S(k)} - m_1 F_{C(k)}}{p^2 - (m_1 q)^2} \right] \qquad (A-4)$$

where,

$$F_{S(k)} = [f_{s(k+1, K+1-k)} - f_{s(K, K+2-k)}], \quad F_{C(k)} = [f_{c(K+1, K+1-k)} - f_{c(k, K+2-k)}]$$

$$f_{s(k,l)} = \sin(px'_k) \sin(qy'_l), \quad f_{c(k,l)} = \cos(px'_k) \cos(qy'_l), \quad J_{nm} = \frac{16(-1)^{n+m}}{L^2}$$

In the above $p=\frac{n\pi}{L}$, $q=\frac{m\pi}{L}$, and $x'_i=x_i-\frac{L}{2}$, $y'_i=y_i-\frac{L}{2}$, where $i=1, 2,....,$ $K+1$.

TABLES

Table 1.

Magnitudes of Uniform Discretized Subloads on Beam

Sub-load Index (f_i)	Magnitude of Sub-load (lb/in)	Normalized Magnitude of Sub-load
1	0.36763D + 02	0.46654D-02
2	0.75501D + 02	0.95812D-02
3	0.11843D + 03	0.15029D-01
4	0.16836D + 03	0.21366D-01
5	0.22929D + 03	0.29098D-01
6	0.30769D + 03	0.39047D-01
7	0.41575D + 03	0.52760D-01
8	0.58172D + 03	0.73822D-01
9	0.89719D + 03	0.11386D + 00
10	0.19552D + 04	0.24812D + 00

Total Contact Load = 394.00 (lb)

Table 2.

Magnitudes of Non-Uniform Discretized Subloads on Beam

Sub-load Index (f_i)	Magnitude of Sub-load (lb/in)	Normalized Magnitude of Sub-load
1	0.98136D + 02	0.12501D-01
2	0.19846D + 03	0.25281D-01
3	0.30382D + 03	0.38704D-01
4	0.41028D + 03	0.52265D-01
5	0.51934D + 03	0.66158D-01
6	0.61781D + 03	0.78703D-01
7	0.70898D + 03	0.90316D-01
8	0.77580D + 03	0.98829D-01
9	0.81094D + 03	0.10330D + 00
10	0.43167D + 03	0.54991D-01

Total Contact Load = 392.50 (lb)

Table 3.

Constitutive Coefficients for Magnesium and Graphite-Epoxy

C_{ij} (10^6 Psi)	Magnesium (Mg)	Graphite-Epoxy (G-E)
C_{11}	8.097	19.577
C_{12}	3.013	0.760
C_{13}	3.013	0.777
C_{22}	8.855	2.078
C_{23}	3.624	1.047
C_{33}	8.855	2.105
C_{44}	2.615	0.510
C_{55}	2.403	0.800
C_{66}	2.403	0.820

Note $C_{ij} = C_{ji} (i, j = 1, 2, 3)$ and the unlisted coefficients are zero.

FIGURES

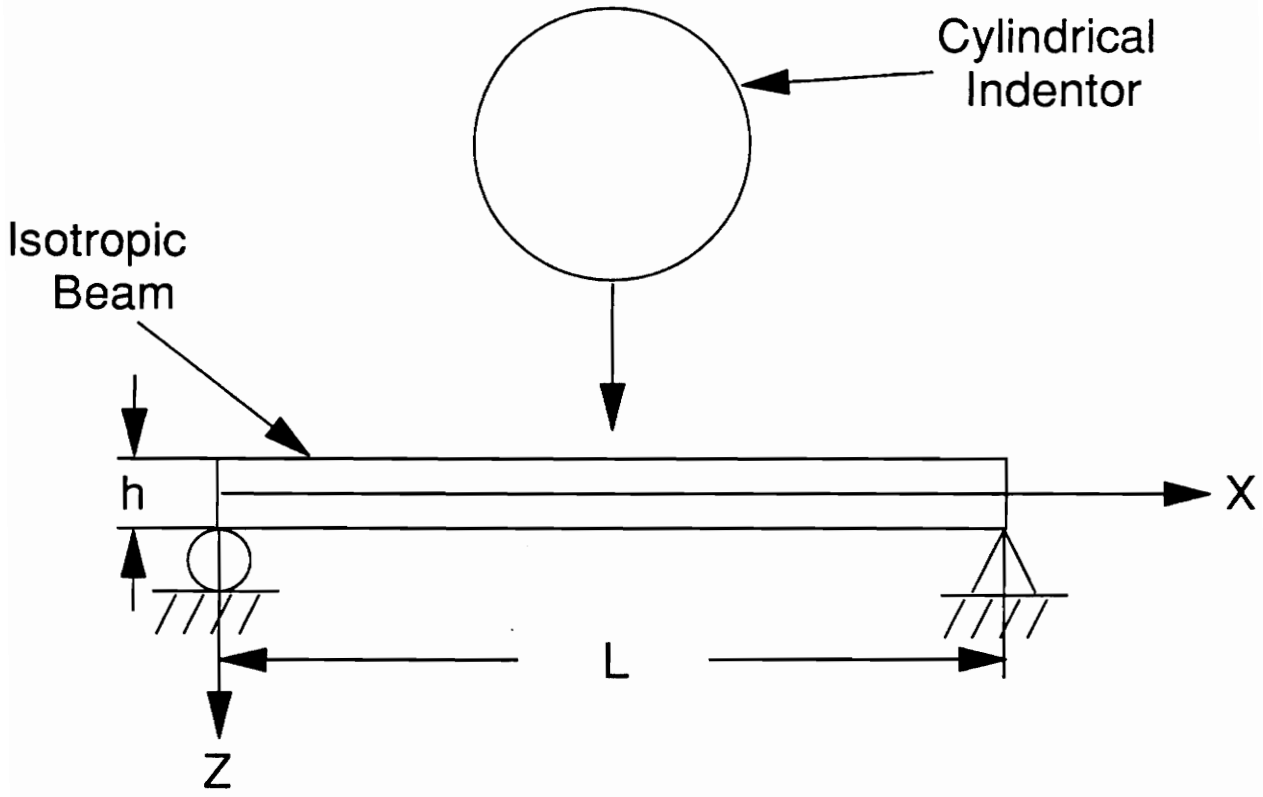

Figure 1. Beam Under Cylindrical Indentation

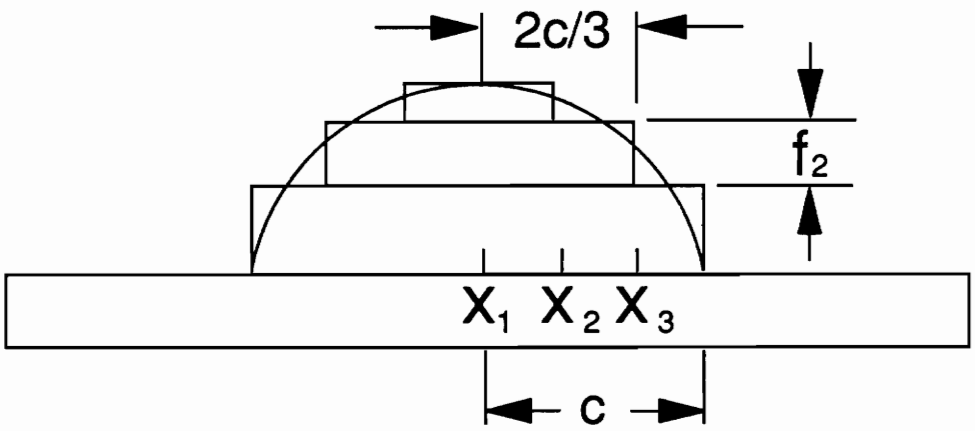

Figure 2. Discretization of Contact Stress
(Indentation of a Beam)

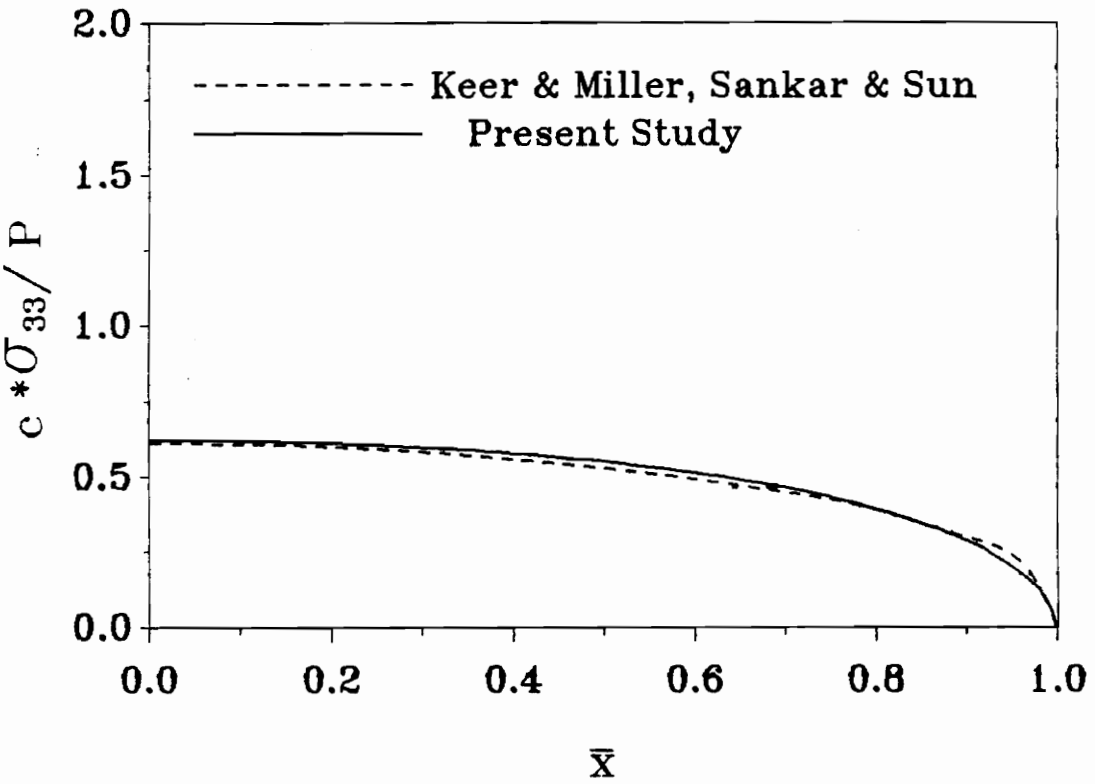

Figure 3. Contact Stress Distribution for Beam
c =0.5 h

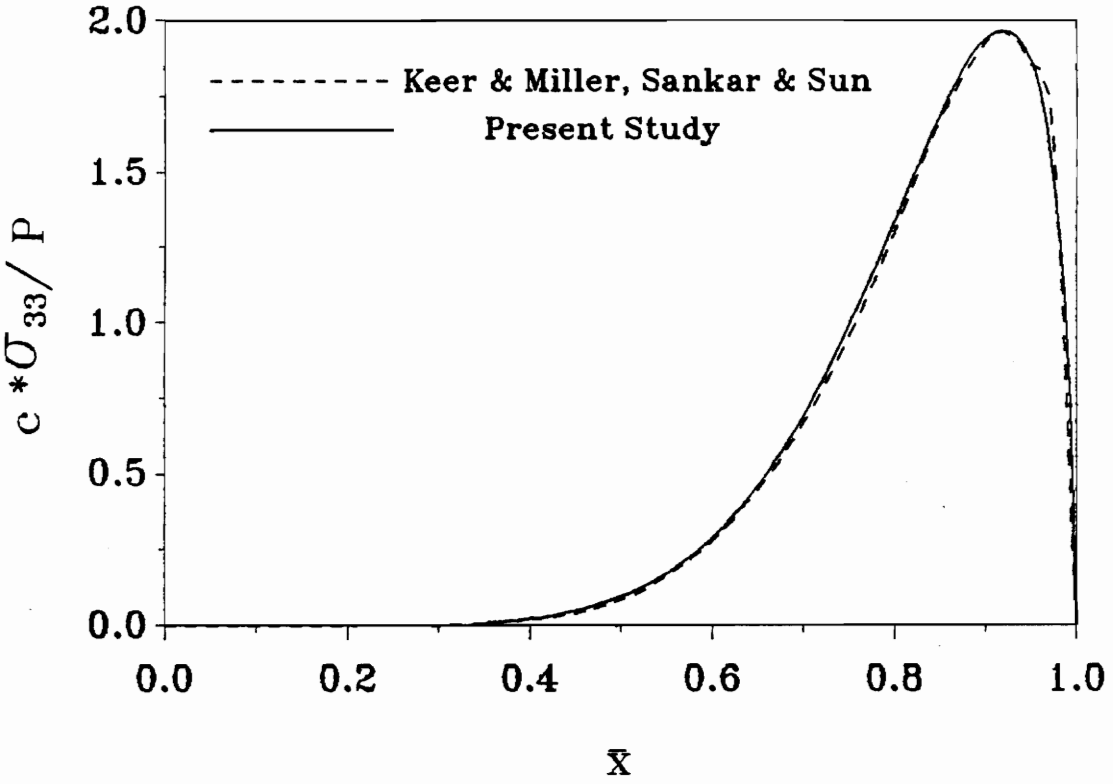

Figure 4. Contact Stress Distribution for Beam
c = 4.0 h

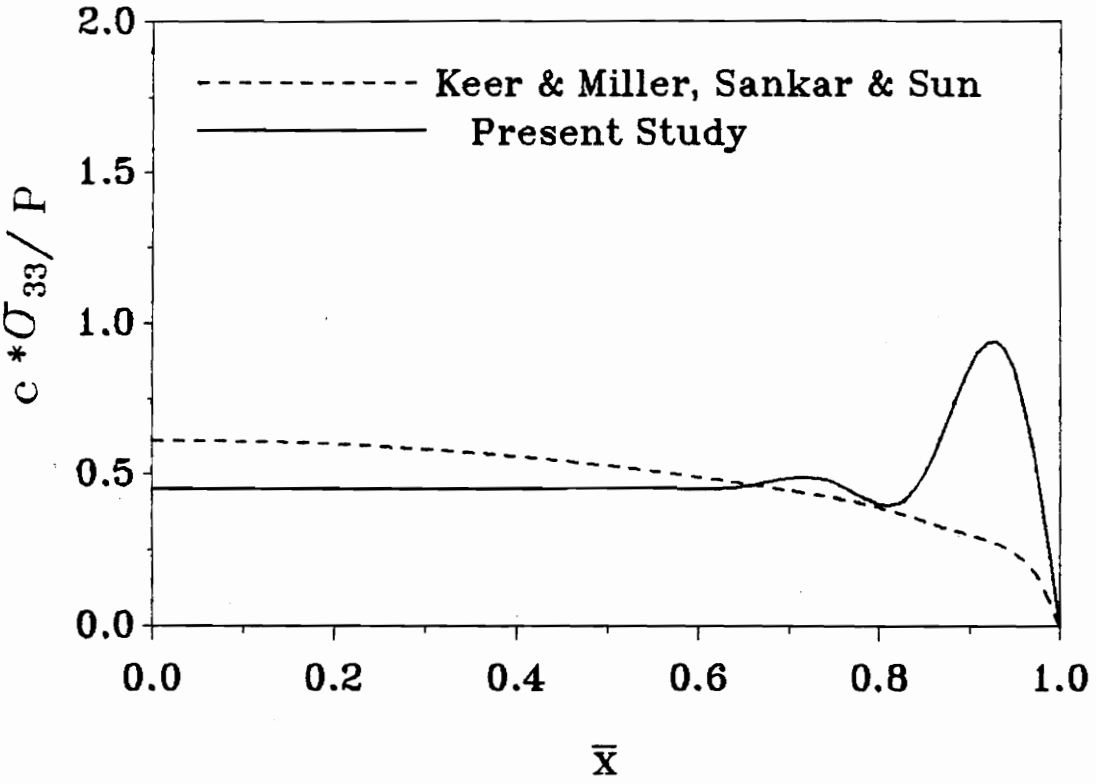

Figure 5. Contact Stress Distribution for Beam, c = 0.5 h
Ref. Pt.s, $x_{i+1} = c*(2*i+1)/(2K)$

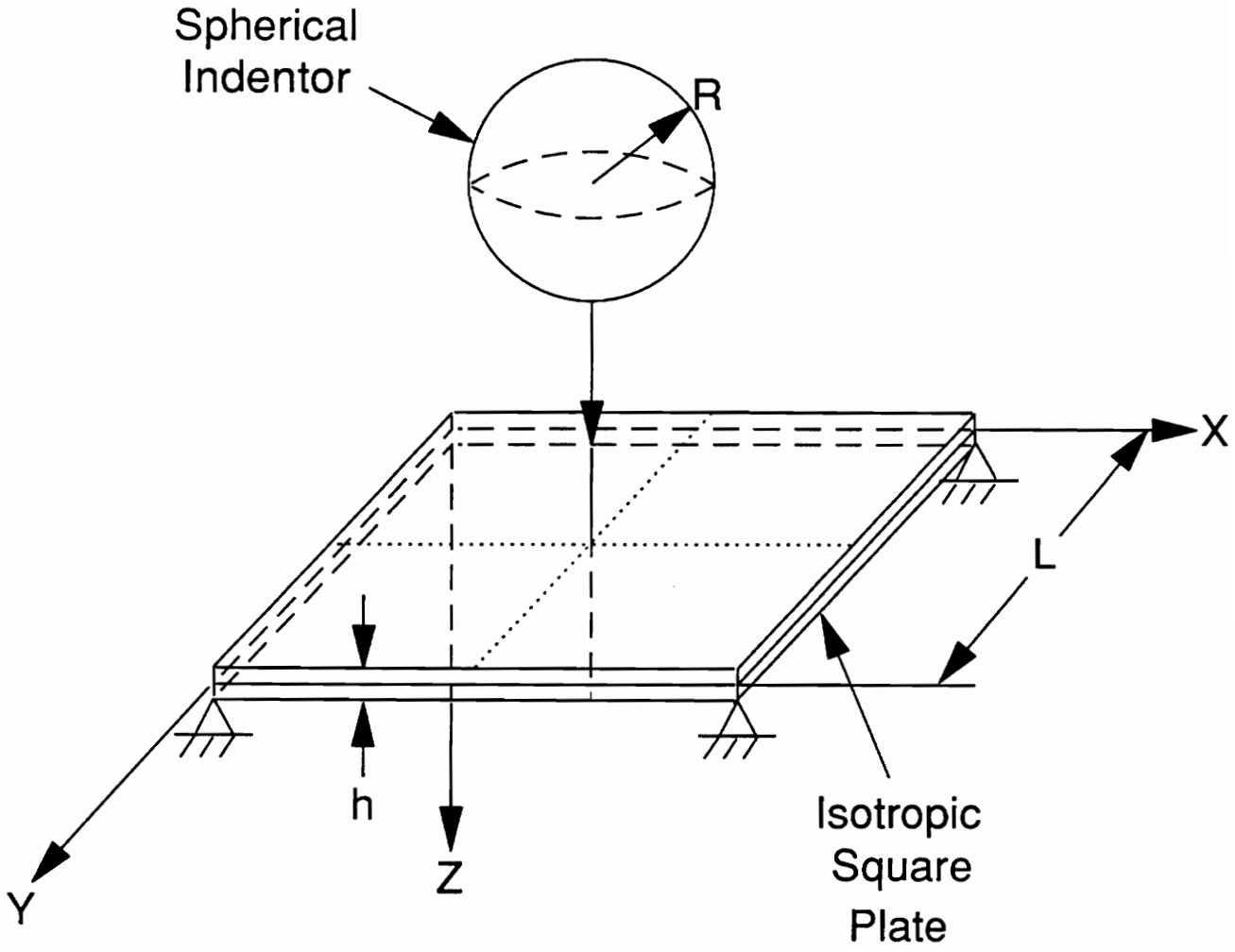

Figure 6. Isotropic Square Plate Indented by a Spherical Indentor

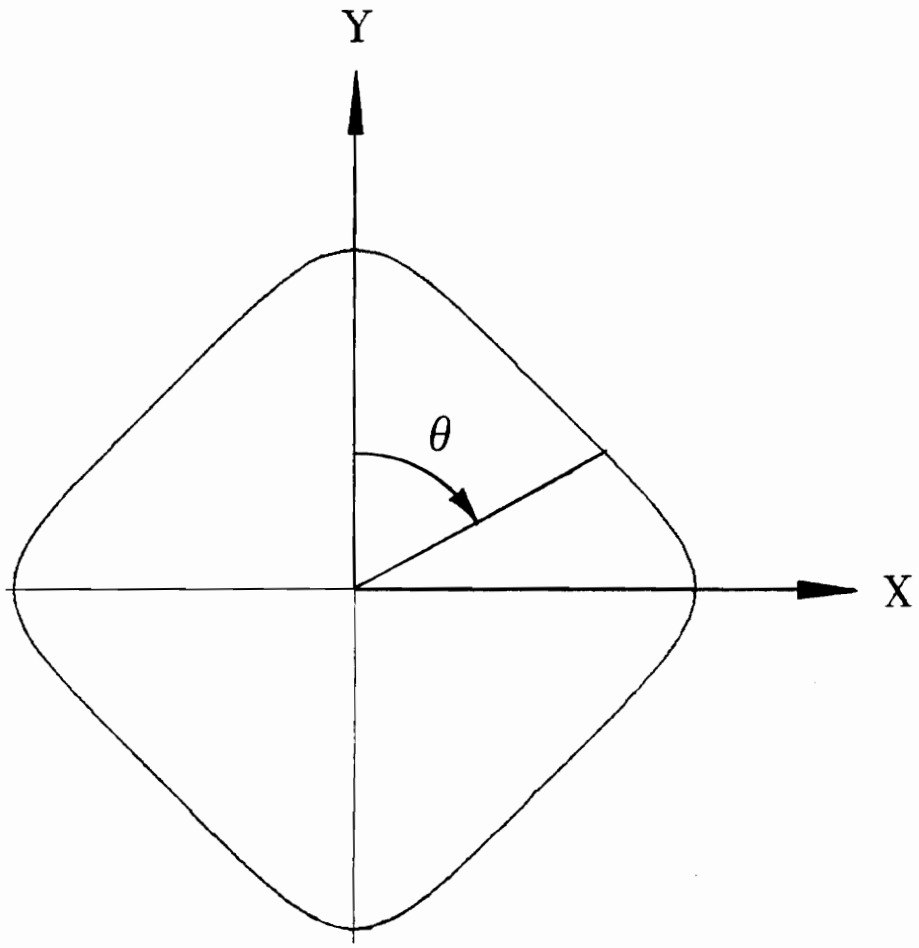

Figure 7. A Typical Hypotrocoid of 4 Lobes

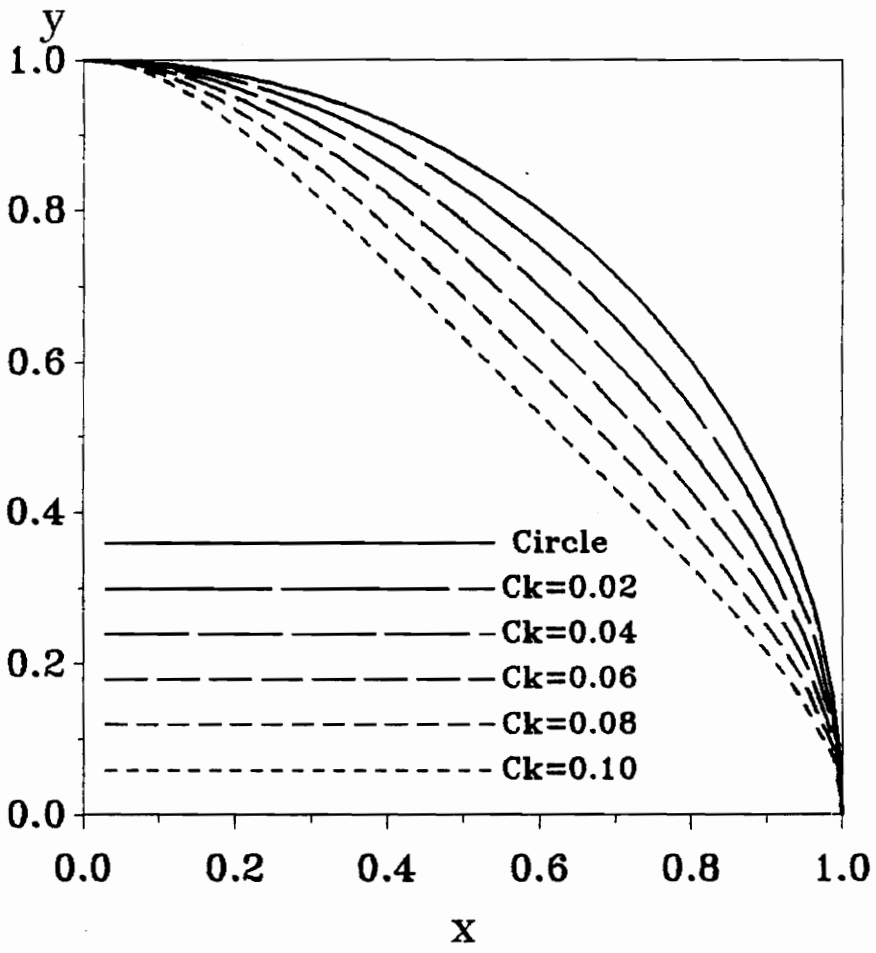

Figure 8. Hypotrocoids of 4 Lobes (Group A)
Kx=1.0, Ck=t/rs

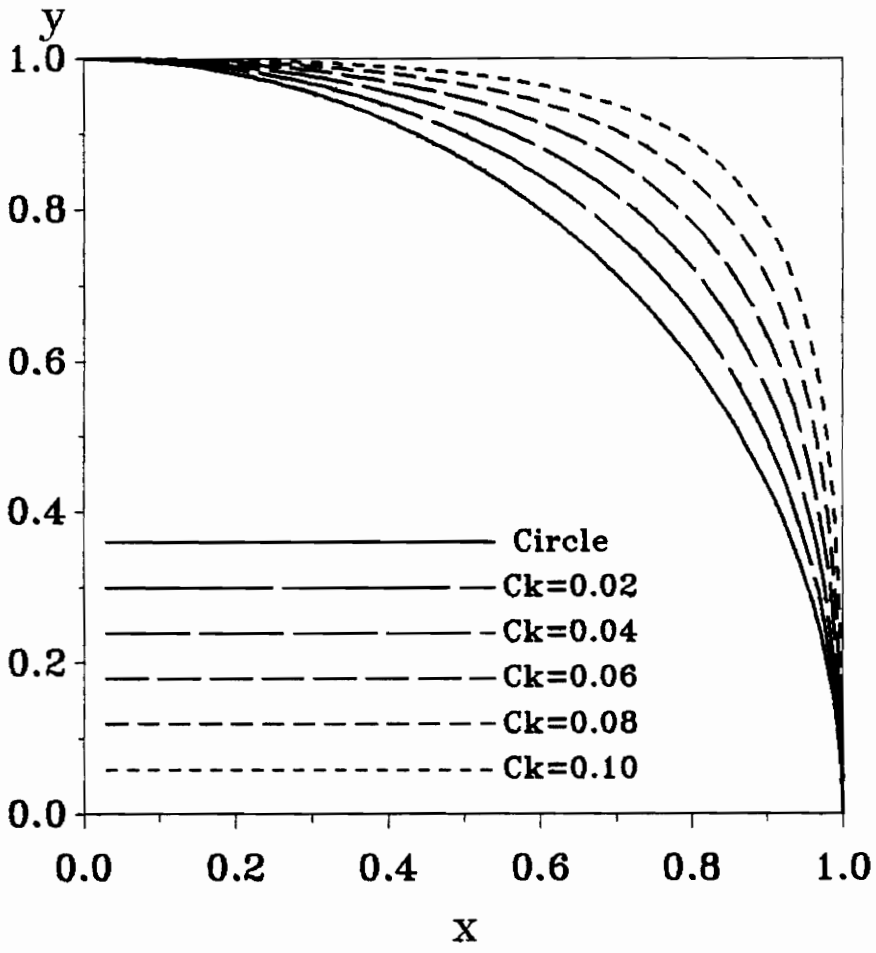

Figure 9. Hypotrocoids of 4 Lobes (Group B)
Kx=1.0, Ck=t/rs

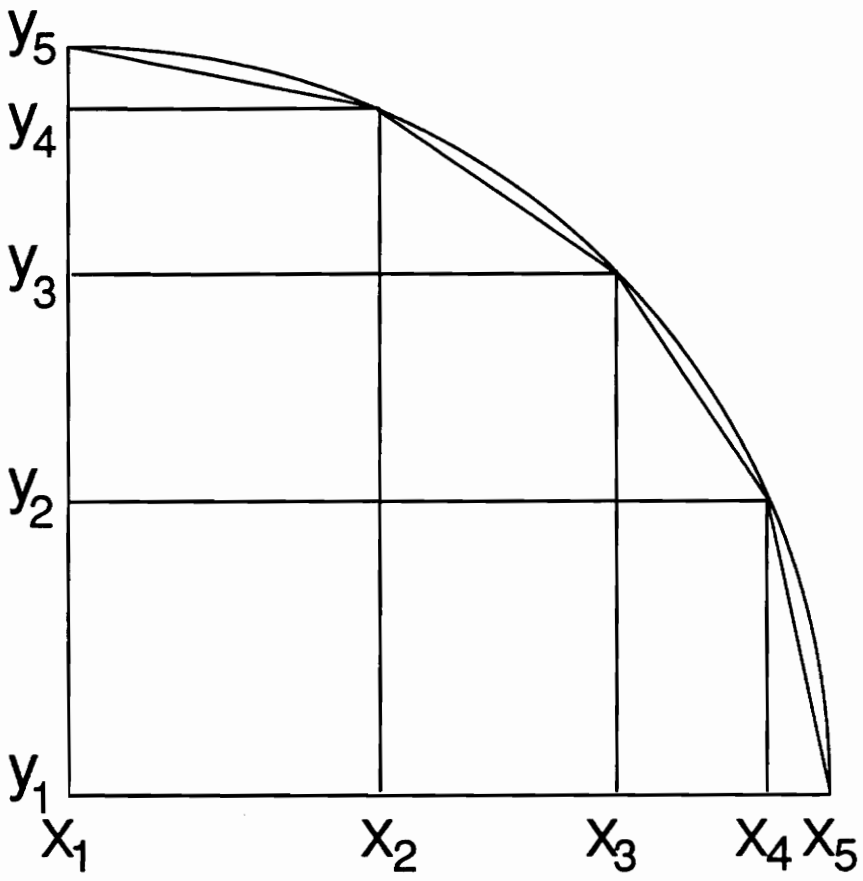

Figure 10. Discretization of a Proposed Contact Area

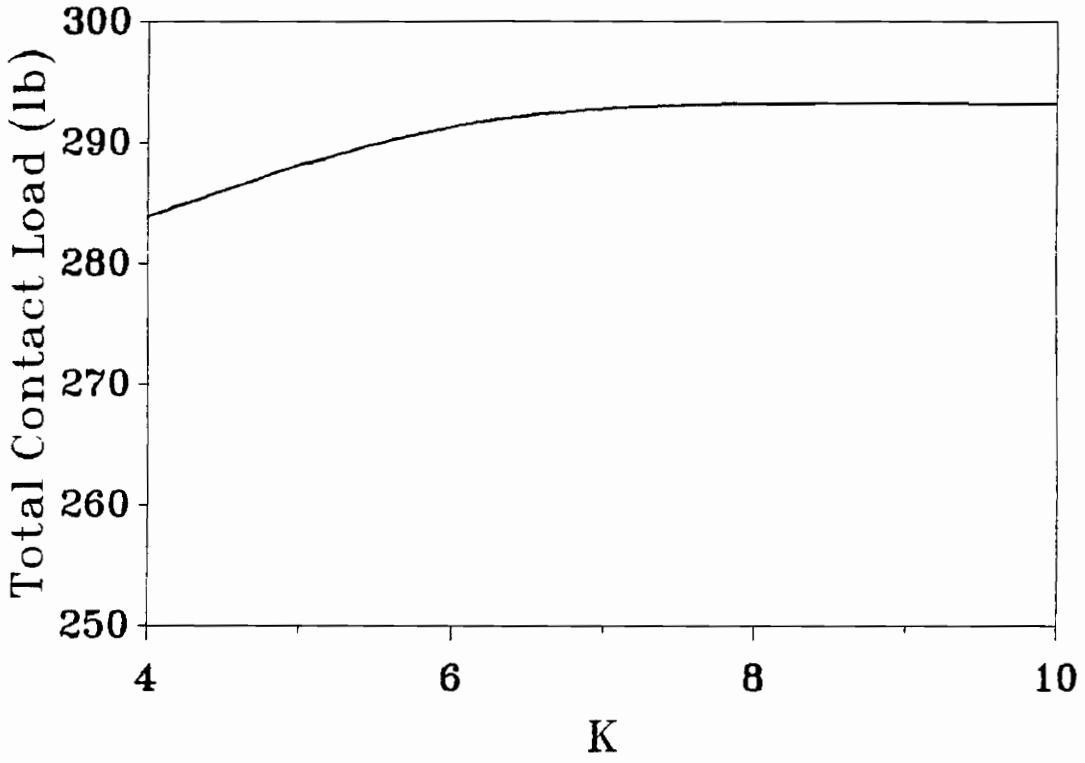

Figure 11. Convergence of Total Contact Load
Isotropic Plate, c=0.5 h
K = No. of Divisions on c

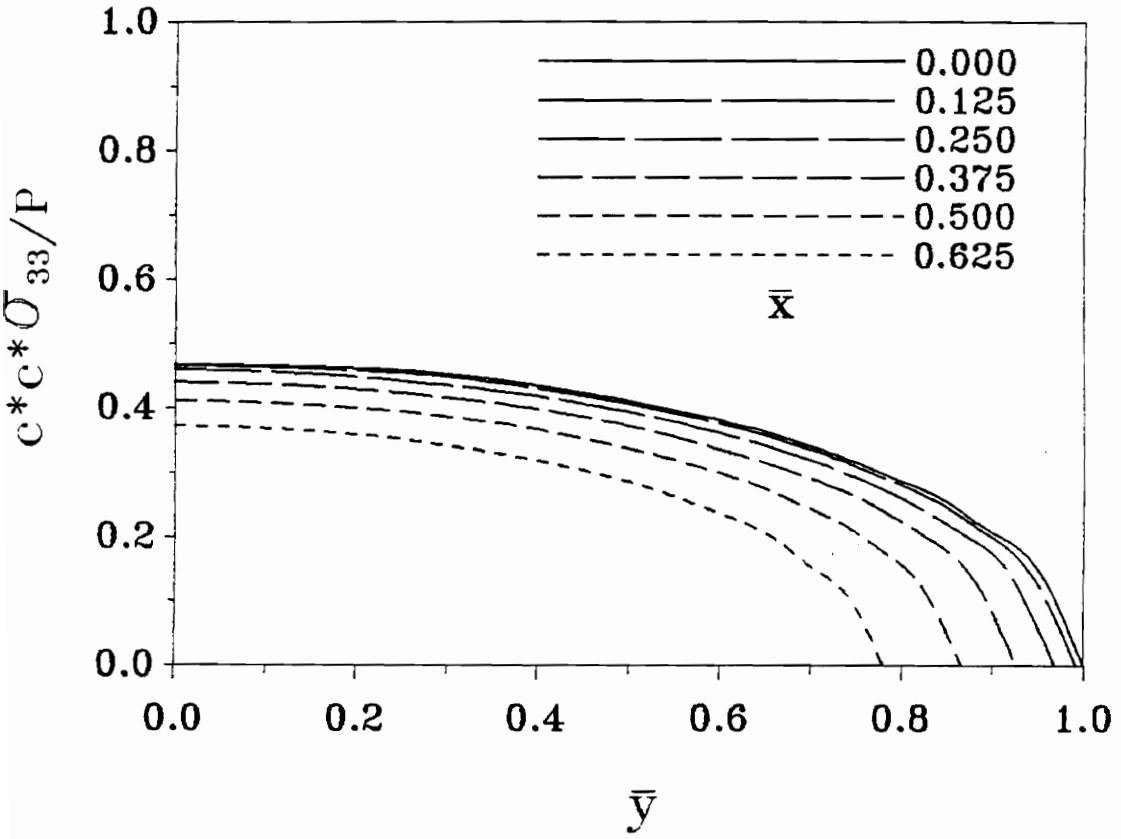

Figure 12. Contact Stress Distribution
Isotropic Plate : c=0.5 h
Circular Contact Area

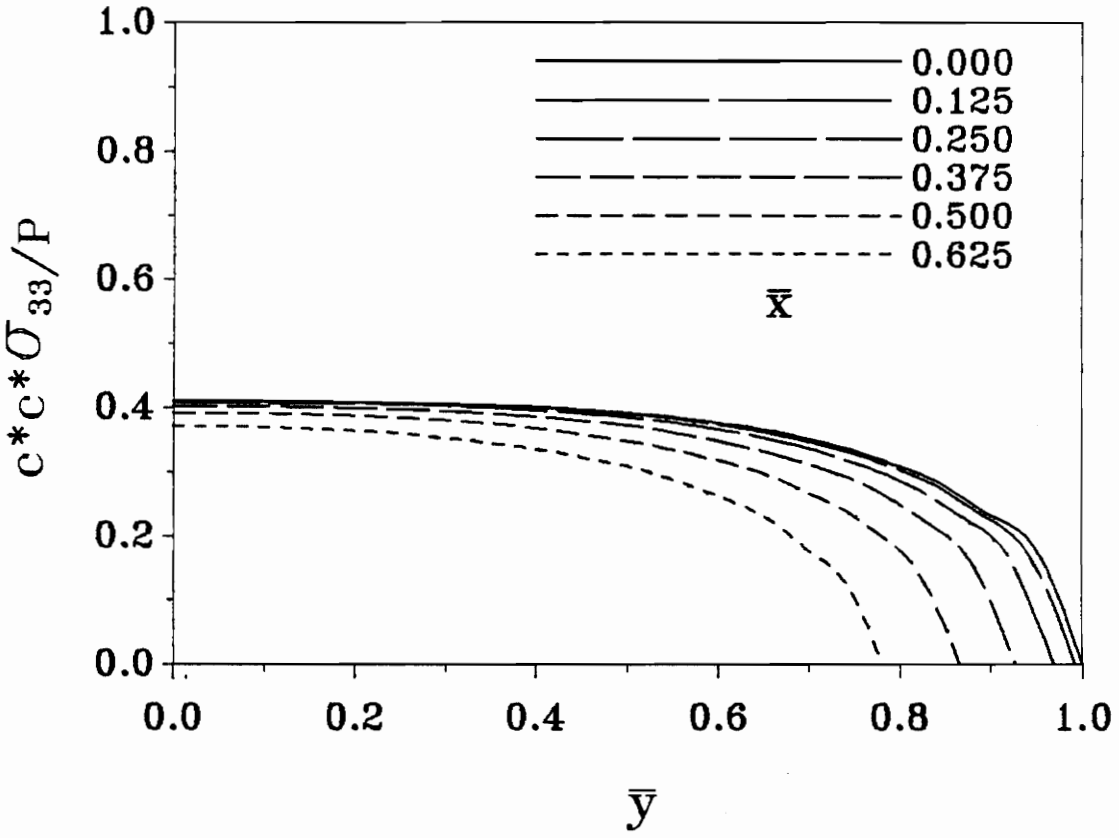

Figure 13. Contact Stress Distribution
Isotropic Plate : c=1.0 h
Circular Contact Area

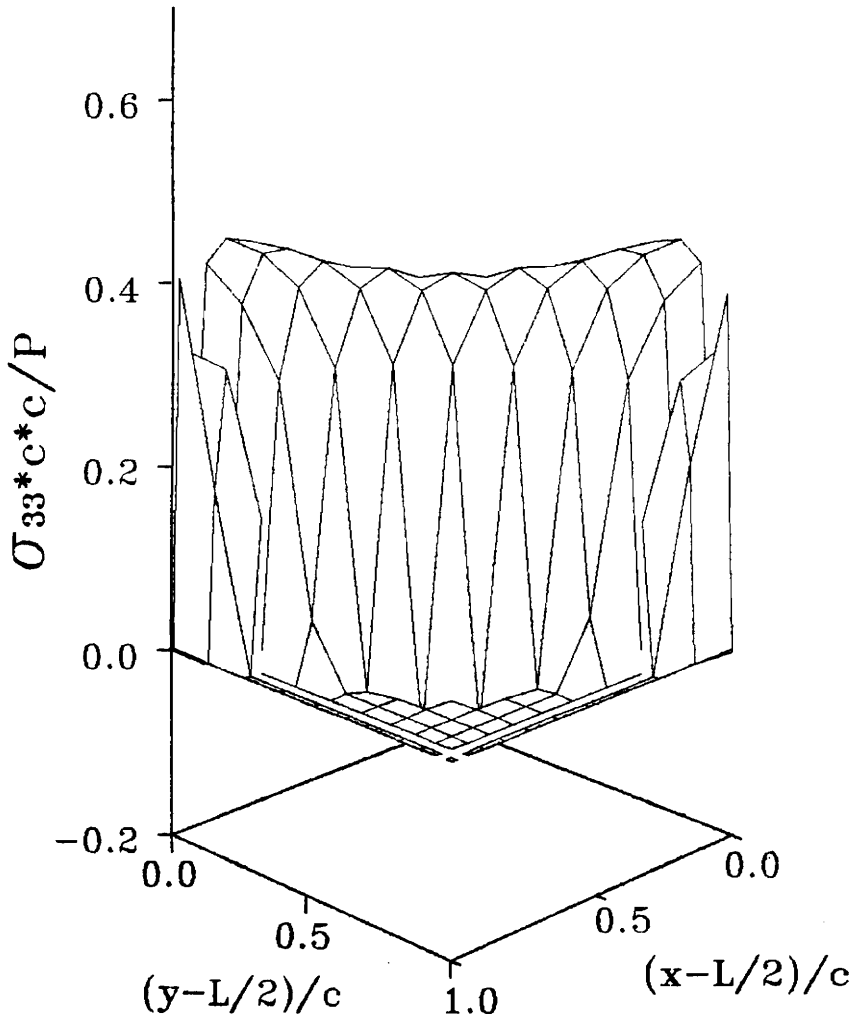

Figure 14. Three Dimensional profile of Contact Stress Isotropic Plate, Circular Contact Area, c=2.0 h

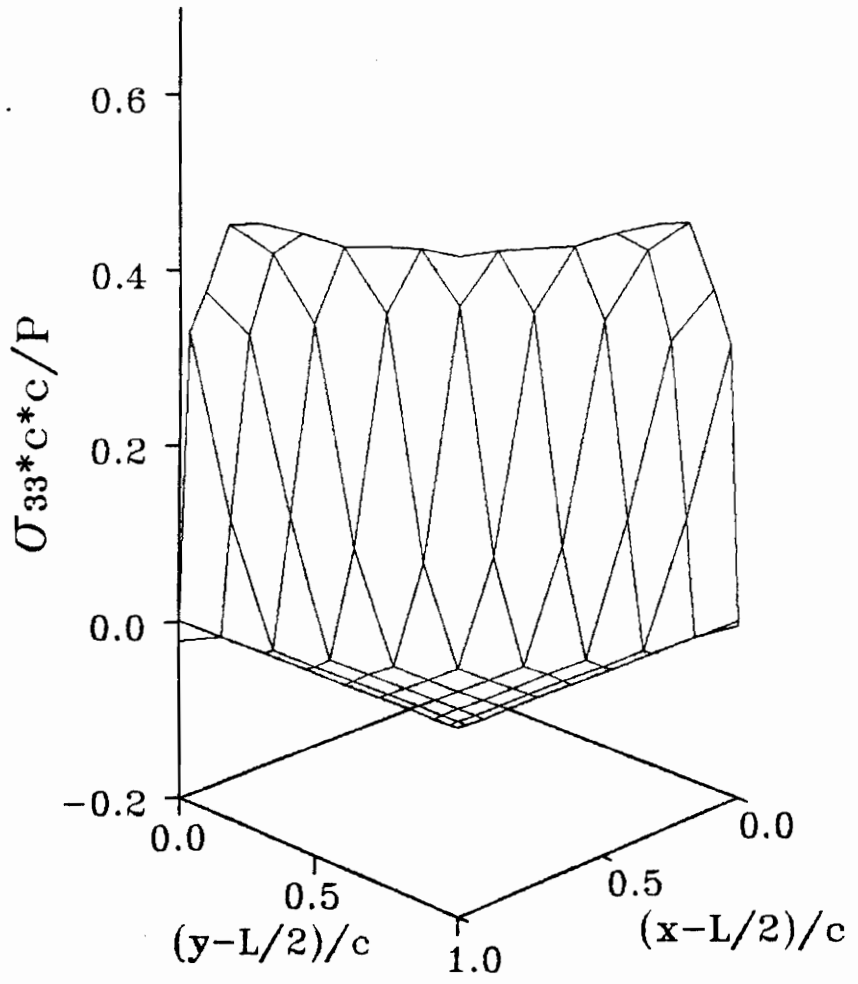

Figure 15. Three Dimensional profile of Contact Stress
Isotropic Plate, c=2.0 h
Hypotrocoidal Contact Area, t/r_s=0.01

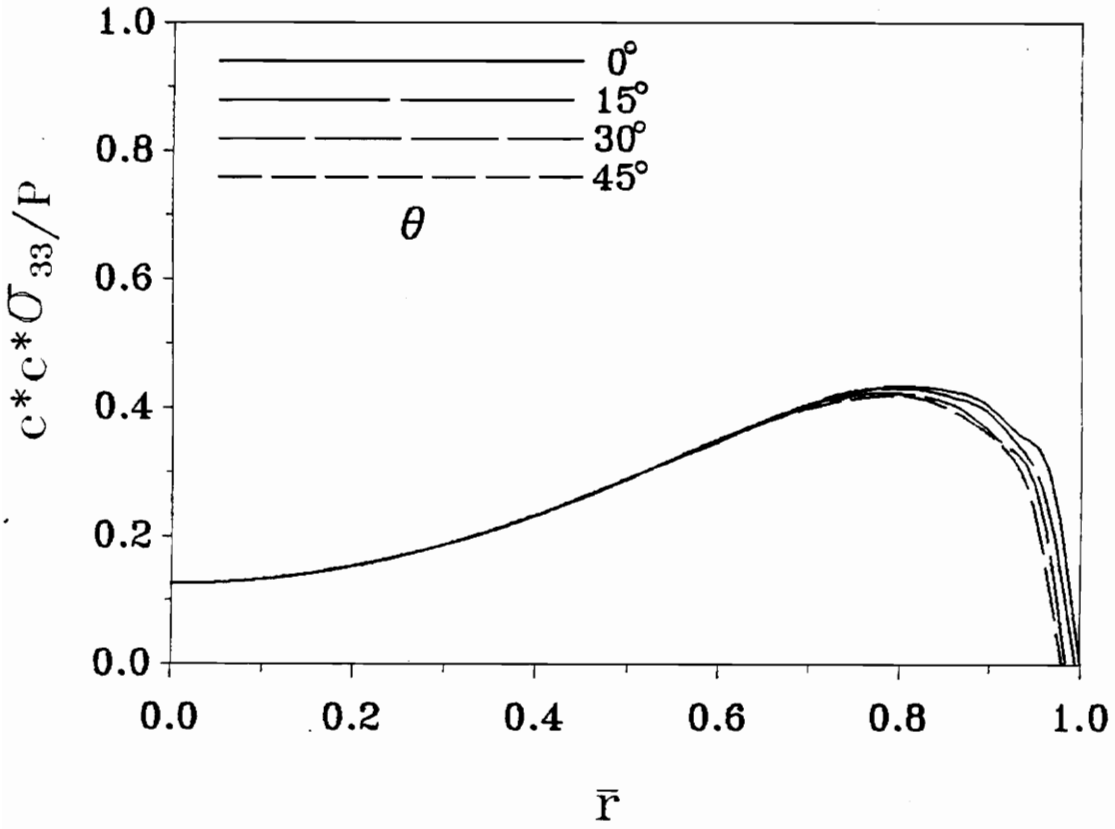

Figure 16. Contact Stress Distribution
Isotropic Plate : c=2.0 h
Hypotrocoidal Contact Area, Ck=0.01

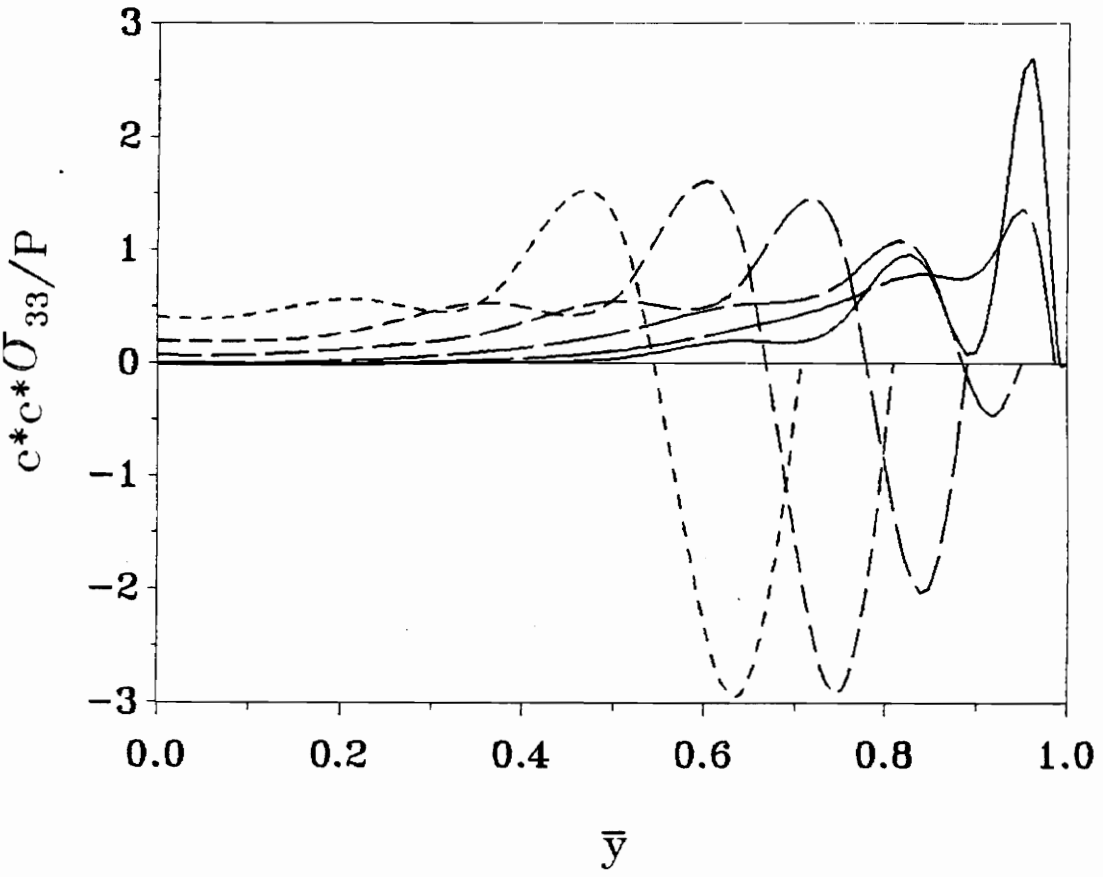

x̄ ——— 0.0 ——— .078
— — — — .233 — — — — .382
- - - - - - .521 - - - - - - .647

Figure 17. Contact Stress Distribution
Isotropic Plate : c=4.0 h
Assuming Circular Contact Area

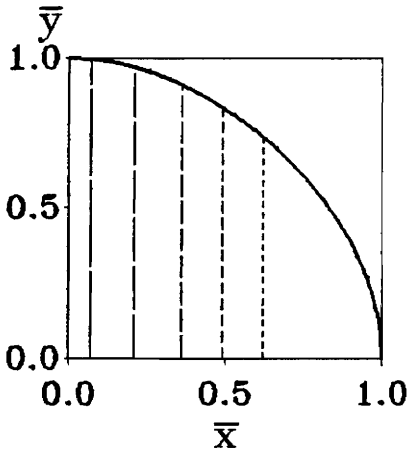

Proposed Contact Area : Hypotrocoid
Parameter, Ck=t/rs=0.02

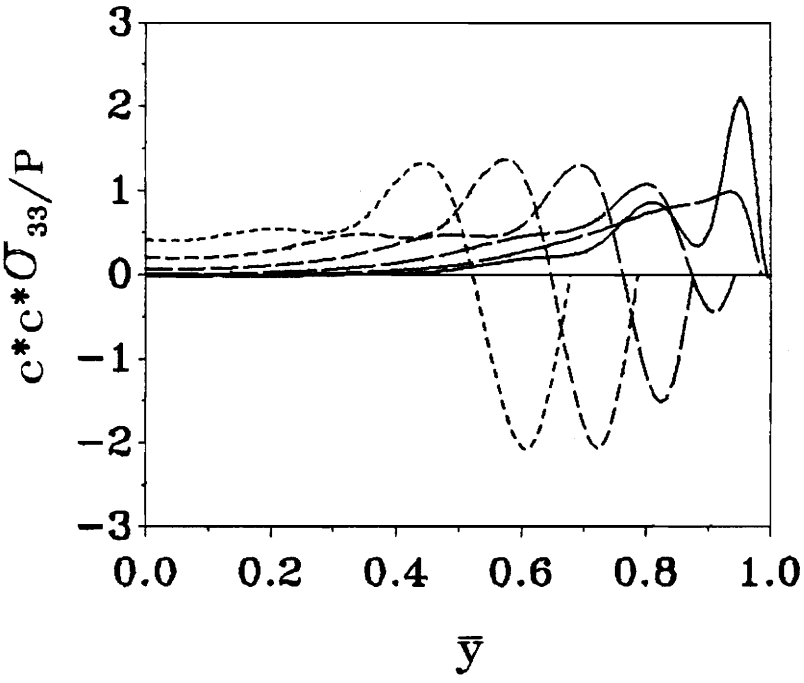

$\bar{x}$ ——— 0.0 ——— .072
— — — — .215 — — — — .356
---------- .491 ---------- .618

Figure 18. Contact Stress Distribution
Isotropic Plate, c=4.0 h

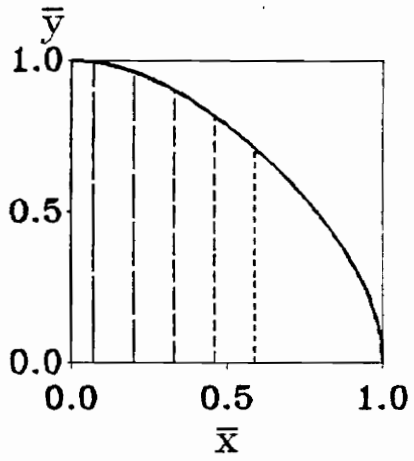

Proposed Contact Area : Hypotrocoid
Parameter, $C_k = t/r_s = 0.04$

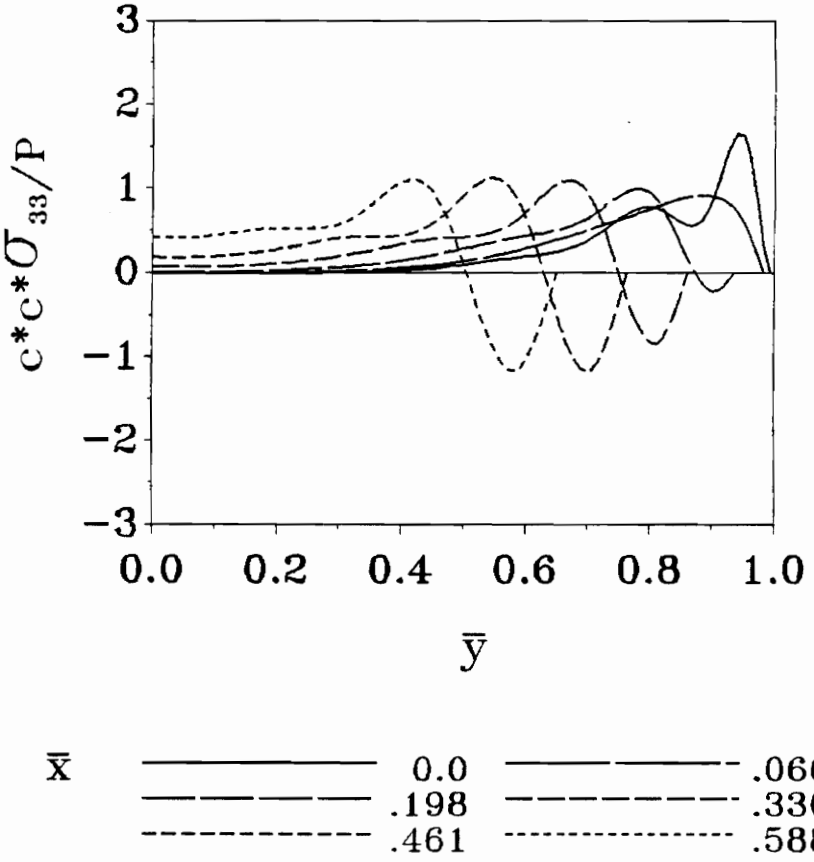

Figure 19. Contact Stress Distribution
Isotropic Plate, c=4.0 h

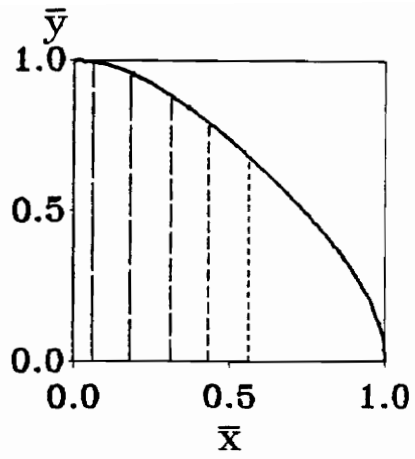

Proposed Contact Area : Hypotrocoid
Parameter, Ck=t/rs=0.06

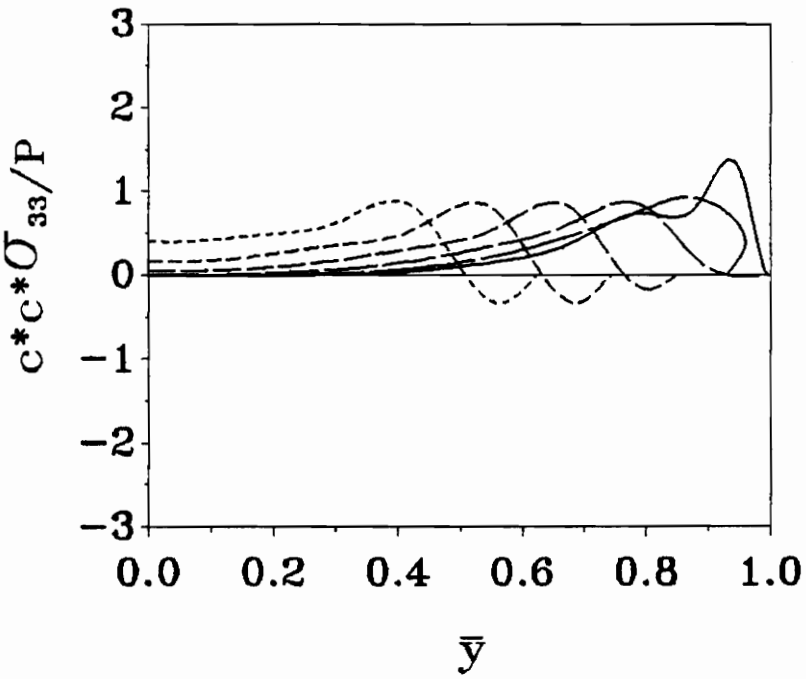

x̄ 0.0 .060
.181 .305
.431 .559

Figure 20. Contact Stress Distribution
Isotropic Plate, c=4.0 h

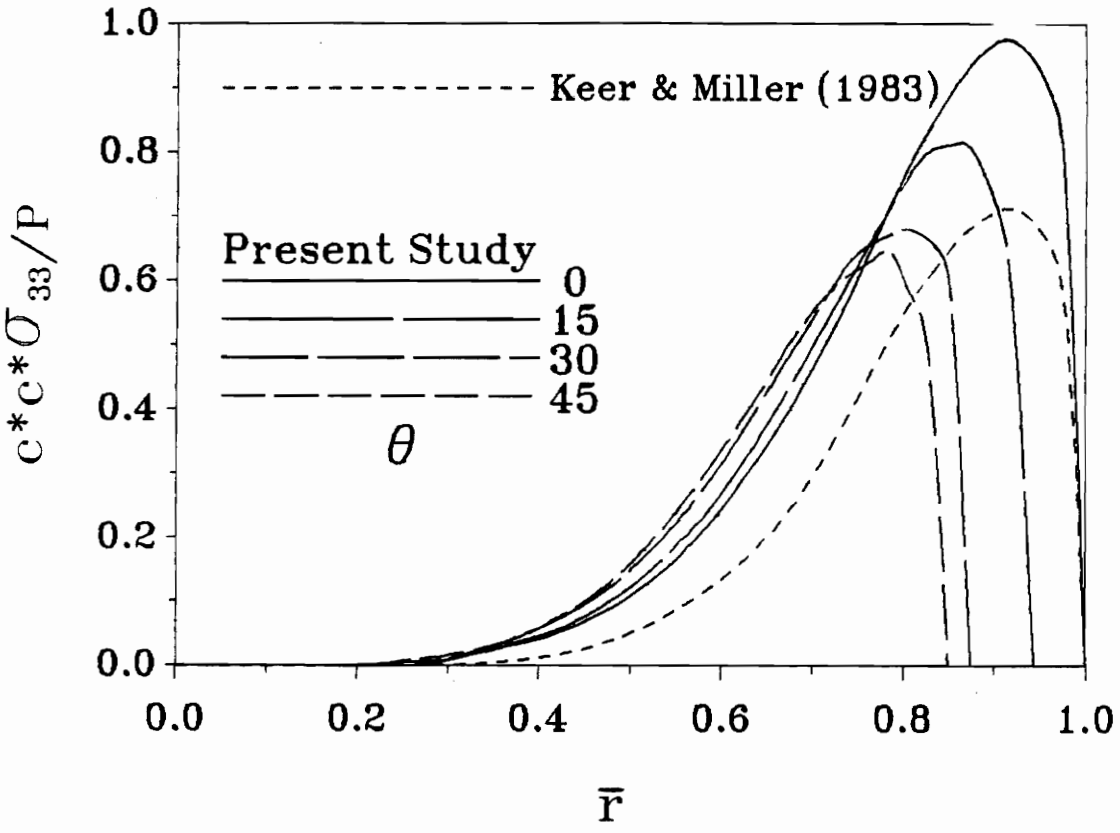

Figure 21. Contact Stress Distribution
Isotropic Plate : c=4.0 h
Hypotrocoidal Contact Area, Ck=0.075

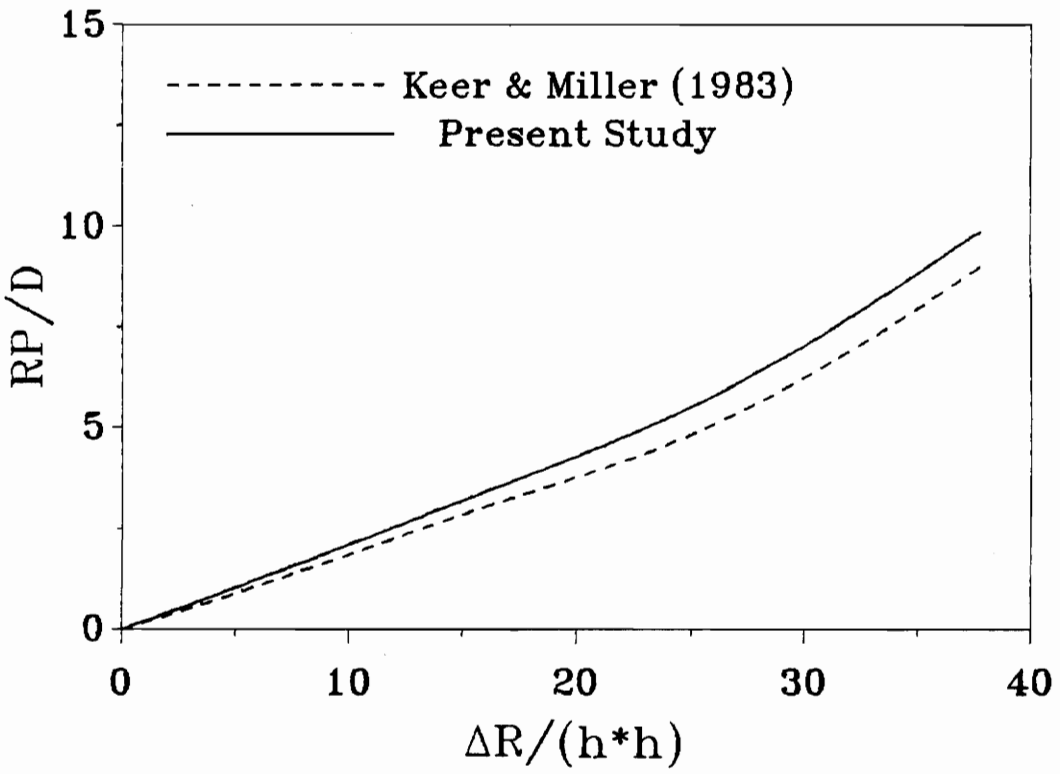

Figure 22. Load–Displacement Relation for Isotropic Plate
D=Bending Rigidity, P=Total load, Δ=Indentor Displacement

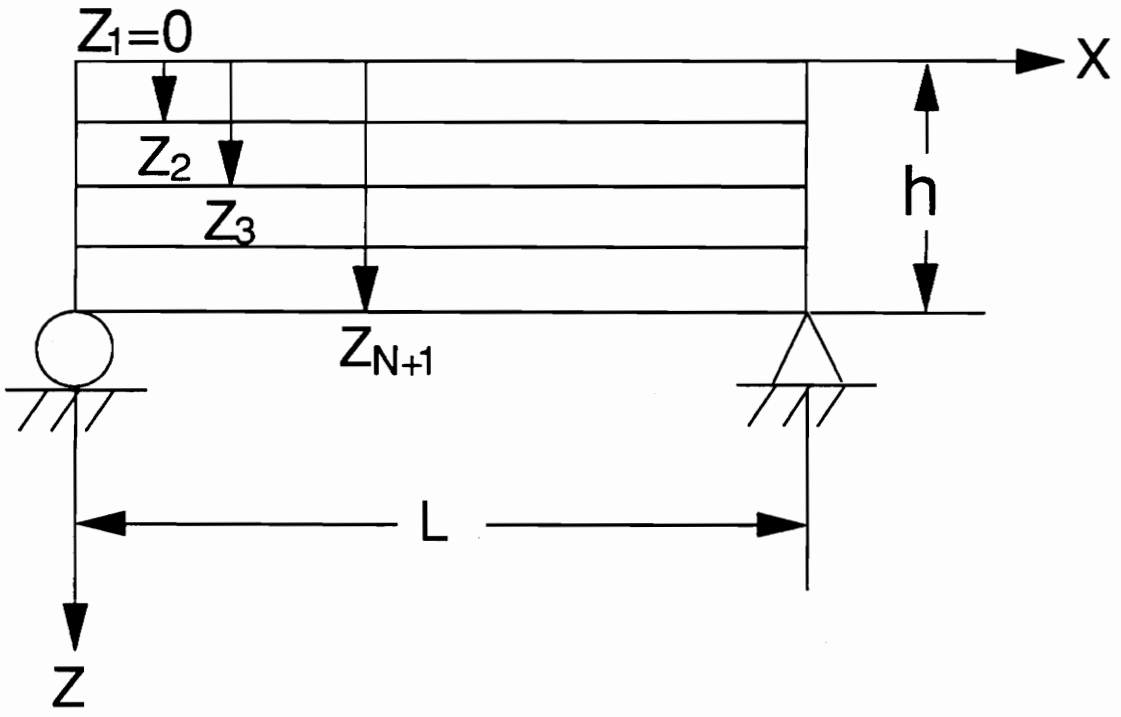

Figure 23. Through-the-thickness Configuration for the Laminate

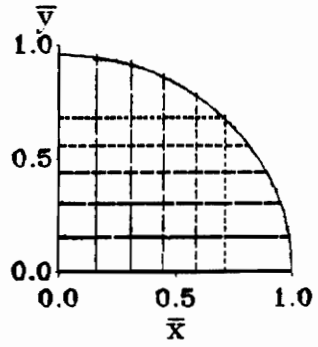

Contact Area : Ellipse
a=c=1.0 h, b=0.960 a

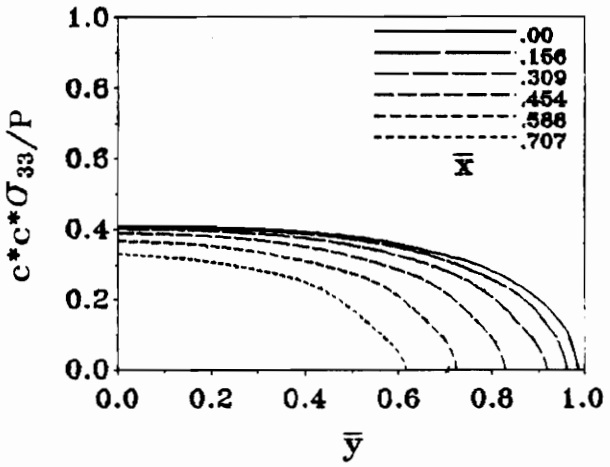

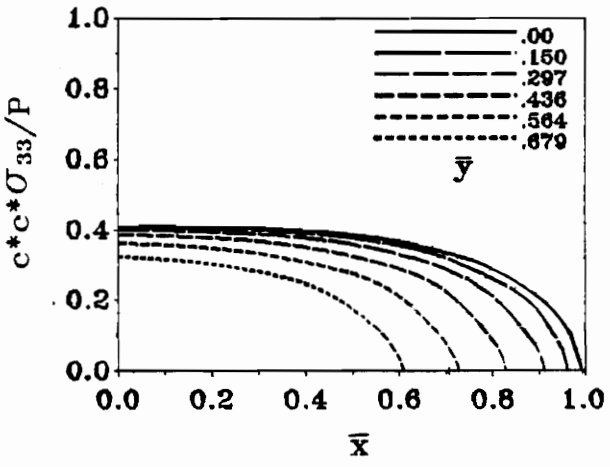

Figure 24. Contact Stress for Mg. Plate
c=1.0 h

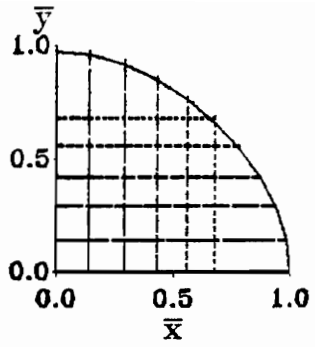

Contact Area : Modified Hypotrocoid
a=c=2.0 h, Ck=0.04, b=0.975 a, Yc=0.975

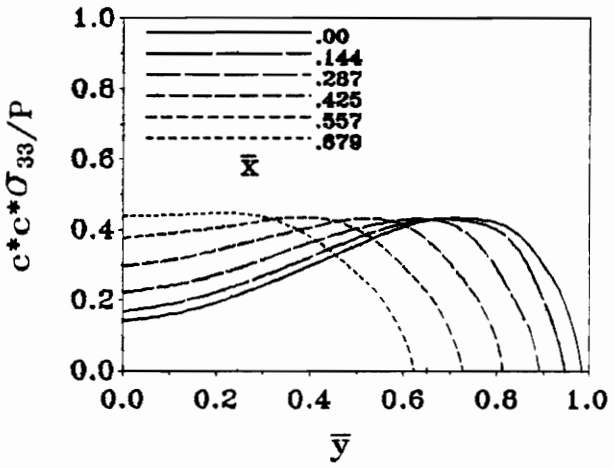

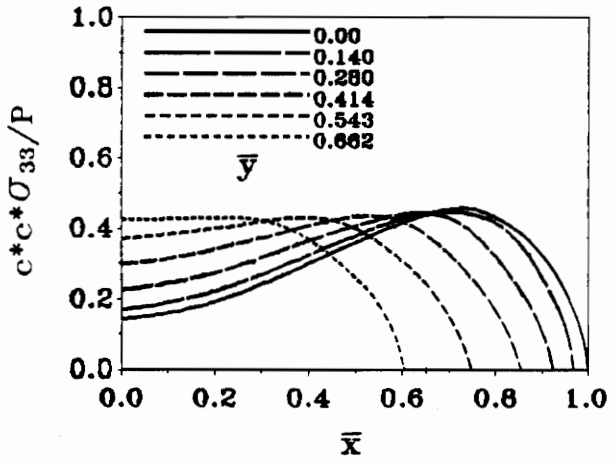

Figure 25. Contact Stress for Mg. Plate
c=2.0 h

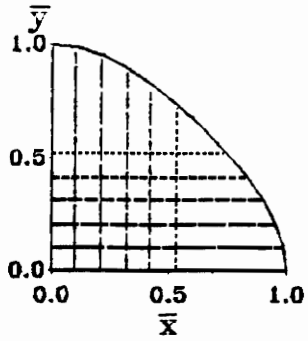

Contact Area : Modified Hypotrocoid
a=c=3.0 h, Ck=0.05, b=0.975 a, Yc=0.975

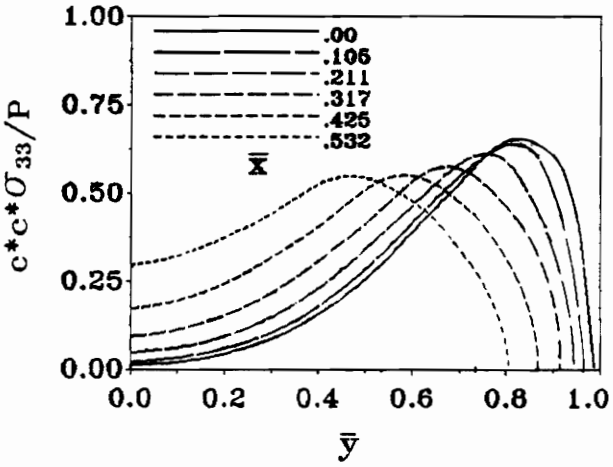

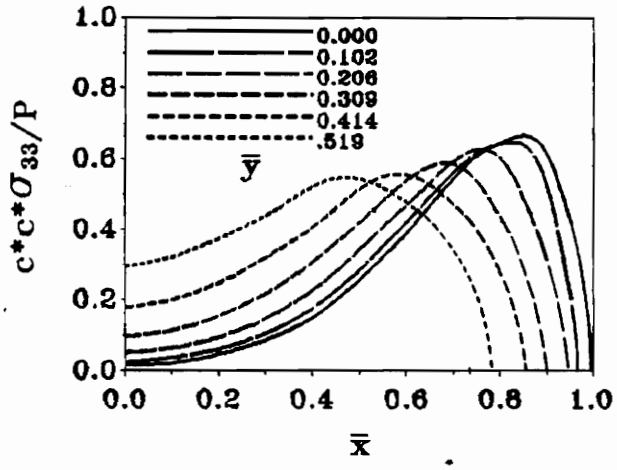

Figure 26. Contact Stress for Mg. Plate
c=3.0 h

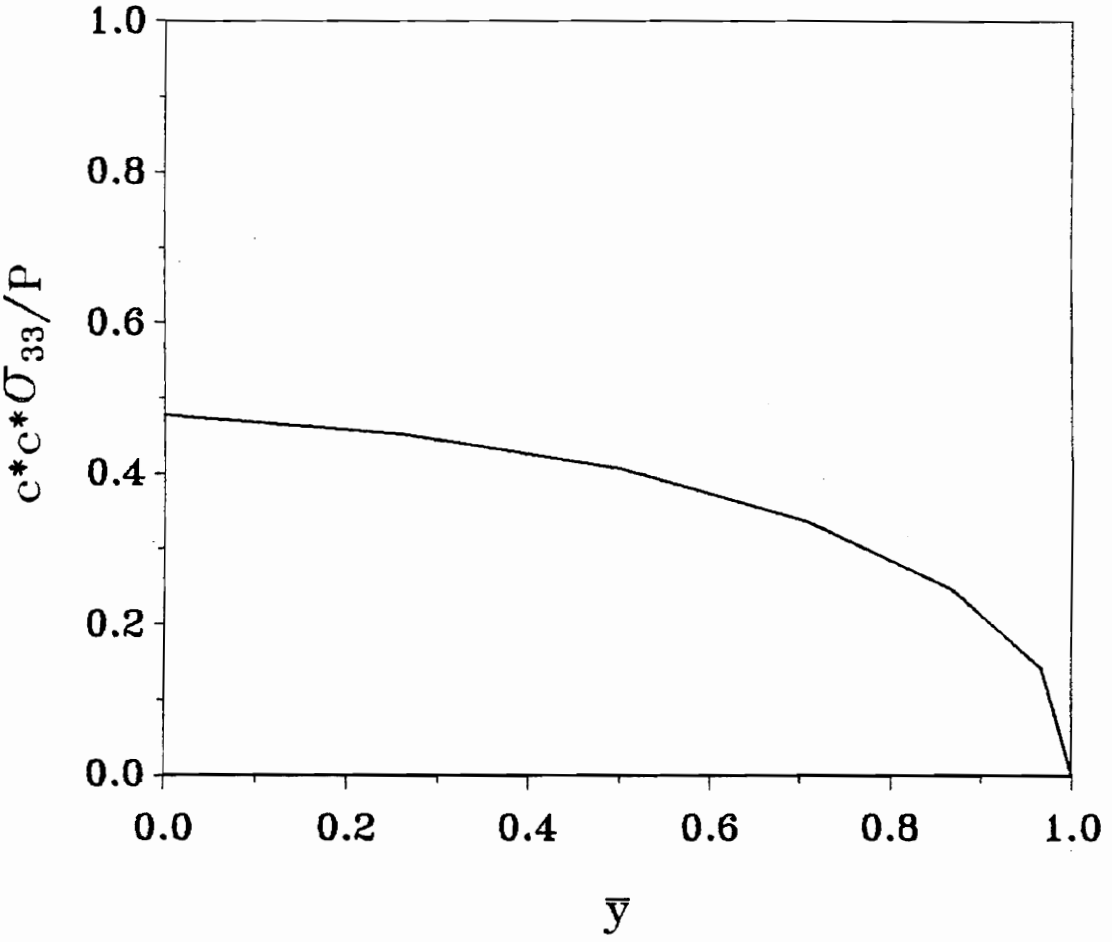

Figure 27. Contact Stress for G–E Plate
Single Layer, c=0.5 h

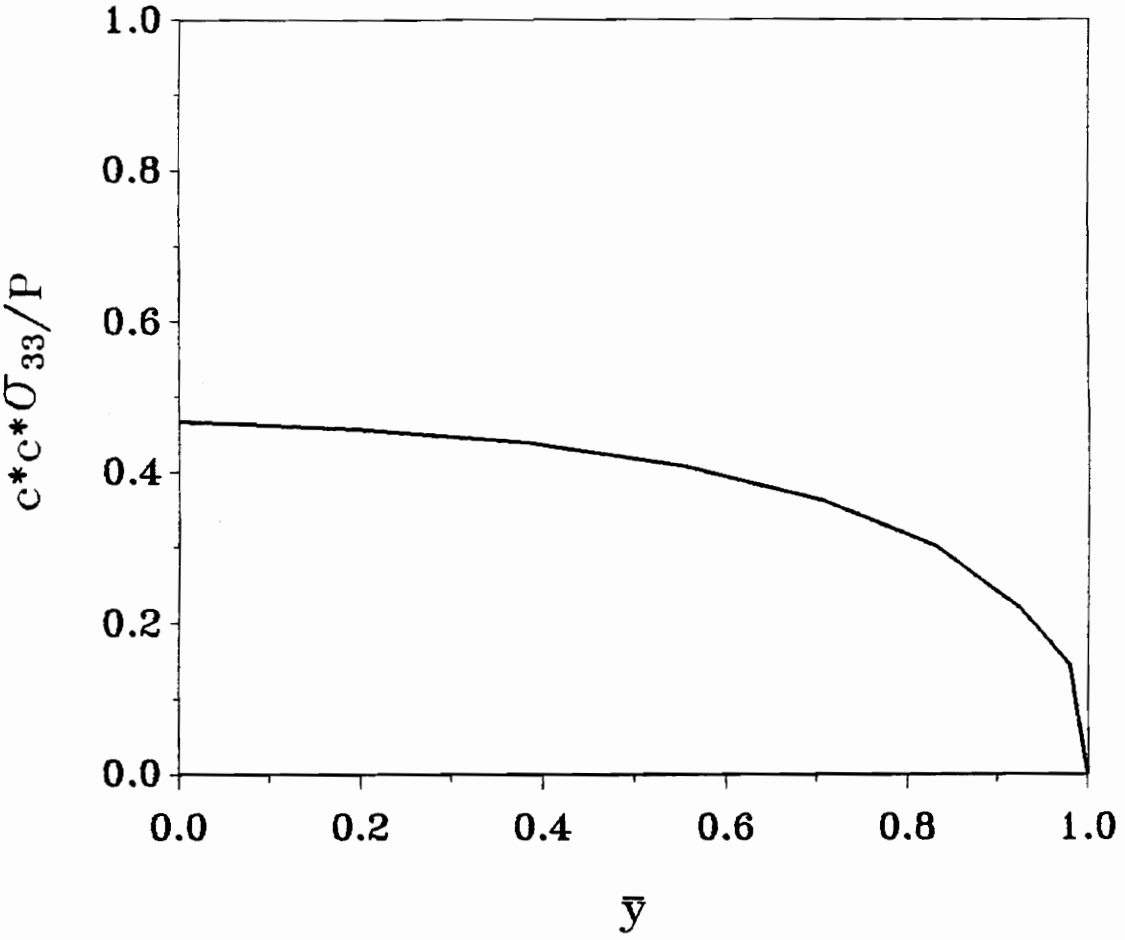

Figure 28. Contact Stress for G–E Plate
Single–Layer, c=1.0 h

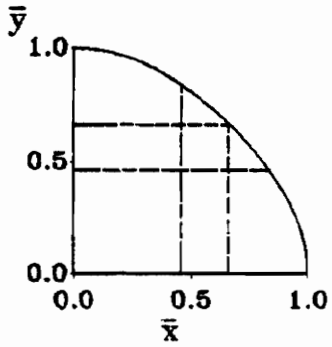

Contact Area : Hypotrocoid
a=c=0.75 h, Ck=0.03, b=a

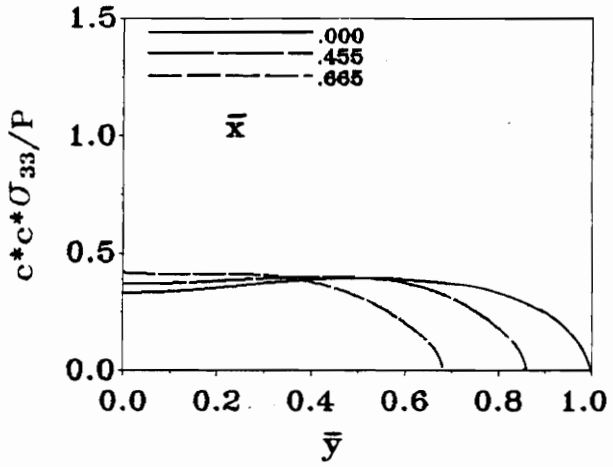

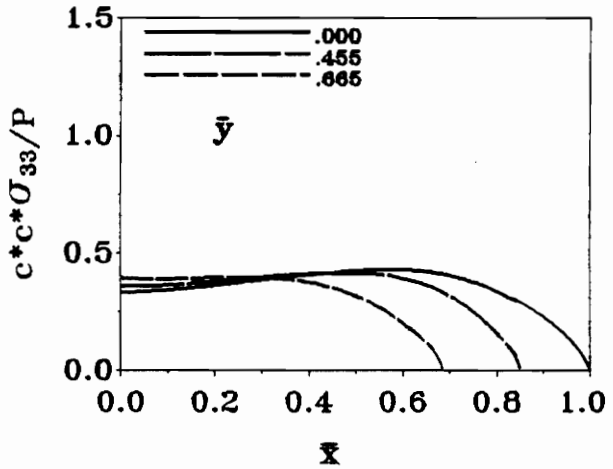

Figure 29. Contact Stress Distribution
Ortho. Lam. (G–E, 2–Layer), c=0.75 h

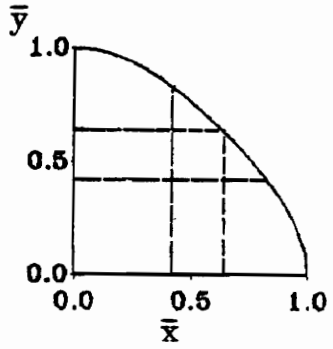

Contact Area : Hypotrocoid
a=c=1.0 h, Ck=0.05, b=a

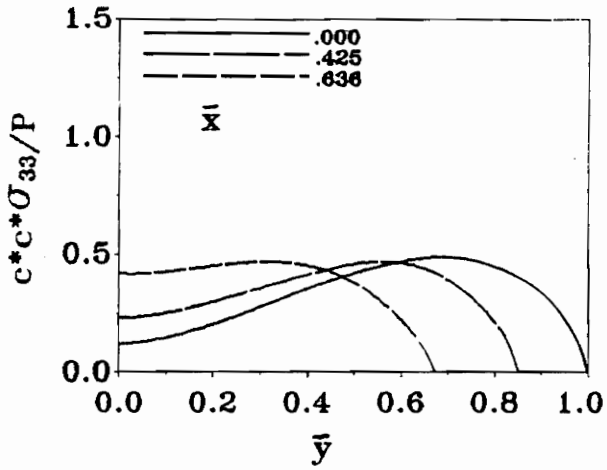

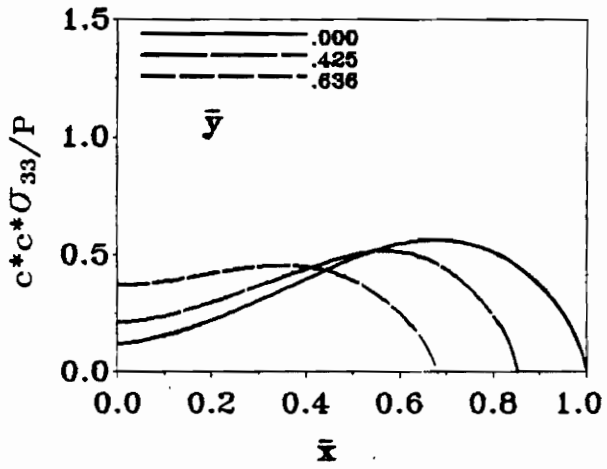

Figure 30. Contact Stress Distribution
Ortho. Lam. (G-E, 2-Layer), c=1.0 h

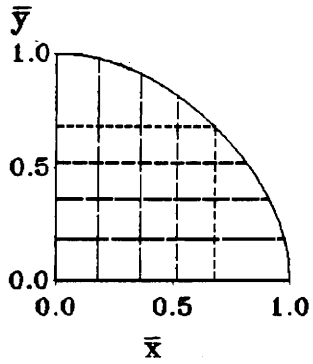

Contact Area : Hypotrocoid
a=c=1.5 h, Ck=0.02, b=a

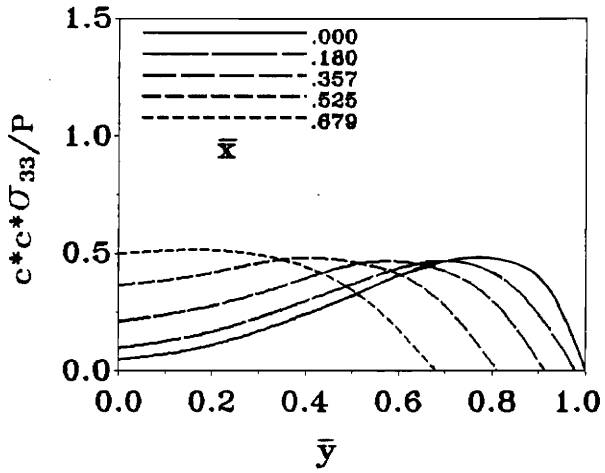

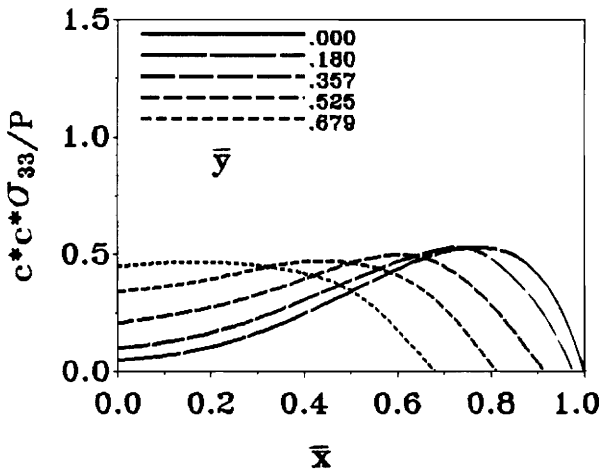

Figure 31. Contact Stress Distribution
Ortho. Lam. (G-E, 2-Layer), c=1.5 h

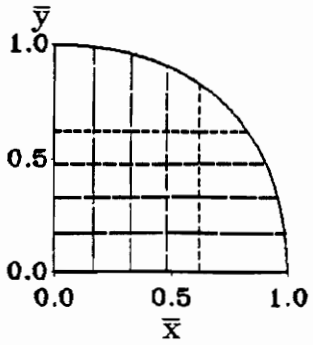

Contact Area : Hypotrocoid (B)
a=c=1.6 h, Ck=0.02, b=a

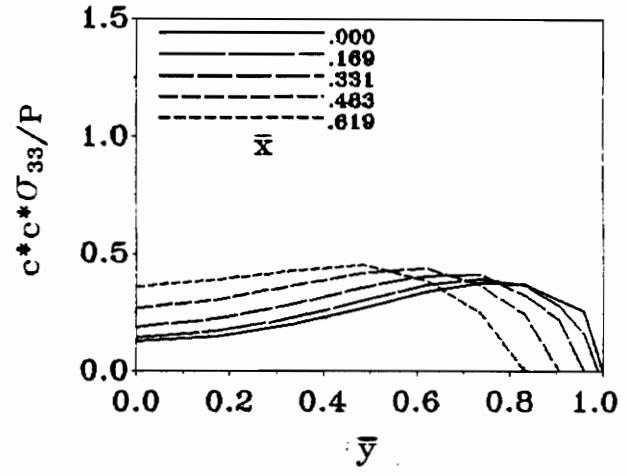

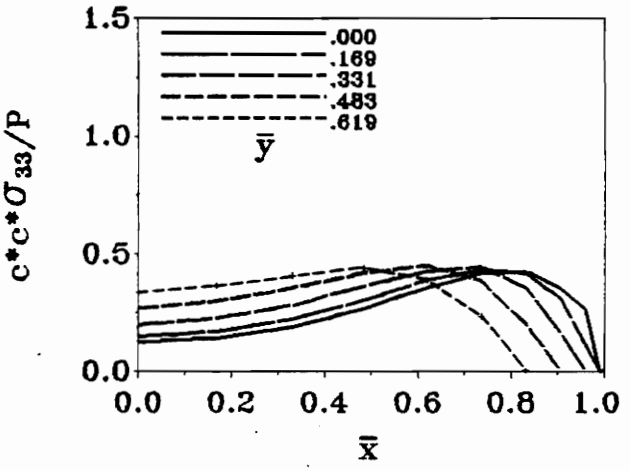

Figure 32. Contact Stress Distribution
Ortho. Lam. (G-E, 2-Layer), c=1.6 h

Vita

Chun-Fu Chen was born on June 20, 1958. He received his B. S. in Mechanical Engineering from National Chiao-Tung University in 1980. After two years of military service, he entered Energy Research Laboratory, Industrial Technology Research Institute in Taiwan in 1982 where he served as an assistant engineer for three years. He enrolled in Department of Engineering Science and Mechanics at Virginia Tech in 1985 and received his M. S. degree in Engineering Mechanics in 1987. He then continued his doctoral study in the same department and completed his Ph. D. degree in April 1991.